THE DISSOLUTION RATES AND MECHANISMS OF TETRAGONAL FERROUS SULFIDE (MACKINAWITE) IN ANOXIC AQUEOUS SYSTEMS

Thesis by

James Frederick Pankow

In Partial Fulfillment of the Requirements

for the degree of

Doctor of Philosophy

California Institute of Technology

Pasadena, California

1979

(Submitted September 28, 1978)

ACKNOWLEDGMENTS

The author would like to thank Professor James J. Morgan for supervising this research project. His chemical insight and encouragement (and puns!) were always very much appreciated. The many helpful discussions which the author held with Professor Fred C. Anson are also gratefully acknowledged. The help of Professors Pol Duwez and Jean-Paul Revel in the areas of X-ray diffraction and electron microscopy were indispensible.

The many informative discussions which the author had with Dr. Michael Barcelona, James Hunt, and Howard Liljestrand are appreciated. Special thanks also go to Dr. George Jackson for his suggestion of the mathematical analysis on diffusion and reactions in porous media presented in Section 7.2.

The expert help of Elton Daly and Joe Fontana in the design and fabrication of much of the dissolution apparatus laid the groundwork for the experimental phase of this research. Thanks also go to Sylvia Garcia, David Byrum, Richard Eastvedt, and Larry McClellan for their technical assistance. The expert help of Patrick Koen with the electron microscope work is also gratefully acknowledged.

Financial support from the U.S. Public Health Service N.I.E.H.S. Training Grant and the Du Pont Environmental Fellowship is gratefully acknowledged.

And, saving the best for last, the author wishes to express his deeply felt appreciation to Elaine Granger, Adelaide Massengale and Bonnie Sherburn for their generous donations of time and patience in metamorphosing my palsied scrawl into a legible first draft. The professional typing of the final draft by Donna Straight speaks for itself and will be appreciated by anyone who reads this thesis.

ABSTRACT

An experimental study was carried out on the rates and mechanisms of the non-oxidative dissolution of mackinawite (tetragonal FeS) in anoxic aqueous systems of varying pH (3-7), T (5-35°C), and ionic strength (0.05-0.60 M). A special glass and teflon dissolution reactor was constructed. The main design criterion was the need to keep the reaction medium absolutely free of oxygen.

The flux F_S (moles/cm^2-min) from the surfaces of pellets pressed from ~1μ FeS particles was found to obey the rate equation

$$F_S = k_1 a_{H^+} + k_2$$

k_1 and k_2 are rate constants and a_{H^+} is the activity of the hydrogen ion At 25°C, k_1 = 0.22 cm/min with a relative standard deviation of 18%. The value of k_2 was measured to be 1.9 moles/cm^2-min with a relative standard deviation of 22%. The actual exposed FeS surface area A′ was related to the projected area A by the expression A′ = 1.7A. The factor of 1.7 accounts for the roughness of the surface. The actual rate constants k_1' and k_2' were therefore obtained by dividing k_1 and k_2 by 1.7: k_1' = 0.13/min and k_2' = 1.1 x 10^{-9} moles/cm^2-min. The k_1' term dominates at pH < 4.3 and k_2' dominates at pH > 5.6. pH 4.3-5.6 is a transition region.

It is argued that these rate constants are relatable to dissolution mechanisms at the FeS crystal surface. k_1' is envisioned to arise from an attack at the surface by H^+. k_2' is linked to a mechanism which relies upon normal thermal vibrations and H_2O solvation effects to liberate

lattice constituents. Both k_1' and k_2' are thought to reflect a rate-limiting departure of surficial S(-II) lattice constituents. The activation entropies $\Delta S^{\ddagger}$ for these two processes are calculated accordingly. The activation enthalpies $\Delta H^{\ddagger}$ were determined from the E_a data. Concentrations of Cu(II) in the ppm range were found to strongly inhibit the dissolution rate.

The k_2' term would dominate at pH's typical of natural waters. This term was used to determine how quickly FeS dissolves when anaerobic sediments are disturbed. When anoxic and oxic sediments are adjacent to one another, the dissolution of FeS in the anoxic portion takes place primarily near the oxic front.

If FeS-containing anaerobic sewage sludge is discharged to anoxic receiving waters, the particles of FeS may be expected to dissolve. Expressions were developed by which the lifetimes of such particles may be calculated. Both transport and non-transport controlled situations are analyzed. The effects which the agglomeration of such FeS with other sewage particles would have on the dissolution rate were considered. The implications which this work holds for sediment pyritization rates were also discussed.

TABLE OF CONTENTS

TABLE OF CONTENTS (CONT.)

TABLE OF CONTENTS (CONT.)

TABLE OF CONTENTS (CONT.)

LIST OF FIGURES

LIST OF FIGURES (CONT.)

LIST OF TABLES

LIST OF NOTATION AND ABBREVIATIONS (CONT.)

Roman

a_i	activity of species i (moles/cm^3)
a	area density of lattice constitutents (number/cm^2)
A	constant of proportionality in Arrhenius Activation Energy equation (dimensions vary)
A	area of solid exposed for dissolution (cm^2)
A'	area exposed for dissolution taking surface roughness into account (cm^2)
Å	angstroms (10^{-8}cm)
c	concentration (moles/cm^3)
c_s	concentration at saturation (moles/cm^3)
D	diffusion coefficient (cm^2/sec)
E_a	energy of activation for a reaction (kcal/mole)
F	flux (moles/cm^2-sec or moles/cm^2-min)
F_s	flux of dissolved metal sulfide (units same as F)
F_{H^+}	flux of protons (units same as F)
Fe_{TOT}	total dissolved iron (II) (moles/liter)
g	fraction of sediment area which is FeS
ΔG	change in free energy for a reaction (kcal/mole)
$\Delta G^{\ddagger}$	activation free energy (kcal/mole)
$\Delta H^{\ddagger}$	activation enthalpy (kcal/mole)
HOAc	acetic acid
I	ionic strength (moles/ℓ)
IAP	ion activity product (dimensions vary)

LIST OF NOTATION AND ABBREVIATIONS (CONT.)

Roman

k	Boltzmann's constant (ergs/°K)
k_1	a constant in rate equation for pressed pellets assuming actual area = projected area (cm/min)
k_2	same as k_1, but units are moles/cm^2-min
k_1'	k_1 corrected for real surface area (cm/min)
k_2'	k_2 corrected for real surface area (moles/cm^2-min)
k_1^*	a constant in rate equation for non-porous surfaces (cm/min)
k_2^*	a constant in rate equation for non-porous surfaces (moles$^{1.5}$/cm$^{3.5}$-min)
$\tilde{k}_1$	rate constant describing the reaction between surface S(-II) groups and protons (cm^3/mole-sec)
$\tilde{k}_2$	rate constant for dissolution (sec^{-1})
ℓ	dimension of particle (cm)
ℓ_o	initial particle size (cm)
K_1	see equation (5.6)
K_2	see equation (5.7)
$^*K_1$	see equation (5.8)
K_{FeCl}	see equation (5.9)
m	mass of particle (g)
m_o	initial mass of particle (g)
MES	morpholino ethane sulfonic acid
MOPS	morpholino propane sulfonic acid
n_s	area density of S(-II) sites on FeS crystal (moles/cm^2)

LIST OF NOTATION AND ABBREVIATIONS (CONT.)

Roman

n_{sa}	area of density of S(-II) active sites on FeS crystals which may dissociate unaided by H^+ (moles/cm^2)
N_A	Avogadro's number
rds	rate determining step
K_{so}	solubility product (dimensions vary)
M	"molar" (moles/liter)
pK	-log K (dimensionless)
s	surface area of particle (cm^2)
S	molar surface area (m^2/mole)
S_{TOT}	total dissolved sulfide (moles/liter)
$\Delta S^{\ddagger}$	activation entropy (eu/mole)
t_f	time to complete dissolution for a particle (min)
r	radius of pore (cm)
r_c	initial radius for hole formation (cm)
R	gas constant (cal/mole-deg)
T	temperature (°K)
V	volume of solvent (cm^3)
W	molecular weight (g)

Greek

α_0	fraction of S(-II) present as H_2S (dimensionless)
α_1	fraction of S(-II) present as HS^- (dimensionless)
α_2	fraction of S(-II) present as S^{2-} (dimensionless)

LIST OF NOTATION AND ABBREVIATIONS (CONT.)

Greek

α_{FeOH}	fraction of Fe(II) present as $FeOH^+$ (dimensionless)
γ	overall surface tension of solid-liquid interface ($ergs/cm^2$)
γ_i	activity coefficient of species i (dimensionless)
δ	thickness of diffusion boundary layer (cm)
κ	rate constant for general reaction (dimensions vary)
ρ	density (g/cm^3)
σ	edge free energy (ergs/cm)
σ_s	surface free energy ($ergs/cm^2$)
μ	10^{-6} meter
ϕ	porosity (dimensionless)
Ω	K_{so}/IAP for hole formation (dimensionless)

CHAPTER 1

INTRODUCTION

1.1 General Comments

This thesis is concerned with an experimental study of the rates and mechanisms of the non-oxidative dissolution reaction of tetragonal FeS (mackinawite; FeS_{mack}) in anoxic aqueous systems of varying pH, temperature, and ionic strength. A rather insoluble compound, FeS_{mack} often forms in reducing sediments and is believed to form in "anaerobically-digested" (microbiologically degraded in the absence of oxygen) sewage sludge (Morgan and Sibley, 1975). The trace metal constituents of these systems which also form insoluble metal sulfides (e.g., Ag^{+}, Cd^{2+}, Cu^{2+}, Pb^{2+}, Zn^{2+}) very likely associate with the much more predominant iron sulfides. This material may be expected to at least partially dissolve: 1) when reducing sediments are disturbed by animal life, dredging, or by more subtle events; and 2) when anaerobic sewage sludge is disposed of in the marine environment.

The non-oxidative dissolution of FeS_{mack} may be written quite simply as

$$FeS_{mack} \longrightarrow Fe^{2+}_{aq} + S^{2-}_{aq} \qquad (1.1)$$

(The aqueous species Fe^{2+}_{aq} and S^{-2}_{aq} will, of course, react with water to form their equilibrium distributions of H_2S, HS^{-}, $FeOH^{+}$, etc.) If oxygen is present, an oxidative dissolution of the FeS_{mack} will result:

$$FeS_{mack} \xrightarrow{O_2} Fe(III) + S(0) + S(II) \quad (1.2)$$

+ other oxidation states of sulfur

The reactions involved in (1.1) and (1.2) are not well understood. Moreover, it is not clear what role, if any, the non-oxidative dissolution plays in (1.2).

The purpose of this research was to characterize the dissolution reaction (1.1) and to investigate the implications which the data obtained hold for the rates at which iron, trace metals, and sulfur are: 1) cycled in the environment under natural conditions; and 2) released to anoxic as well as oxic marine waters as a result of the ocean disposal of anaerobic sewage sludge.†

1.2 Formation of Metal Sulfides

The occurrence of the H_2S in natural waters and sewage sludge which leads to the precipitation of metal sulfides is usually the result of the microbiological respiration of biogenic organic matter by sulfate-reducing bacteria. Special conditions, however, are required before such sulfate reduction can begin.

In a non-sterile natural water system containing biodegradable organic compounds, the dissolved oxygen present will be consumed by

†The interest in this problem from the perspective of sewage sludge is easily understood when it is realized that currently, approximately 5, 7, 9, 95 and 120 metric tons per year of silver, cadmium, lead, copper and zinc, respectively, are being discharged into the waters off Southern California from the anaerobic sewage sludge outfall of the City of Los Angeles "Hyperion" facility.

aerobic microorganisms. Using the carbohydrate $C_6H_{12}O_6$ as a model compound, the overall reaction is

$$C_6H_{12}O_6 + 6\ O_2 \xrightarrow{\text{microorganisms}} 6\ CO_2 + 6\ H_2O \qquad (1.3)$$

In the presence of high levels of organics, if the oxygen is not replenished, its concentration will go to zero. The system is then described as being "anaerobic." (This occurs in the waters in certain sediments, as well as in anaerobic sewage sludge digesters.) The continued respiration of the remaining organic matter may occur via either fermentation,

$$C_6H_{12}O_6 \xrightarrow{\text{fermenting microorganisms}} 3\ CO_2 + 3\ CH_4 \qquad (1.4)$$

or through the use of whatever nitrate and sulfate is present as oxidants. In the case of sulfate we have

$$C_6H_{12}O_6 + 3\ SO_4^{=} \xrightarrow{\text{sulfate reducing bacteria}} 6\ HCO_3^- + 3\ H_2S \qquad (1.5)$$

Soon after the disappearance of the oxygen, CH_4 and H_2S production begins.

Once enough H_2S has formed to exceed the solubility product of the sulfide of a given metal present, that metal sulfide may be expected to precipitate. Based on a K_{so} of $10^{-17.5}$ for $FeS_{mack} \rightleftharpoons Fe^{2+} + S^{2-}$ (Berner, 1967), at a pH of 8 and temperature of 25°C, the total sulfide ($H_2S + HS^- + S^{2-}$) concentration required to initiate the precipitation of 10^{-5} M Fe^{2+} would be $\sim 5 \times 10^{-6}$ M.

1.3 Selection of Mackinawite as a Model Compound for Dissolution Experimentation

The sulfides of iron are the only sulfides which are easily recognized in marine and lake sediments. Consequently, they have been the subject of almost all the research concerning metal sulfides in natural systems. In particular, since iron can form a variety of sulfides (e.g., mackinawite, tetragonal FeS; pyrrhotite, hexagonal FeS; pyrite, cubic FeS_2; marcasite, orthorhombic FeS_2; and greigite, spinel Fe_3S_4), it has been of considerable interest to study the various conditions of their formation and intertransformations (Berner, 1964a; Berner, 1967; Rickard, 1969; Rickard, 1975). Of all these iron sulfides, mackinawite is probably of greatest interest to the natural water chemist.

Mackinawite has been characterized fairly recently (Evans, et al., 1964) and was first identified in recent sediments by Berner (1964a).† If not always the first, researchers in this area feel that it is one of the initial iron sulfides to form in iron-bearing sediments upon the onset of H_2S production, with greigite and pyrite being other possible early precipitates (Goldhaber and Kaplan, 1974). It has been shown (Berner, 1964a) that FeS_{mack} can form over a broad range of pH (4-9) and temperature (20-85°C) when iron reactants are exposed to

†Many workers in this field believe that mackinawite is non-stoichiometric (sulfur deficient) and can be represented by the formula FeS_{1-x} where $x \leq 0.05$ (Clark, 1966; Ward, 1970). This issue is by no means resolved (e.g., where in the tetragonal FeS lattice would such "excess" Fe atoms reside?), and for the sake of simplicity, in this thesis mackinawite will be assumed to be stoichiometric.

aqueous H_2S. Among such reactants are aqueous Fe^{2+}, steel and iron chips and even goethite (orthorhombic FeOOH). In the case of goethite, a portion of the H_2S reduces the Fe(III) forming Fe(II) and S(0). FeS_{mack} then precipitates. (Some FeS_{mack} goes on to react with the S(0) to form pyrite FeS_2. This latter reaction will be discussed later.)

As a result, mackinawite is a mineral phase of considerable importance regarding the geochemical cycling of sedimentary iron and sulfur. In addition, as is mentioned in Section 1.1, it is to be anticipated that it plays an important role in determining the behavior of sulfide forming trace metal constituents in anaerobic sediments as well as in anaerobic sewage sludge. This is due in large part to the fact that iron is typically present in much greater amounts than trace elements like cadmium, etc.[†] This predominance makes very likely the association of these sulfide-forming trace metals with the coexisting mackinawite. Such an association might manifest itself in three possible ways:

1. Adsorption of metal ion M^{z+} on FeS: $FeS\text{-}M^{z+}$
2. Solid solution of metal sulfide MS in FeS: (Fe,M)S
3. Non-solid solution aggregation of metal sulfides: ((MS)(FeS))

The third possibility would be favored by the availability of the FeS surface as a source of nucleation sites for the precipitation of other metal sulfides. In each of the above three cases, in the event that the

[†]By dry weight, mackinawite iron can sometimes comprise as much as 0.5% of anaerobic sediments (Berner, 1964b). Total iron in anaerobic sewage sludge (also by dry weight) has been found to be as high as $\sim$ 1% (Faisst, 1976).

FeS_{mack} dissolves, the rate of release to the solution phase of these other metals will be a strong function of the dissolution rate of the FeS_{mack}.

The fact that FeS_{mack} can be a precursor phase for pyrite (cubic FeS_2) adds further impetus for studying the kinetics of dissolution of this compound. Zero-valent sulfur, S(0), can combine (albeit slowly) with FeS_{mack} to form pyrite (Roberts et al., 1969; Berner, 1970; Sweeney and Kaplan, 1973):

$$FeS_{mack} + S(0) \rightarrow FeS_{2\ pyrite} \qquad (1.6)$$

The product FeS_2 has been observed to crystallize on the surface of the elemental sulfur (Berner, 1970). The non-oxidative dissolution of the FeS must therefore comprise a step in the mechanism of (1.6). Since pyrite is a common authigenic mineral in recent marine as well as lacustrine sediments (sometimes comprising as much as 1% by dry weight of marine sediments) (Berner, 1964b), a study of the non-oxidative dissolution kinetics of FeS_{mack} could be of considerable help in understanding the mechanism of sediment pyritization. Furthermore, because much of the sedimentary FeS_{mack} is ultimately converted to pyrite, if any trace metals associated with the FeS_{mack} are not incorporated into the pyrite, the rate of pyritization and therefore the FeS_{mack} non-oxidative dissolution rate may again determine the rate of release to pore waters of trace metal constituents.

The kinetics of the non-oxidative dissolution of FeS_{mack} therefore has a direct bearing on the rates of several environmentally important

phenomena. They are:

1. the non-oxidative release of Fe, trace metals, and S from sulfide phases in anoxic sediments and sewage;
2. the oxidative release of these species from the same system;
3. the pyritization of recent sediments.

The objectives of this thesis are to present the results of an experimental study of the rate of reaction (1.1) as well as to discuss the above phenomena in the light of the results obtained from this research.

CHAPTER 2

DISSOLUTION THEORY

2.1 Introduction

In the simplest case, two distinct steps may be visualized to occur during the dissolution of a solid compound:

1. the detachment from the crystal lattice of the ions or molecules which comprise the solid; and
2. the transport of these newborn solute species away from the dissolving crystal face.

In the event that some particular solute participates in the solubilization reaction, another step will be involved, namely the transport of this reactant to the crystal surface.

In the earliest "theoretical" treatments of dissolution, Noyes and Whitney (1897) and later Nernst (1904) assumed that the processes responsible for step (1) would always be fast enough to maintain solution saturation near the surface. Their hypothesis was therefore that dissolution rates in general will be controlled by step (2), the diffusion step. Additional assumptions made by Nernst were that: 1) in a well-stirred system, the concentration gradient of the dissolving species is restricted to a thin layer (of thickness δ) of solution which adheres to the dissolving surface; 2) increasing the intensity of the stirring will decrease δ; and 3) the concentration decreases linearly over this distance from the saturation value c_s to the bulk value, c (moles/cm^3). These assumptions allowed Nernst to express the diffusive flux, F (moles/cm^{2}sec) of material escaping from

the surface into solution as being

$$F = D \frac{(c_s - c)}{\delta} \tag{2.1}$$

The distance δ is referred to as the "Nernst diffusion layer thickness" (cm), and D is the solution diffusion coefficient of the dissolving material (cm^2/sec). For a solid of surface area A (cm^2) dissolving in a solvent system of volume V (cm^3) we have

$$\frac{dc}{dt} = \frac{AF}{V} = \frac{AD}{V\delta} (c_s - c) \tag{2.2}$$

Experiments carried out with stirred suspensions as well as rotating disks and cylinders of a variety of different substances such as alkali metal and alkaline earth halides, nitrates, and sulfates (e.g., Haussühl and Müller, 1972; Barton and Wilde, 1971) indicate that under the conditions employed by these researchers, the dissolution rates of such compounds seem indeed to be diffusion-controlled.† The rates exhibited the first order dependence on the subsaturation contained in equation (2.2), and an increase in stirring (decrease in δ) was always accompanied by an increase in the dissolution rate. The types of values of δ which may be extracted from such data are generally in the range 0.01 - 0.03mm (10-30μ).

†It is important to remember that experimental design will always play a very large role in determining whether or not any given heterogeneous process is diffusion-controlled. Thus, the fact that any dissolution process has been observed to be diffusion-controlled is really only a result of the inability of the mixing processes employed to prevent the development of concentration gradients near the solid surface.

As simplistic as this theory may seem, it continues to be invoked in the interpretation of a wide variety of dissolution phenomena. In many cases, particularly those involving ionic compounds of intermediate to high solubility, it is not surprising that diffusion controlled dissolution should tend to be observed. This may be understood in terms of Eyring's (1935) theory of chemical kinetics.

According to this theory, the rate at which a chemical reaction will proceed is proportional to the quantity $\exp(-\Delta G^{\ddagger}/RT)$. $\Delta G^{\ddagger}$ is the so-called "activation free energy" for the reaction, and is a measure of the free energy difference between the reactants and an unstable intermediate species called the "activated complex" (see Figure 2.1). This unstable species may be thought of as having properties intermediate between those of the reactants and the products, and as such, may decompose spontaneously into either the original reactant or the final product species. In a dissolution reaction then, the transition state probably involves a partially hydrated ion or pair of ions somewhere on the surface of the crystal lattice. In the case of a reasonably soluble ionic compound, since this solubility is due to the ability of the water molecules to successfully compete with the lattice for the constituent ions, the activated complex will be stabilized considerably by the strong ion-solvent interactions. The result is that $\Delta G^{\ddagger}$ will tend to be small and the solubilization rate will tend to be large. One may conclude, therefore, that unless extremely efficient mixing is provided, the dissolution rate of a fairly soluble ionic compound is <u>likely</u> to be diffusion controlled. With relatively insoluble compounds

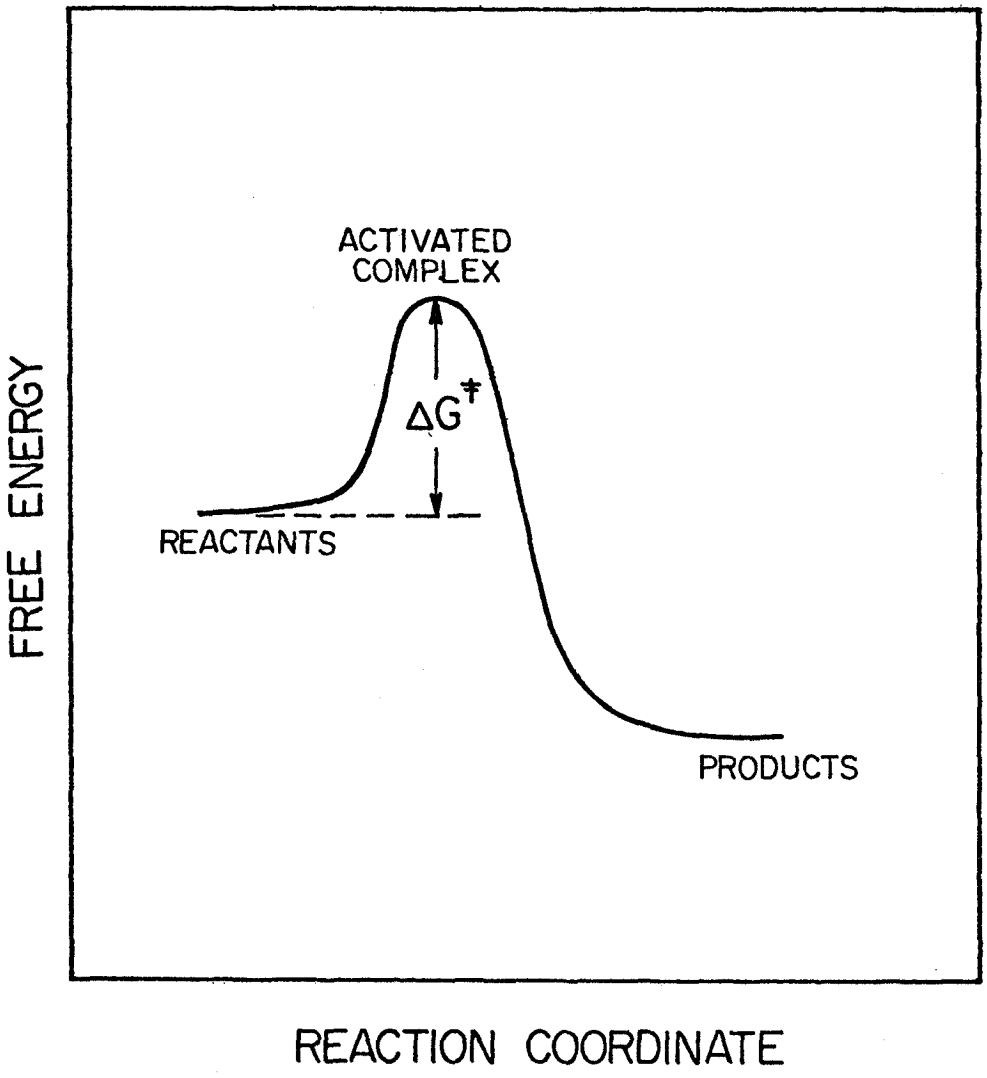

Figure 2.1 The energy barrier for a system of reactants and products.

(e.g., $BaSO_4$, FeS, etc.) on the other hand, $\Delta G^{\ddagger}$ will probably be considerably greater since this greater lattice stability must be overcome before the dissolution transition state can be formed. As a result, the dissolution rates of such compounds are less likely to be diffusion-controlled and the rates of surface reactions (step (2) above) may begin to play a role in determining the overall dissolution rate. (Although they are useful as guidelines, caution should nevertheless be exercised in the application of these generalities since there is always an element of danger present when trying to extract kinetic information from thermodynamic properties.)

Although not extensively investigated, some attention has been given to the study of the dissolution rates of stirred suspensions of sparingly soluble salts such as $BaSO_4$, $PbSO_4$ (Bovington and Jones, 1976, 1970) and $SrSO_4$ (Campbell and Nancollas, 1969). They have been found to be adequately described by a power law rate equation of the form

$$F = k(c_s - c)^2 \qquad (2.3)$$

where k has units of $moles^{-1}cm^4sec^{-1}$. Despite the fact that very low energies of activation E_a[†] (2-6 kcal/mole) have been observed for the dissolution rates of these compounds, on the basis of the quadratic form of the rate law, the above authors suggest that the dissolution rates of stirred suspensions of these compounds are not film diffusion controlled. The quadratic dependence on the relative subsaturation is

---

[†] E_a is closely related to $\Delta G^{\ddagger}$.

attributed to a slow removal from the lattice and subsequent hydration of a pair of oppositely charged ions.

Both of the above dissolution models are rather phenomenological in nature, and treat the dissolving solid as if it was devoid of any rate-affecting microstructure. In the first, diffusion-limited case (equation 2.1), the surface is simply viewed as a material source. In the second case, although some special conditions might be required before a given ion-pair on the surface of these 2-2 electrolytes is released to the aqueous phase, no conjectures have been forwarded as to what those conditions might be.

A more atomistic, albeit somewhat qualitative, approach to the study of the dissolution of crystalline materials has been advanced by Cabrera and Vermilyea (1958) and Ives and co-workers (Ives, 1965; Ives, 1963; Ives and Hirth, 1960). In this treatment, a model of the surface first proposed by Kossel (1927) is adopted. According to this model, crystalline surfaces are thought to be composed of "facets" (i.e., planes) of low index (e.g. [100]) which are separated by ledges of monomolecular height. These ledges in turn are not completely straight, but by virtue of the presence or absence of the crystal's basic molecular or ionic constituents, possess within them a certain concentration of "kink sites" which are denoted by "k" in Figure 2.2. The presence of steps on a low index crystal surface may, in general, be due to either: 1) the partial dissolution of the surface; or 2) the presence of crystal imperfections such as screw dislocations (Frank, 1949; Burton, Cabrera and Frank, 1951). The concentration of kink sites on

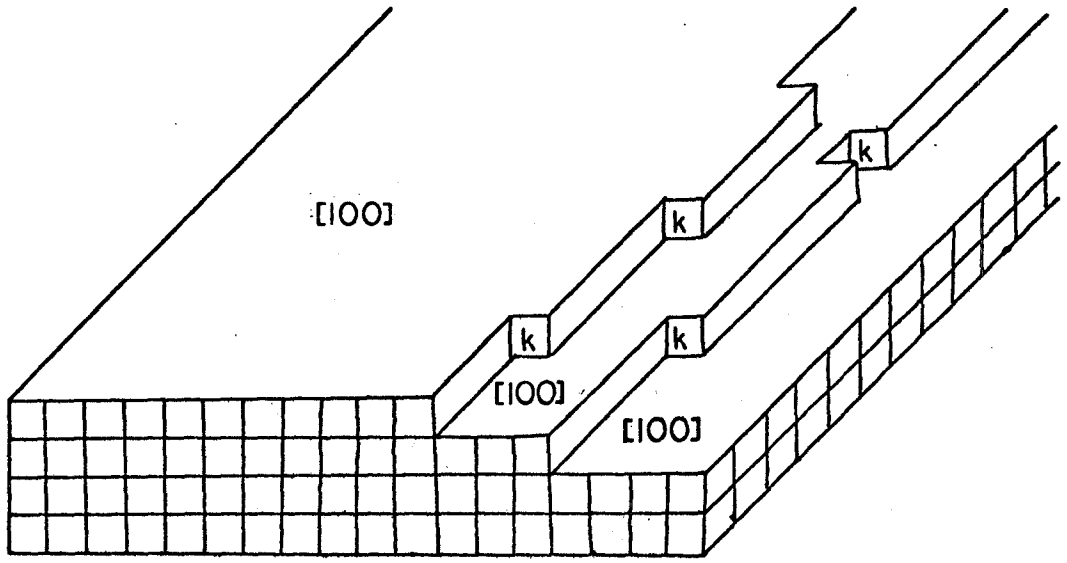

Figure 2.2. Model of a crystal surface according to Kossel (1927)

a given step will be determined by statistical-thermal fluctuations (Burton, Cabrera and Frank, 1951).

If a crystal dissolves, the constituent species will tend to be removed preferentially from the kink positions since there the bonding to the crystal lattice is weakest and the exposure to the solution the greatest. When such a kink constituent is removed, a new kink is formed. Thus, these kinks transverse the ledge until the ledge is completely removed from the surface. In addition to being sites for the preferential loss of constituent ions, these kinks are also sites for preferential adsorption from solution of these same ions (viz., crystal growth) as well as other dissolved species since they present several (three, for hexacoordinated solids) "bonding" positions to the adsorbate. (The attachment of such a species to the flat surface on the other hand would only provide one such "bonding" interaction.) In the event that some foreign species is very strongly adsorbed at some kink site, that kink may be immobilized (i.e., "poisoned"), thereby delaying the removal of that ledge from the crystal until a new kink site can be formed within the ledge through the removal of one of the ions composing that ledge.

Although some progress has been made in the mathematical modeling of kink site/ledge kinematics as regards crystal <u>growth</u> (Burton, Cabrera and Frank, 1951) very little has been done to develop these concepts into an integrated model of dissolution. There has, however, been considerable interest in recent years in what is attributed to be the action of kink poisons in decelerating crystal dissolution rates

(Berner and Morse, 1974; Cabrera and Vermilyea, 1958; Galilly and Friedlander, 1965; Ives, 1965; Morse, 1974; Nestaas and Terjesen, 1968, 1969). Considering the much greater insolubility of metal sulfides such as CuS ($K_{so} \simeq 10^{-35}$) relative to FeS_{mack} ($K_{so} \simeq 10^{-17.5}$), a priori it seems very possible that when present, ions such as Cu^{2+} could act as kink poisons during the dissolution of FeS. Since Cu^{2+} and other metal sulfide forming ions are present in sewage sludge and may be present in sediments, the mechanisms by which kink poisons inhibit dissolution are of considerable interest in this thesis.

One of the most quantitative treatments of the inhibitory affects of kink poisons on dissolution rates has been produced by Berner and Morse (1974) in their study of the dissolution of calcite (hexagonal $CaCO_3$) in the presence of orthophosphate (PO_4^{3-}) ion. In this study they make use of a hypothesis advanced by Cabrera and Vermilyea (1958) regarding the rates of dissolution in the presence of kink poisons. This treatment assumes that on the average, inhibitor species will remain at kink sites for times longer than are required to form new kink sites somewhere along the ledge. Thus, the dissolution of a "poisoned ledge" may continue, but only through the formation of "embayments" of radius r on the ledge (see Figure 2.3a). (The average value of r will depend upon the density of absorbed inhibitor species, an estimate of which may be obtained experimentally.) For small values of r, these embayments have considerable curvature, and as such, have a high edge free energy. In other words, a high percentage of the energy price paid to form the embayment was required for the disruption

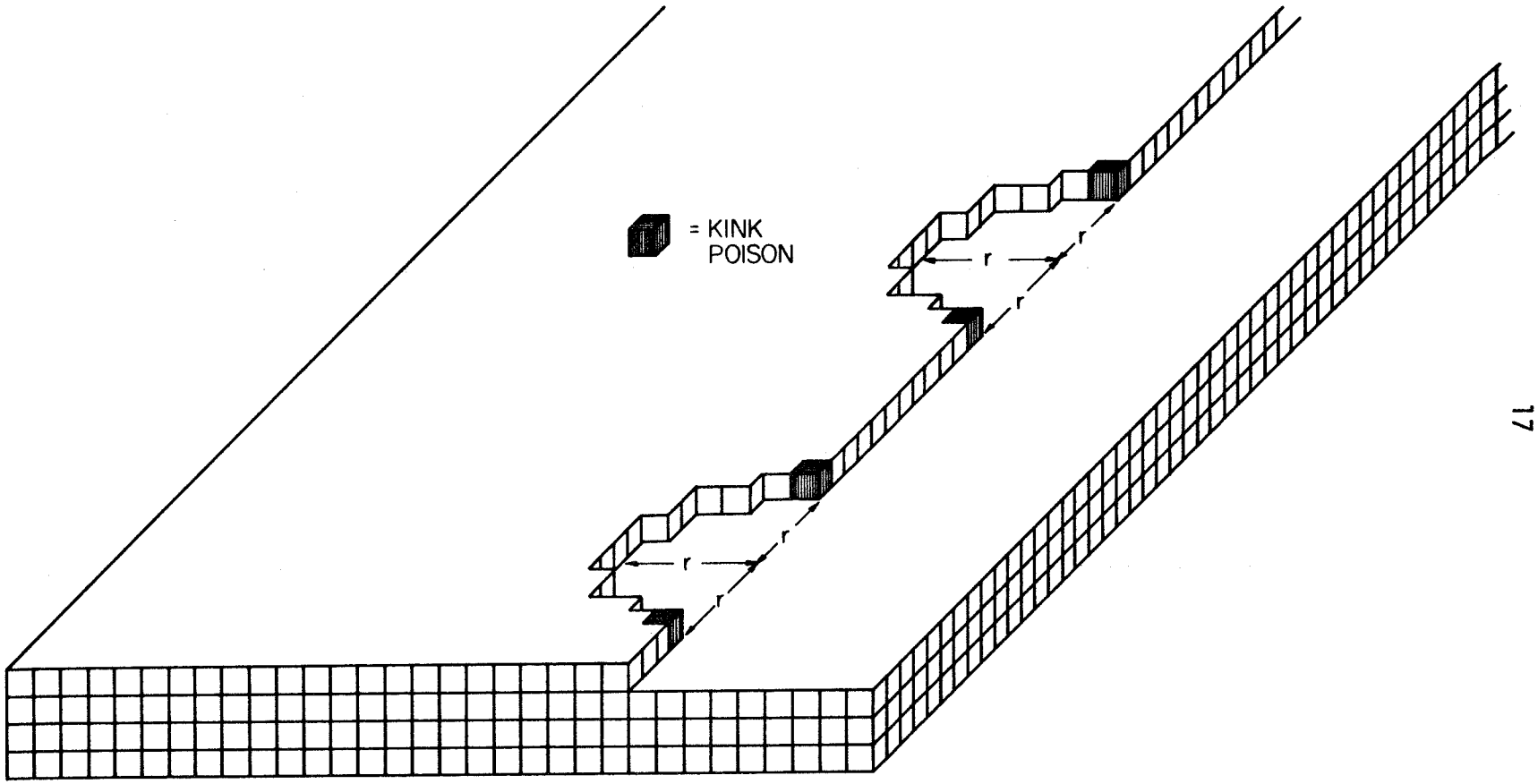

Figure 2.3a The dissolution of a poisoned ledge continuing through the formation of embayments. The radius of smallest stable hole, termed the critical radius, is dependent upon the degree of undersaturation.

of the edge bonds (see Figure 2.3b). Embayments (or equivalently, holes) of small radius make such efficient solute traps that they tend to be filled up even though the overall system may be slightly undersaturated. This hole is the negative analogue of a surface nucleus (aggregate) of monomolecular height and radius r. The critical (i.e., minimum) value for the radius, r_c, which would imply stability for such surface nuclei or holes is given by classical nucleation theory to be (Burton, Cabrera and Frank, 1951):

$$r_c = \frac{\sigma}{a\,k\,T\,\ln\Omega} \tag{2.4}$$

where r_c = radius of critical (circular) nucleus or hole (cm)
σ = edge free energy (ergs/cm)
a = area density of lattice constituents (number/cm^2)
T = temperature (°K)
k = Boltzmann's constant (ergs/°K)
Ω = IAP/K_{so} for surface nucleus formation (viz. crystal growth)
Ω = K_{so}/IAP for hole formation (viz. dissolution)
IAP = ion activity product

If the solution is supersaturated (IAP/K_{so} > 1), r_c refers to the radius of the smallest stable surface nucleus. Nuclei with radii smaller than r_c will redissolve and those larger than r_c will continue to grow. Similarly, if the solution is undersaturated (K_{so}/IAP > 1), r_c refers to the radius of the smallest stable hole. Holes of radius larger than r_c will continue to grow while those smaller will be filled.

If the average distance between poisoned kinks on a given ledge is less than the diameter of the critical hole, this theory implies that

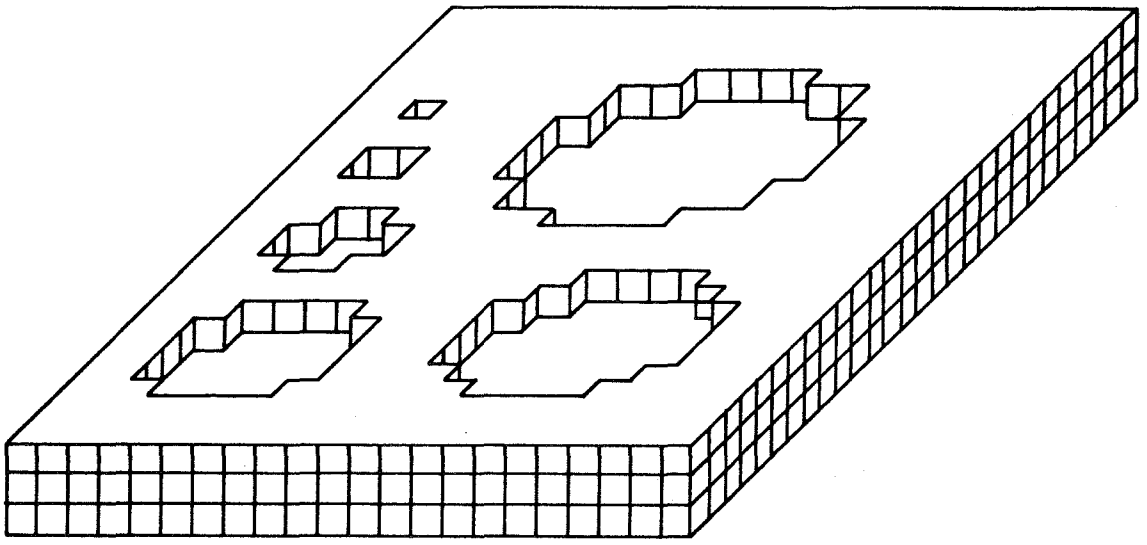

Figure 2.3b Several holes of varying radius r are illustrated for a hexacoordinated solid. The values of r range from 0.5a to 5a where a is the approximate diameter of the lattice constituents. Inside the crystal, each constituent has six "bonds" to its six nearest neighbors. The number of edge bonds which must be broken to form the six holes illustrated above are, from the smallest to the largest, 4, 8, 16, 24, 32, and 40. The total number of bonds which must be broken are 5, 16, 44, 108, 172, and 260, respectively. In order to form these holes, 1, 4, 12, 32, 52, and 80 lattice constituents, respectively, must be removed from the surface. Per lattice constituent then, on the average, 5, 4, 3.7, 3.4, 3.3, and 3.2 bonds, respectively, must be broken during hole formation. Since the thermodynamically-predicted solubility is based upon the disruption of three bonds per lattice constituent, relatively high under - saturations will be required to stabilize the smaller holes.

any embayments which may manage to form between the poisoned kinks will not be stable and will be refilled. The dissolution process will not be completely halted, however, since the kink poisons are not forever bound to a certain kink, but may occasionally diffuse away either on the crystal surface or into the bulk solution. Dissolution may then continue in that portion of the ledge, but will be terminated once again when the newly-formed kinks become poisoned.

The research efforts which have been mentioned and in some cases briefly abstracted in this chapter together provide a good overview of the present understanding of the kinetics of dissolution processes. As is apparent from the above discussion, this understanding is neither very deep, nor quantitative in nature. Such deficiencies are the result of the hesitancy of scientists to study these complicated phenomena as well as the considerable difficulties encountered by those who have tried to understand the dynamics of dissolution processes. The discussions of the results of the FeS dissolution experiments carried out in this thesis research will draw upon the concepts presented in this chapter and hopefully add, in some measure, to the understanding of dissolution processes.

CHAPTER 3

MACKINAWITE SYNTHESIS AND CHARACTERIZATION

3.1 Introduction

At the outset of this research, there was the option of using either natural or synthetic FeS_{mack}. There is some basis to the argument that the results of a laboratory study of naturally-occurring FeS_{mack} might be more easily extrapolatable to real world situations. However, the facts that

1. authigenic FeS_{mack} is rarely present in recent sediments at levels higher than 1% (Berner, 1964b)

and

2. the FeS_{mack} which is present in such sediments is inextricably associated with other sulfides as well as sedimentary detritus

left no other alternative than to synthesize the required FeS_{mack} in the laboratory.

3.1.1 Homogeneous Precipitation of FeS_{mack}

The combination of a solution of ferrous iron with either aqueous H_2S or aqueous sulfide salt is perhaps the easiest way to prepare large amounts of FeS[†] with a minimum of effort in a short period of time. Due to the tremendous supersaturations encountered in such a procedure, however, the resulting precipitate is extremely fine-grained (with particle sizes of ~ 50Å and corresponding molar surface areas S of $\sim 10^4$ m^2/mole) and in the presence of sufficiently low

[†]In this, as well as subsequent chapters, the notation "FeS" may be taken to refer to mackinawite. "FeS_{mack}" will be reserved for those occasions when it is to be emphasized that mackinawite is the form of FeS being discussed.

background electrolyte (I ~ 0.01) can form a stable colloid. X-ray analysis of such FeS shortly after formation reveals a barely discernable mackinawite spectrum (Berner, 1964a; Berner, 1967; Rickard, 1969). Aging the suspension at room and elevated temperatures increases the crystallinity as evidenced by the narrowing and intensifying of the X-ray diffraction peaks (Berner, 1964a).

In principle, the solubility of any compound depends upon the sizes of its constituent particles. This phenomenon, commonly known as the Kelvin effect, is treated in detail elsewhere (Stumm and Morgan, 1970) and becomes noticeable only for very highly-divided materials with large values of $\mathcal{S}$. The equation of interest here is

$$\log K_{so_{(\mathcal{S} = \mathcal{S}')}} = \log K_{so_{(\mathcal{S} = 0)}} + \frac{\frac{2}{3} \gamma \mathcal{S}'}{2.3\ RT} \qquad (3.1)$$

where $K_{so_{(\mathcal{S} = \mathcal{S}')}}$ and $K_{so_{(\mathcal{S} = 0)}}$ are the solubility products for the compound with $\mathcal{S}$ values of $\mathcal{S}'$ and essentially zero, respectively. γ represents the surface tension of the solid-liquid interface. R and T have their usual meanings. Although no measurements of γ have been made for the FeS-H_2O interface, the values of γ (T=25°C) for similar systems ($Cu(OH)_2$, CuO-H_2O) are in the range 400-800 ergs/cm^2 (Schindler et al., 1965). At 25°C and with $\gamma \cong 400$ ergs/cm^2, if $\mathcal{S} = 10^4$ m^2/mole, the theoretical effect on log K_{so} is approximately 0.5.

Since the thermodynamic behavior of a compound is therefore a function of $\mathcal{S}$, it seems probable that its dissolution kinetics may also exhibit a similar dependency. Due to its highly divided nature, freshly

precipitated FeS was consequently not considered an attractive form of FeS with which to conduct this research. The preparation and consistent use, however, of FeS of low $\mathcal{S}$ would eliminate this potential problem.

If larger and more well-defined crystals of FeS are desired, and if they are to be precipitated directly from a homogeneous solution,[†] it is clear that the supersaturations encountered during the reaction must be reduced. It was felt that such a reduction could be realized by tying up the Fe^{2+} with an organic chelate so that the rate of FeS formation would be limited by the rate of the Fe^{2+}-ligand decomposition kinetics.[‡] It was hoped that further reductions could be achieved by also limiting the rate at which the $H_2S_{(g)}$ was allowed to enter the aqueous phase.

Precipitation procedures which employed both of these ideas were tested. In the first case, ligands (EDTA, Citrate) were added to the aqueous Fe^{2+} solution in slight excess of the Fe^{2+} present. $H_2S_{(g)}$ was then bubbled directly into the solution. In the second case, the rate of addition of the H_2S to the Fe^{2+}/ligand solution was kept at a low

---

[†]The use of thermal aging to ripen the "amorphous" FeS was not considered since it was felt that material so produced could not be prepared in a reproducible manner.

[‡]A method which employs thioacetamide as the S(-II) source (via its acid or base catalyzed thermal decomposition) was not used since other workers (Framson and Leckie, 1978; Flaschka, 1955) had difficulty in preparing pure FeS by this method. Contamination with small amounts of ferrous hydroxide was a major problem (Framson and Leckie, 1978).

level by either just touching the $H_2S_{(g)}$ bubbler to the solution or by raising the bubbler completely out of the solution.

3.1.2 Heterogeneous Synthesis of FeS_{mack}

Berner (1964a) noted in his early work on iron sulfides that mackinawite is the form of FeS which results upon the corrosion of elemental iron with aqueous H_2S:

$$Fe + H_2S \xrightarrow{H_2O} FeS_{mack} + H_{2(g)} \qquad (3.2)$$

Furthermore, the FeS_{mack} so obtained was observed by him to have a very well-defined X-ray diffraction pattern. This indicates that the FeS formation processes involved in reaction (3.2) are much slower than those typical of the simple reaction of aqueous Fe^{2+} with H_2S, allowing relatively large (~ 1μ) crystals of FeS_{mack} to form. An added dividend of using this reaction in a synthesis procedure is that the FeS need not be washed free of dissolved salts. The FeS must merely be separated from the residual Fe. Drying will then remove the H_2O and the residual (volatile) H_2S. Since this synthesis method seemed to be an easy avenue to FeS_{mack} with a relatively small S value, experiments of this type were carried out with an eye toward the large (gram) quantity preparation of low-S FeS_{mack}.

3.2 Experimental Methods and Materials

3.2.1 General Information

Unless otherwise stated, all chemicals employed in this study were of A.C.S. reagent grade and were used without further purification.

Prior to use, all glassware was washed in a hot solution of a detergent containing sulfonated organics and polyols (PEX Laboratory Detergent, Peck's Products, St. Louis, MO) rinsed first with tap deionized water, then 4 M HNO_3, and finally with distilled-deionized water. In the case of the heterogeneous synthesis apparatus, soaking in hot 6 M HNO_3 was substituted for the 4 M HNO_3 rinse.

3.2.2 Apparatus, Procedures, Product Characterization: Homogeneous Precipitation

Synthesis.

All homogeneous precipitations were carried out in the apparatus shown in Figure 3.1. If an organic chelate was to be used in a given precipitation, it was added as a salt to vessel 6 along with the solution to be used as the aqueous phase. The resulting solution was thoroughly de-oxygenated (at least 5 hrs.) with oxygen-free nitrogen (less than 0.5 ppm O_2) obtained from Linde Corp. (Torrance, CA). The "course" which the N_2 followed during this de-oxygenation was $1 \rightarrow 3 \rightarrow 4 \rightarrow 6 \rightarrow 7 \rightarrow 8$. The Fe(II) was then added (either as $FeCl_2 \cdot 4H_2O$ or as $Fe(NH_4)_2(SO_4)_2 \cdot 6H_2O$). Extreme caution was used during this step to prevent the entry of atmospheric oxygen to the separatory funnel.

After further deoxygenation, gaseous H_2S was passed through $2 \rightarrow 3 \rightarrow 4 \rightarrow 5$ for 1 hour. (If the H_2S was to be merely passed over the reactant solution, the bubbler was pulled up above the solution level at this time.) H_2S was then allowed to enter vessel 6, following the course $2 \rightarrow 3 \rightarrow 4 \rightarrow 6 \rightarrow 7 \rightarrow 8$. The NaOH trap was included so as to reduce the quantity of H_2S vented to the fume hood.

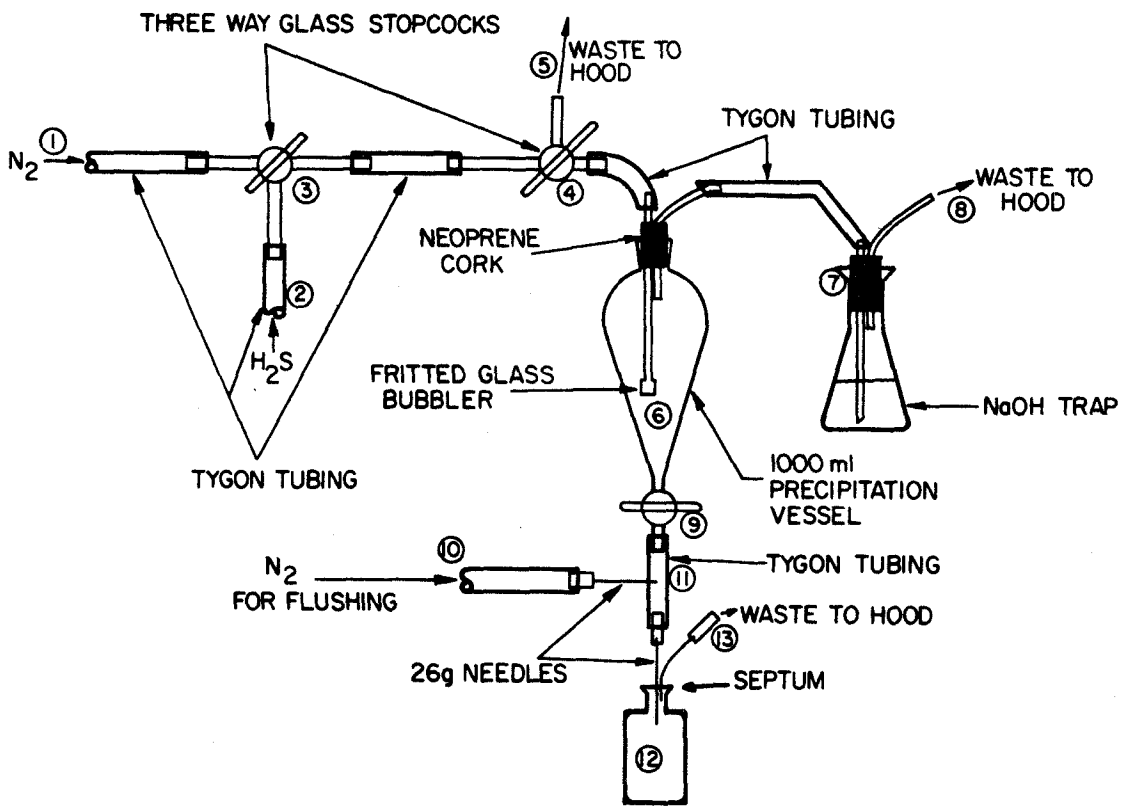

Figure 3.1. Homogeneous synthesis apparatus

When it was felt that all of the Fe(II) had been converted to FeS, the suspended FeS was allowed to settle and was then transferred (along with a minimum of reactant solution) through a 26 gauge stainless steel needle to a 250 ml polyethylene bottle which had been fitted with a septum and thoroughly purged of O_2 with N_2 (10 → 11 → 12 → 13). This suspension was centrifuged at 2500 rpm and the supernatant was removed through a needle while passing in N_2 with a second needle. Using two 100 ml portions of de-oxygenated distilled water and the septum transfer techniques, the FeS was resuspended (i.e., washed) and centrifuged. After removing the second aliquot of wash water, the polyethylene container was placed in a vacuum desiccator and the FeS dried and stored under vacuum.

X-Ray Analysis.

Since the FeS seemed to be quite air-stable when dry, no special care was taken to prevent atmospheric oxygen from coming into contact with the small portion of FeS allotted for X-ray study. Using acetone, a slurry of FeS was made and transferred to a special powder specimen cup from which the acetone was allowed to volatilize. Special care was taken to ensure that the surface of the FeS was flush with that of the cup. The specimen cup was then mounted in the goniometer of a Type 12045 Norelco X-ray diffractometer fitted with a Hamner model NB-19 detector. Using source and detector slit-widths of 1° and 1°/.006", respectively, the X-ray diffraction scan was carried out using Ni-filtered Cu Kα radiation at a rate of 1° of 2θ per minute.

3.2.3 Apparatus, Procedures, Product Characterization: Heterogeneous Synthesis

Synthesis.

A diagram of the special apparatus developed for the heterogeneous synthesis of FeS is presented in Figure 3.2. It was constructed of Pyrex and all stopcocks used were of hi-vacuum quality.

The distilled water which was to mediate the reaction was deoxygenated by bubbling it for 24 hours with O_2-free (< 0.5 ppm O_2) N_2 (1→2→3). Simultaneously, the regions 5 → 9 → 4 → 2 → 3 and 5 → 9 → 4 → 6 → 8 were purged of O_2 by the 24 hour passage of O_2-free N_2. The deoxygenated H_2O was then dropped into the reactor 10, which already contained the iron flakes (Gallard-Schlesinger Chemical Corp., Carle Place, NY). The $H_2S_{(g)}$ flow was then initiated (7 → 6 → 4 → 9 → 10 → 11).

The surfaces of the iron chips became black (FeS) after about 20 minutes. After 3-4 hours, the slow evolution of $H_{2(g)}$ was visible on the surfaces of the flakes. Because of the slowness of this reaction, the synthesis was usually allowed to proceed for approximately one month, after which time most of the iron remained, but a fair amount (1-2 g) of FeS had also collected on the bottom of vessel 10.

Once the FeS had been formed, the lower section of the apparatus 13 - 15 - 17 was evacuated using a 1 μm Hg rated vacuum pump. By increasing the $H_2S_{(g)}$ flow to the reactor 10, oxygen was prevented from entering the system when stopcock 13 was slowly opened to allow the FeS suspension to flow down through stopcock 15 and into vessel 17. After stopcock 15 was closed, the joint between cocks 13 and 15 was

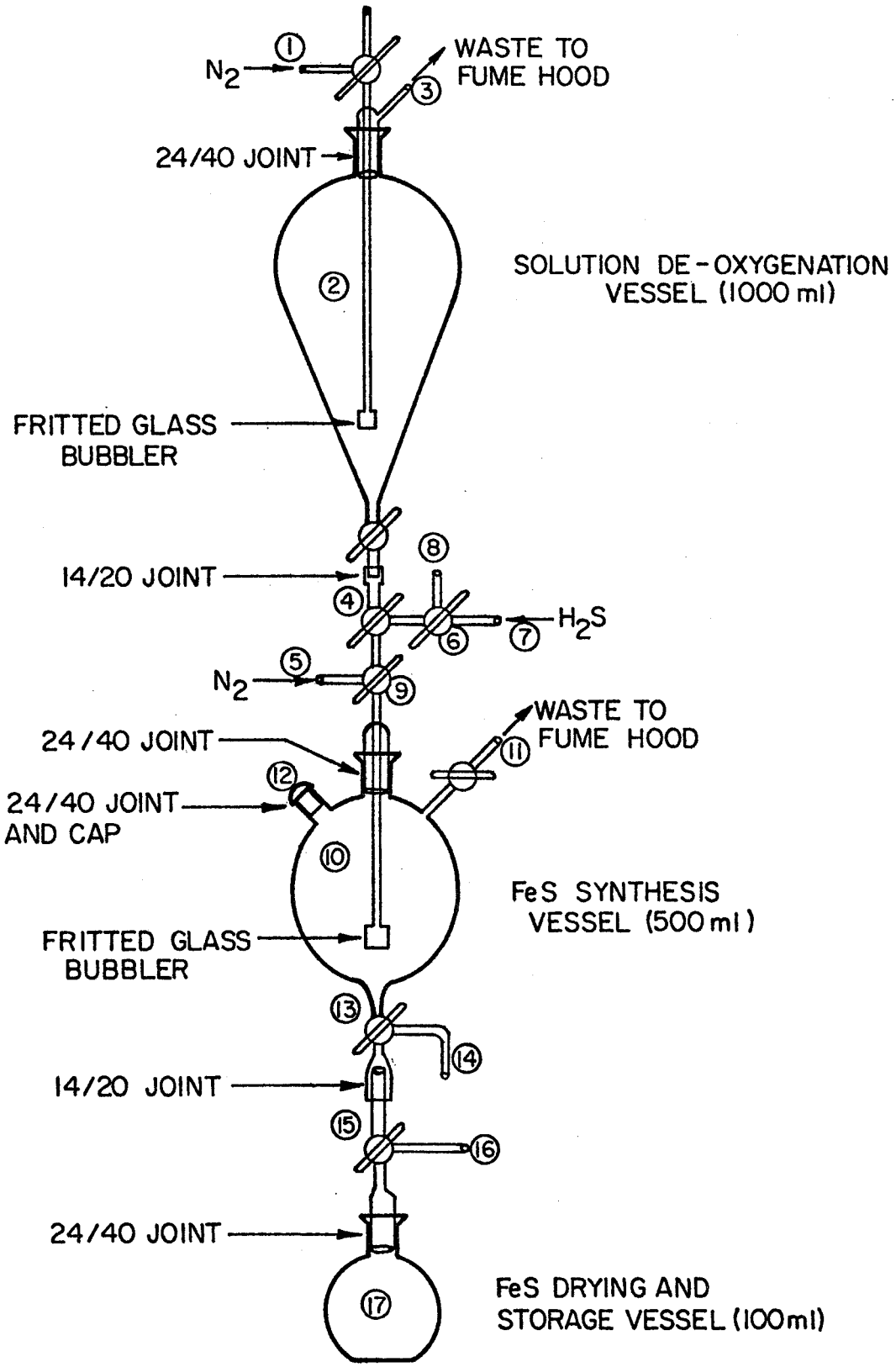

Figure 3.2. Heterogeneous synthesis apparatus

separated, and the suspension was frozen by placing flask 17 in NaCl-saturated ice water. When the FeS suspension had been completely frozen, it was dried by evacuating flask 17 through point 16.

X-ray, Electron Microscope, and Chemical Analysis.

The X-ray analyses were carried out exactly as was described for the FeS prepared by homogeneous precipitation.

The sulfur analyses were conducted by Galbraith Laboratories (Knoxville, TN) on samples of FeS shipped to them under N_2 atmosphere. Iron analyses were carried out according to the following procedure. Small amounts (~.01 g) of FeS were weighed into acid washed 50 ml beakers and covered with watch glasses. 30 ml of distilled water was added to each replicate, followed by 3 ml of 4 N HNO_3 (slowly to prevent loss of sample due to H_2S effervescence). The beakers (with watch glasses) were then heated at 100°C for 2 hours. The resulting solution was usually a clear yellow, but small amounts of elemental sulfur sometimes remained on the bottoms of the beakers. The addition of 7 ml of redistilled conc. HNO_3 and 2 ml of 30% of H_2O_2 and subsequent 1 hour heating at 100°C solubilized this material. This was followed by dilution to an appropriate concentration range and analysis using a Varian (Palo Alto, CA) AA-5 atomic absorption spectrophotometer.

Transmission Electron Microscope Studies.

The direct examination of these FeS_{mack} crystals was made possible through the use of a Siemens (Iselin, NJ) Elmscop 1A 100 kV transmission electron microscope. Formvar electron microscope (e.m.)

substrate was cast on water, and then picked up on conventional e.m. copper grids. Small amounts of the freeze-dried FeS_{mack} were placed on the grids by air-blasting. Photographs of typical crystals were then taken.

3.3 Results

3.3.1 Homogeneous FeS_{mack} Precipitation: Product Characterization

Table 3.1 summarizes the conditions of synthesis and the resulting crystallite sizes[†] of a number of different batches of FeS_{mack}. Consistent with the results of earlier research (Berner, 1964a; Berner, 1967; Rickard, 1969), the product of the direct reaction of Fe(II) with H_2S (Batch 1) was practically X-ray amorphous (see Figure 3.3). The use of EDTA in Batch 2 completely prevented the precipitation of any FeS. This was a surprise. Based on Berner's (1967) solubility product for FeS_{mack} ($10^{-17.5}$ for $FeS \rightleftharpoons Fe^{2+} + S^{2-}$), at a P_{H_2S} of 1 atm, FeS_{mack} should have precipitated.

In contrast, when citrate was the complexing ligand, FeS_{mack} began to form shortly (1-2 minutes) after the initial addition of H_2S (Batches 3-5). (Small amounts of EDTA were also included in Batches 3-5 to complex any contaminating Fe(III) and thereby prevent it from oxidizing the S(-II).)

[†]These were estimated using the well-known Scherrer equation (Cullity, 1956) which relates the broadening of X-ray diffraction peaks to crystallite size.

Table 3.1 Summary of homogeneous precipitation experiments

Batch	Reaction solution composition	Position of H_2S bubbler	Estimated crystal size
1	.05 M $Fe(NH_4)_2(SO_4)_2 \cdot 6H_2O$	in solution	too small to estimate
2	.05 M $Fe(NH_4)_2(SO_4)_2 \cdot 6H_2O$ .051 M Na_4EDTA	in solution	no FeS obtained
3	.05 M $Fe(NH_4)_2 \cdot 4H_2O$, .015 M Na_3 citrate, .0075 M Na_2EDTA	in solution	200 Å
4	.05 M $FeCl_2 \cdot 4H_2O$, .015 M Na_3 citrate, .0075 M Na_2EDTA	just touching solution	200 Å
5	.05 M $FeCl_2 \cdot 4H_2O$, .015 M Na_3 citrate, .0075 M Na_2EDTA	out of solution	250 Å

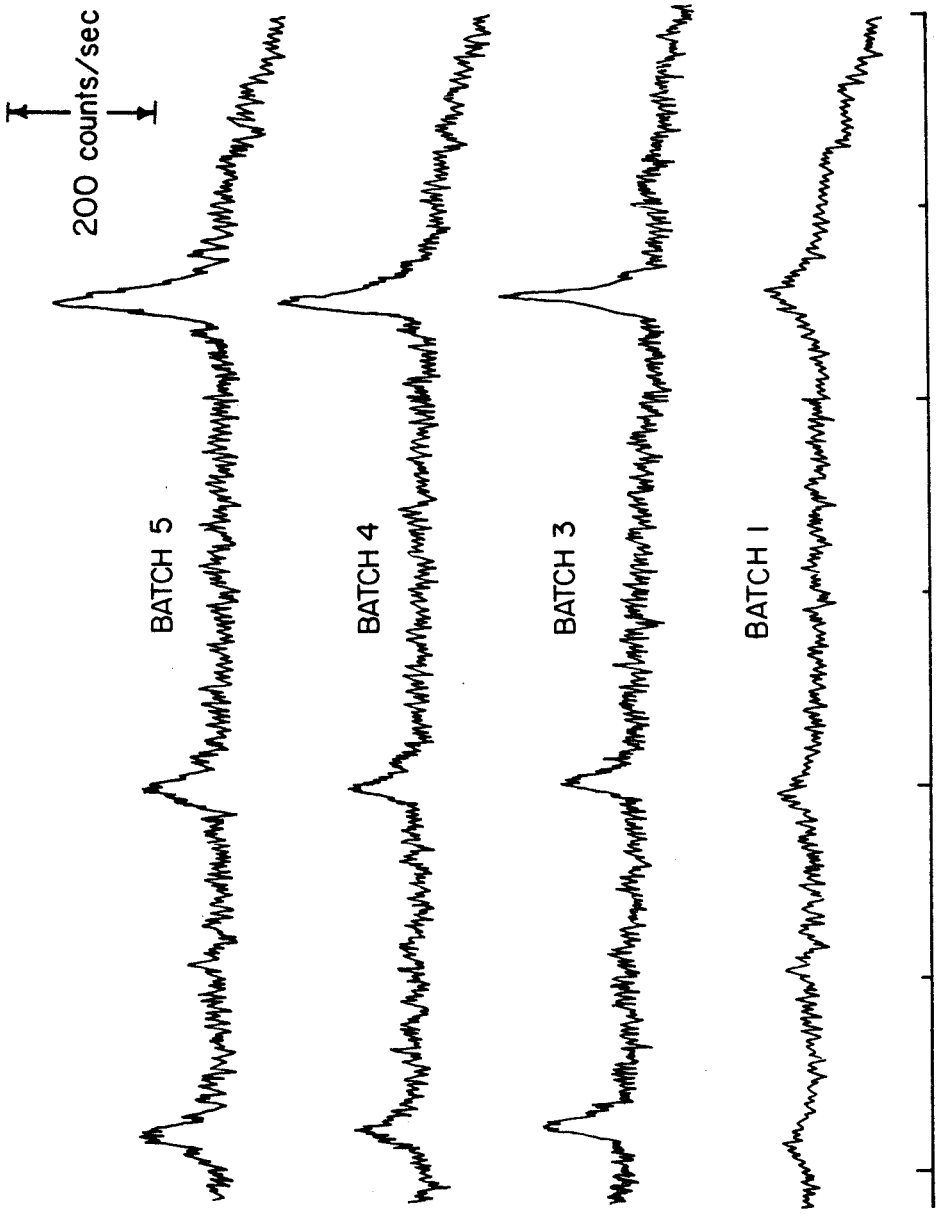

Figure 3.3. X-ray diffraction patterns from homogeneously precipitated FeS_{mack}

The increased crystallinity of Batches 3-5 over that of Batch 1 is clearly evidenced by the considerable narrowing and intensification of the X-ray diffraction peaks. Batch 5 contained the largest crystals ($\sim$ 250 Å) obtained using homogeneous precipitation techniques. If the shape of the crystals is taken to be approximately cubic and 250 Å is the face-width of such cubes, the molar surface area for such particulate FeS would be $\sim$ 4000 m^2/mole. According to equation (3.1), at 25°C and $\gamma \simeq 400$ ergs/m^2, the effects on log K_{so} is $\sim$0.18. In other words, K_{so} is increased by 50%.

3.3.2 Heterogeneous FeS_{mack} Synthesis: Product Characterization

Table 3.2 summarizes the conditions of synthesis and the characteristics of the various batches prepared using the heterogeneous synthesis techniques. Figure 3.4 presents the X-ray diffraction pattern obtained from the FeS synthesized using elemental iron as the Fe source. The very intense, narrow peaks indicate that this material is quite crystalline. The extent of the broadening of the diffraction peaks observed for this sample would imply a crystallite size of approximately 400 Å. The direct examination of these crystals (Figures 3.5-3.6) by electron microscopy, however, revealed that the sizes of the crystallites comprising this material ($\sim 10^3$ - 10^4 Å) are considerably larger than 400 Å.[†] For 1000 Å FeS and γ = 400 ergs/cm^2, the effect on K_{so} would be approximately 12%.

[†]This discrepancy is attributed to the breakdown of the assumptions upon which the Scherrer equation is based.

Table 3.2 Summary of FeS syntheses by heterogeneous methods

Batch	Reaction solution composition	Position of H_2S bubbler	Estimated particle size
6	H_2O/Fe chips	in solution	1μ
7	H_2O/Fe chips	in solution	1μ

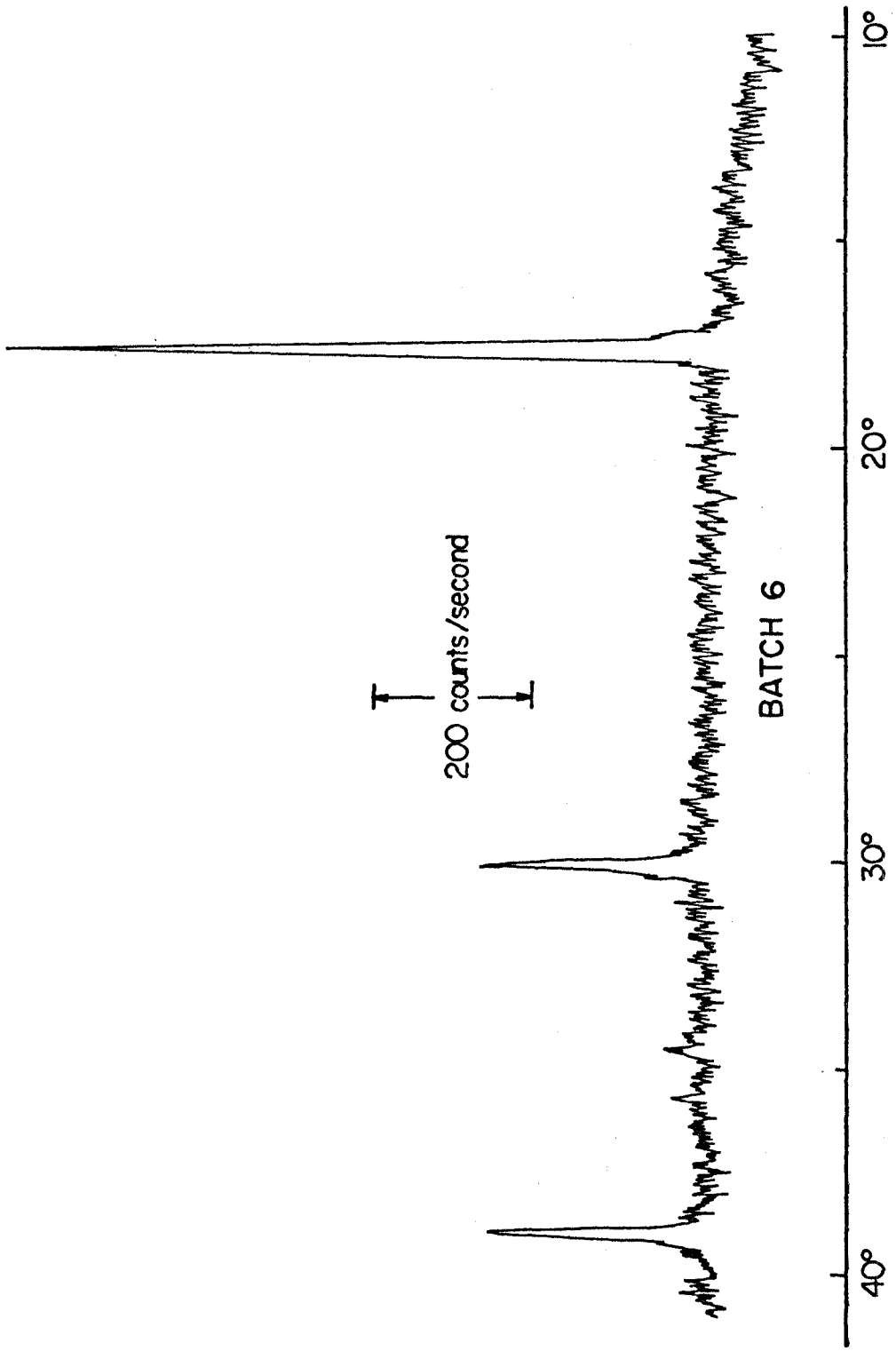

Figure 3.4. X-ray diffraction pattern of FeS_{mack} heterogeneously synthesized using elemental Fe

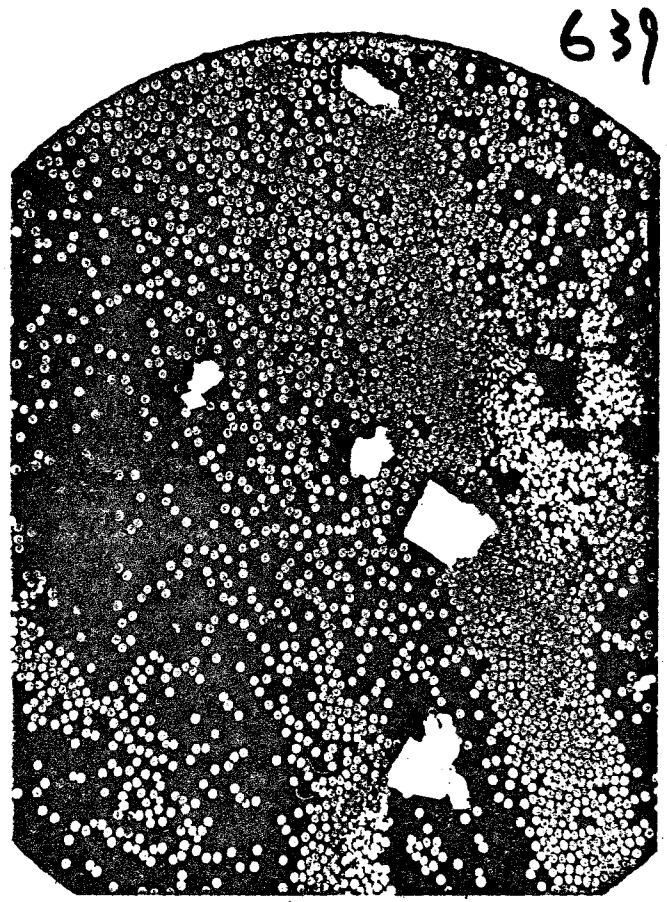

Figure 3.5

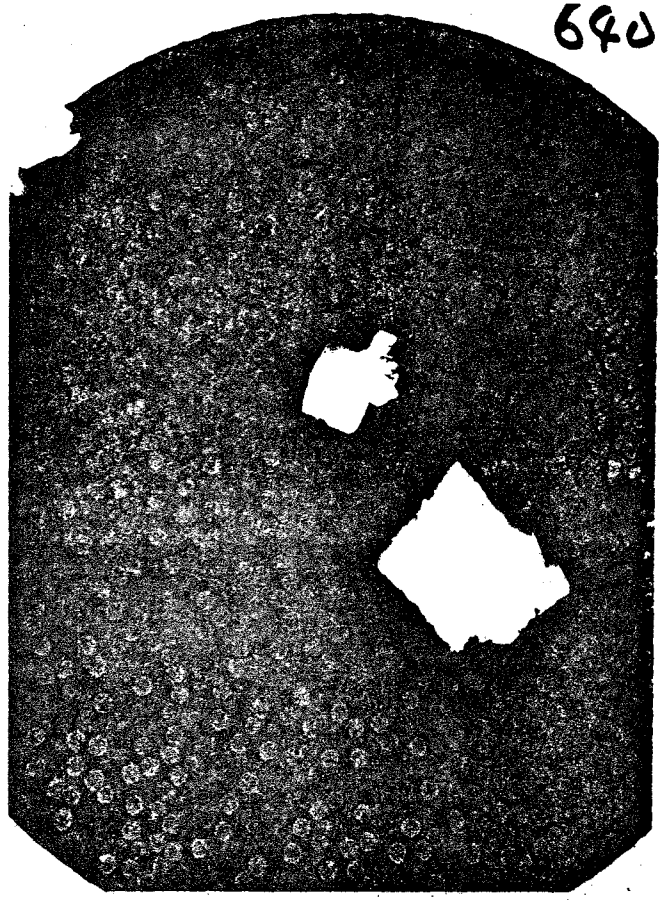

Figure 3.6

Figures 3.5 and 3.6 Transmission electron micrographs of FeS_{mack} crystals synthesized by the action of aqueous H_2S on elemental iron. Spheres in background are 0.109μ polystyrene latex beads.

The results of the chemical analyses carried out on heterogeneously synthesized FeS are presented in Table 3.3. In all cases, the percentages of Fe and S are very close to what would be expected for stoichiometric FeS.

3.4 Discussion and Conclusions

Both the heterogeneous and the "chelate-retarded" homogeneous procedures (CRHP) employed allowed the synthesis of FeS_{mack} which could be used in dissolution studies without the fear of large surface tension effects. The greatest success in this regard was realized using elemental Fe as the iron bearing reactant. The heterogeneous method employing elemental Fe is to be preferred over CRHP since the working-up of the product FeS requires only the drying of the FeS slurry. No washing is needed, and therefore the potential problems of incomplete electrolyte removal and oxygen contamination during washing are not encountered.

For these reasons, the heterogeneous method employing elemental Fe was considered the procedure of choice for this work, and much of the dissolution research was carried out with FeS_{mack} prepared in this manner.

Table 3.3 Summary of analyses of FeS synthesized heterogeneously.

Batch	% Fe	% S	Total
6	64.5	36.1	100.6
7	64.4	35.7	100.1

Theoretical weight percentages for stoichiometric FeS: 63.6% Fe, 36.4% S.

CHAPTER 4

SELECTION AND PREPARATION OF "FIXED-PHASE" FeS_{mack} FOR DISSOLUTION EXPERIMENTATION

4.1 Introduction

In the study of the dissolution characteristics of a finely-divided material, one can examine the behavior of the substance either: 1) as a suspension; or 2) in the form of a compressed solid phase, one face of which is exposed to the solution phase. The advantages and disadvantages which may be associated with the use of stirred suspensions are:

Stirred Suspension

Advantages:

1. certainty that dissolution is occurring at surface of particles.

Disadvantages:

1. difficulty of separating suspended matter from reactant solution for further experimentation;
2. likelihood of grinding of suspended matter by stirbar if magnetic stirring is used;
3. difficulty of maintaining system anoxic through "moving seal" if stir-paddle is used.

Similarly, if the material is compressed into a pellet and this pellet is exposed to various solutions, we have:

Compressed Pellets

Advantages:

1. ability to easily separate reactant solution from FeS, thus allowing reuse of FeS surface;

2. "small" FeS surface area (~1 cm^2) exposed to solution requires only small amount of O_2 to form "monolayer" of oxidized Fe compounds: presence of small amounts of contaminant O_2 immediately indicated by discoloration (yellow) of the black FeS pellet surface.

Disadvantages:

1. possibility that the dissolution may be occurring not only at the exposed pellet surface, but also in the pores of the greater than zero porosity pellet.

Despite this last disadvantage, it was felt that FeS_{mack} dissolution experiments could be carried out and interpreted with greater facility using a fixed FeS_{mack} phase than with stirred suspensions. The majority of the work was conducted using such compressed pellets.

Very preliminary experimentation with the pelletization of FeS_{mack} powder in dies similar to those used in the preparation of KBr pellets for infrared spectroscopy quickly revealed the extreme brittle nature and susceptibility to delamination exhibited by FeS pellets. If such pellets were to be pressed, removed undamaged from the die, and handled in any way, they would have to be manufactured within some type of protective device. A portion of this chapter will be devoted to the description of the pellet holder that was developed, as well as the particulars involved in the pressing of an FeS pellet in this holder.

Many of the experiments, however, were not carried out using freshly pressed pellets. Despite the many precautions taken in the design and use of the dissolution apparatus, occasionally very small amounts of O_2 would leak into the reactor and oxidize the surface of the FeS pellet. In order to be able to continue using such a pellet, the Fe(III) oxide layer had to be removed physically. (Chemical etching was

not considered advisable due to the likelihood of pit formation.) This "surface renewal" was carried out by cutting off a thin layer from the face of the teflon pellet holder/FeS surface. The renewed pellet was then used in further dissolution experiments.

Because they were prepared from $\sim 1\mu$ FeS particles, the pellets were somewhat porous. To determine whether or not these pores were affecting the observed rate, experiments using non-porous FeS_{mack} surfaces were also carried out. Heterogeneous FeS synthesis experimentation disclosed that after exposing elemental Fe to aqueous H_2S for approximately 20-30 minutes, a thin coating of FeS develops on the surface of the Fe. Non-porous FeS_{mack} surfaces were obtained in this manner and used in the dissolution experiments.

4.2 Experimental Aspects of FeS Pelletization and Pellet Characterization

4.2.1 Pellet Holder

Diagrams of this device are found in Figures 4.1a,b,c. The bottom, female portion of the pellet holder serves to hold the FeS powder in place during and after the pressing. The piston of the die applies the compression force to the upper, male section of the pellet holder, which then transmits this force to the powder directly beneath it. Both the upper and lower sections were machined from TFE teflon. The outer diameter of the teflon parts was machined so as to be within 0.025 mm (.001") of the inner diameter of the pellet die. In this way, "flattening" of the pellet during the pressing was prevented. Consequently, since it was not deformed during the pressing, the pellet holder did not tend to contract (and therefore crack the FeS disk) when the

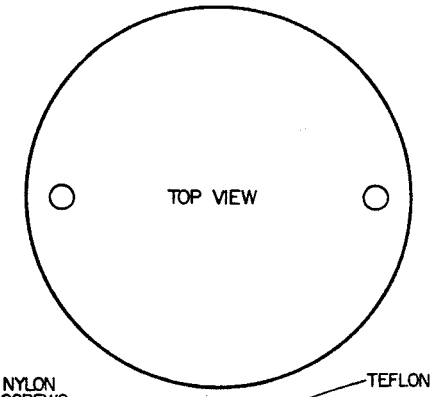

Figure 4.1a

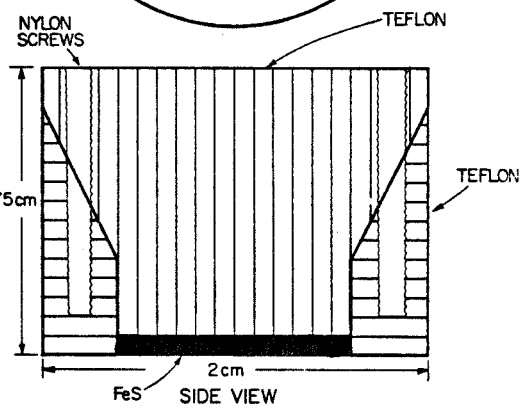

Figure 4.1b

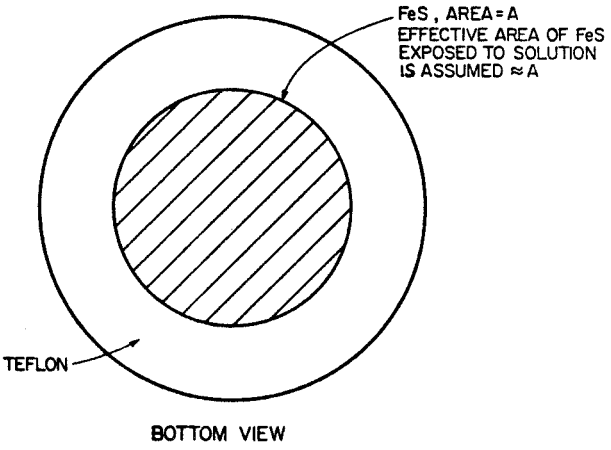

Figure 4.1c

Figure 4.1. Pellet holder

pressure was finally removed. The lower section was drilled and tapped to accept the nylon screws shown in Figure 4.1b. Clearance holes were drilled in the upper section so that the screws would easily slide through them during the pressing operation. Since teflon flows under extreme pressures, after any pellet had been formed, the male and female sections of the pellet holder were very securely attached to one another: the clearance holes of the upper section became "threaded".

4.2.2 Die Assembly and Pressing Procedures

When a new FeS_{mack} pellet was to be prepared, the FeS_{mack} storage vacuum dessicator was filled with O_2-free N_2, and the appropriate amount of FeS quickly weighed out in air,† loaded into the die and the die assembled as shown in Figure 4.2. The die was immediately placed into a special polyethylene bag fitted with a stopcock (as well as with two 1/16" thick stainless steel plates on opposite walls) and the entire bag (closed, except for the stopcock) placed into a large vacuum desiccator which was then evacuated to a pressure of less than 1 μ Hg. Approximately five minutes were required for this entire operation.

After 24 hours, the desiccator was filled with O_2-free N_2 and then opened, the stopcock closed, and the bag removed. The die was then situated between the two metal plates, and the entire bag placed into the press (see Figure 4.3). The actual pressing was carried out at a loading rate of 5,000 psi/3 minutes up to 40,000 psi. Pressure was maintained

†Please see Section 4.2.3 for comment on short term exposure of FeS_{mack} to air.

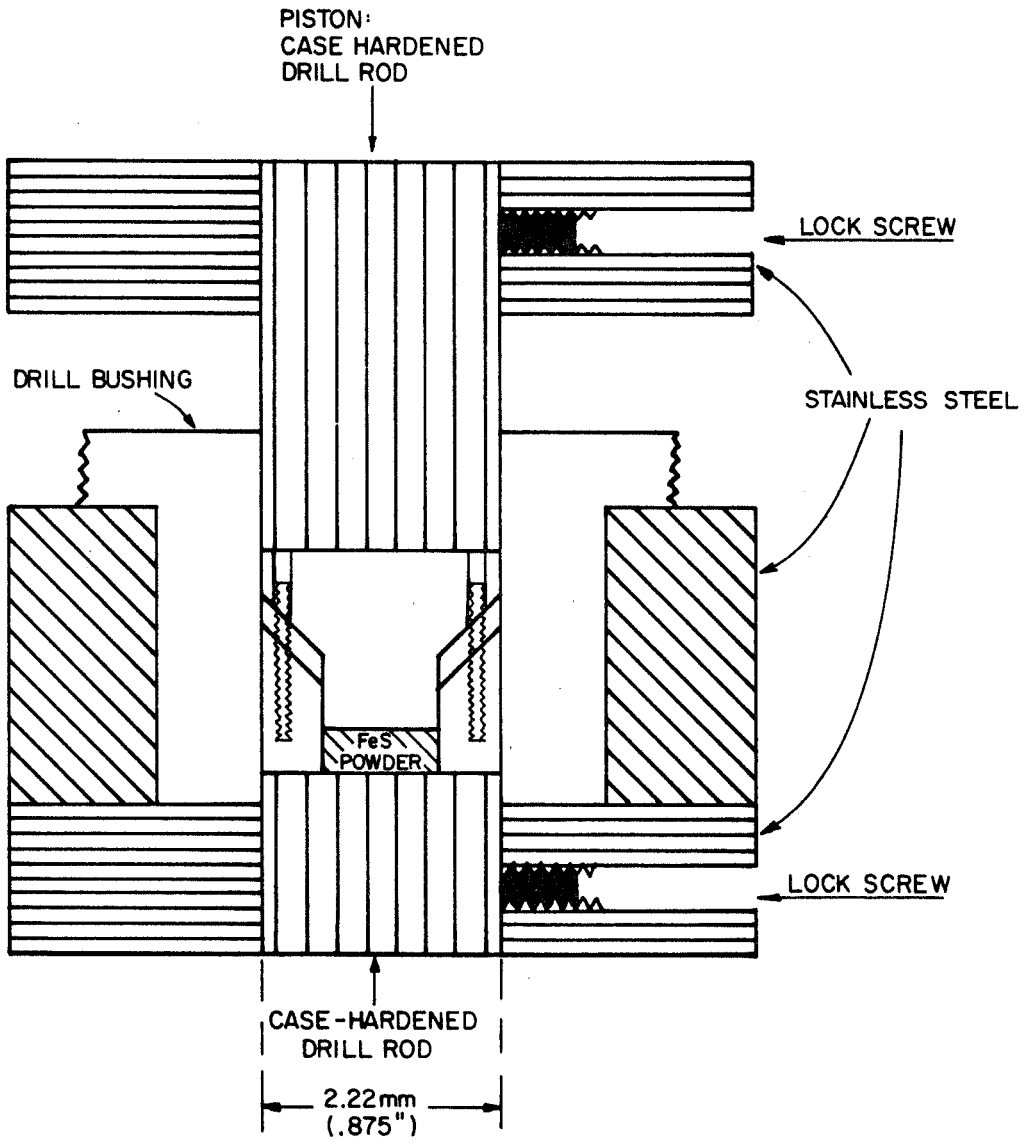

Figure 4.2. FeS pellet holder loaded in die (before pressing).

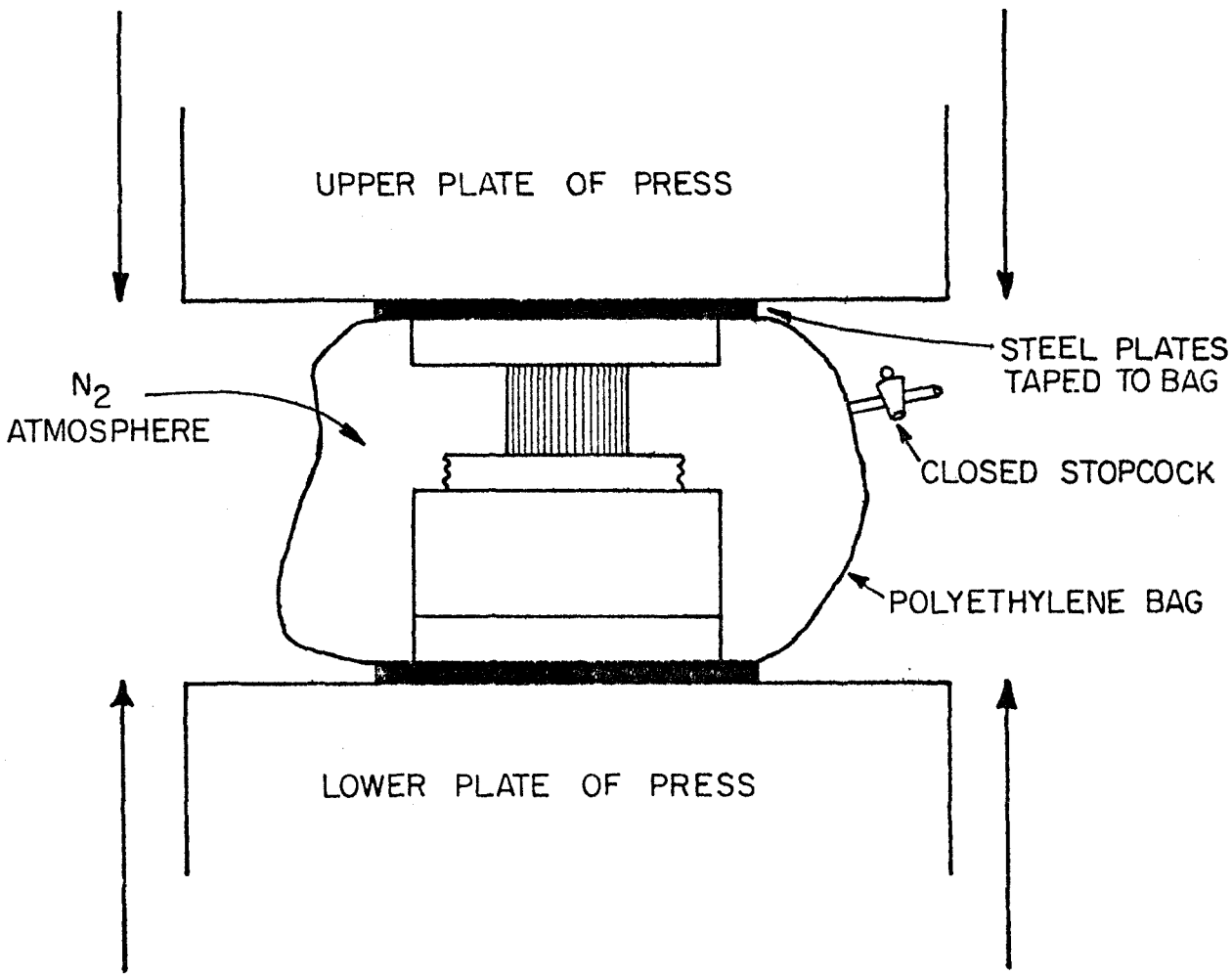

Figure 4.3. Loaded die in N_2 atmosphere during pressing

at this level for 15 minutes, then removed at a rate of 5,000 psi/ 3 minutes. When the pressing was complete, the newly formed pellet was carefully removed from the die and stored under vacuum until needed for experimentation.

4.2.3 Pellet Surface Renewal

Whenever a pellet surface required renewal, its vacuum storage vessel was filled with O_2-free N_2, and the pellet was removed. Working quickly to minimize its exposure to air, the pellet was wrapped in Saran Wrap and mounted in the chuck of a lathe. Approximately 0.1 mm of material (both teflon and FeS) was shaved away from the pellet surface shown in Figure 4.1c with a (dry, acetone washed) carbide cutting tool. A fresh, unoxidized surface of FeS was thereby exposed. The pellet was immediately returned to its container, and full vacuum restored. The entire process required about 5 minutes.

Although temporarily exposed to atmospheric O_2, it is not felt that this new surface suffered any oxidation. In earlier phases of this work, small samples of mackinawite which remained exposed to air for many months did not, as long as they were kept dry, appear to undergo oxidation. Indeed, X-ray studies of such material yielded the diffraction pattern of mackinawite alone. Thus, it is very unlikely that 5 minutes of exposure to air would damage the integrity of the newly exposed surface.

4.2.4 X-Ray, Density and SEM Characterization

The X-ray diffraction pattern of a pressed FeS_{mack} pellet was taken using the same apparatus described in Section 3.2.2. A piece of the pellet was placed in the sample cup, and the scanning carried out at a rate of 1 degree of 2θ per minute.

Density determinations carried out on 40,000 psi-pressed FeS_{mack} were made by simply weighing a pellet (without holder) of FeS, and measuring its thickness. Since the diameter (2.22 mm) of the die used was known, calculating the density was straightforward.

Scanning electron microscope (SEM) studies of the surfaces of both freshly pressed as well as renewed surface FeS pellets were carried out using an ETEC (Hayward, CA) Autoscan SEM. The pellet to be examined was coated with gold using a sputter coater (Model "Hummer") manufactured by Technics Corp. (Alexandria, VA).

4.3 Experimental Aspects of Non-Porous FeS_{mack} Surface Synthesis and Characterization

4.3.1 Synthesis

Disks (0.5" in diameter) of high purity iron (99.998% Fe, obtained from Alfa-Ventron Corp., Danvers, MA) were placed in FEP teflon holders (similar to those used for the powder pellets) and reacted with aqueous H_2S in the same apparatus and according to procedures similar to those described for the heterogeneous synthesis of FeS. After the 30 minutes required to obtain an FeS-coated Fe surface, however, the Fe disk was simply allowed to remain in vessel 10 (see Figure 3.2), the aqueous H_2S

was drawn off under N_2, and vessel 10 evacuated to dry the disk surface. After drying, the disk was removed from vessel 10 in an O_2-free dry box, then stored under vacuum until needed. A diagram of the Fe disk/FeS surface with holder is found in Figure 4.4.

4.3.2 X-Ray, SEM Characterization

The X-ray diffraction pattern of an Fe/FeS surface was taken using the same instruments described in Section 3.2.2. A piece of Fe coated with FeS was placed in the sample cup, and the scanning carried out at a rate of 1° of 2θ per minute. SEM studies were carried out as with the pellets.

4.4 Results

4.4.1 FeS_{mack} Pellet Characterization

The X-ray diffraction pattern obtained for pelletized FeS is presented in Figure 4.5. Except for the considerable intensification of the various mackinawite peaks, the pattern is identical to the FeS_{mack} powder pattern of Figure 3.4. Certain proof was thereby obtained that the pressure pelletization of the FeS_{mack} did not alter its crystalline form. The intensification of the peaks is due to the fact that the pellet is much denser than the powder used to obtain Figure 3.4.

Several determinations of the density of the 40,000 psi-pressed, heterogeneously synthesized FeS were made. All of the values obtained centered closely around 2.9 g/cc. Since the crystalline form of mackinawite is known to be primitive tetragonal, there are two Fe atoms

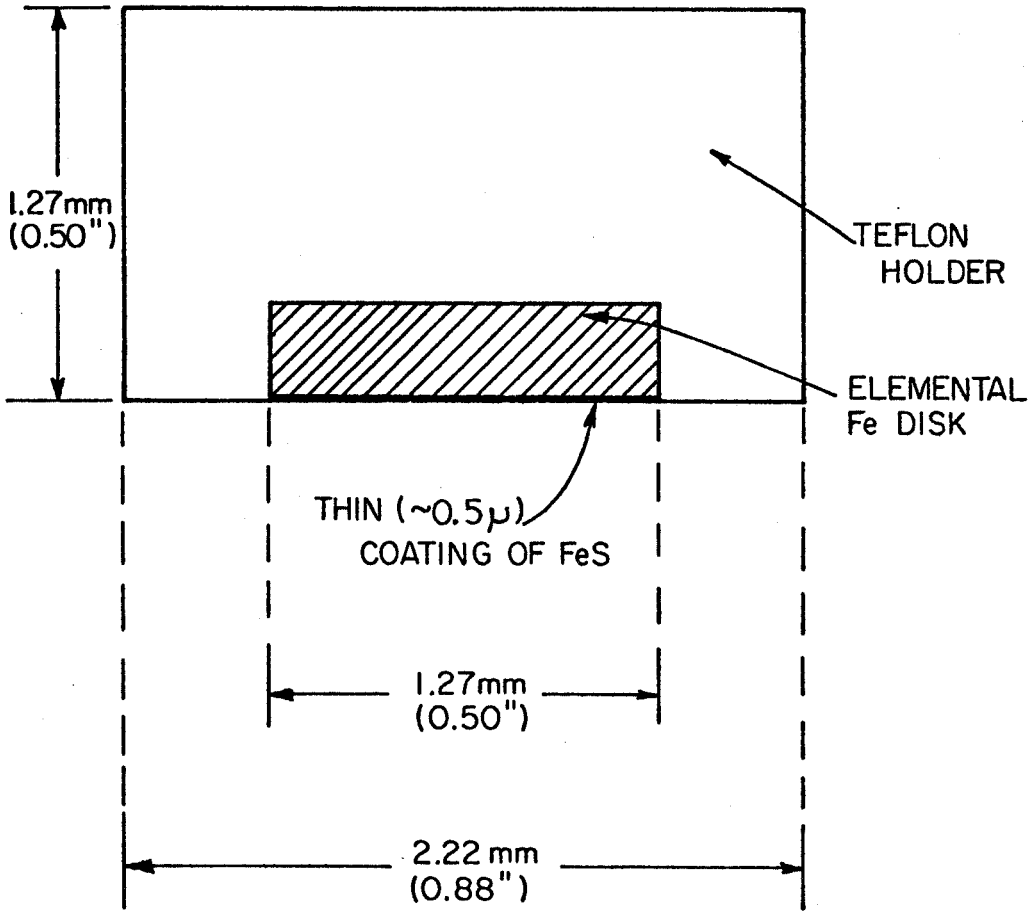

Figure 4.4. Fe surface coated with FeS

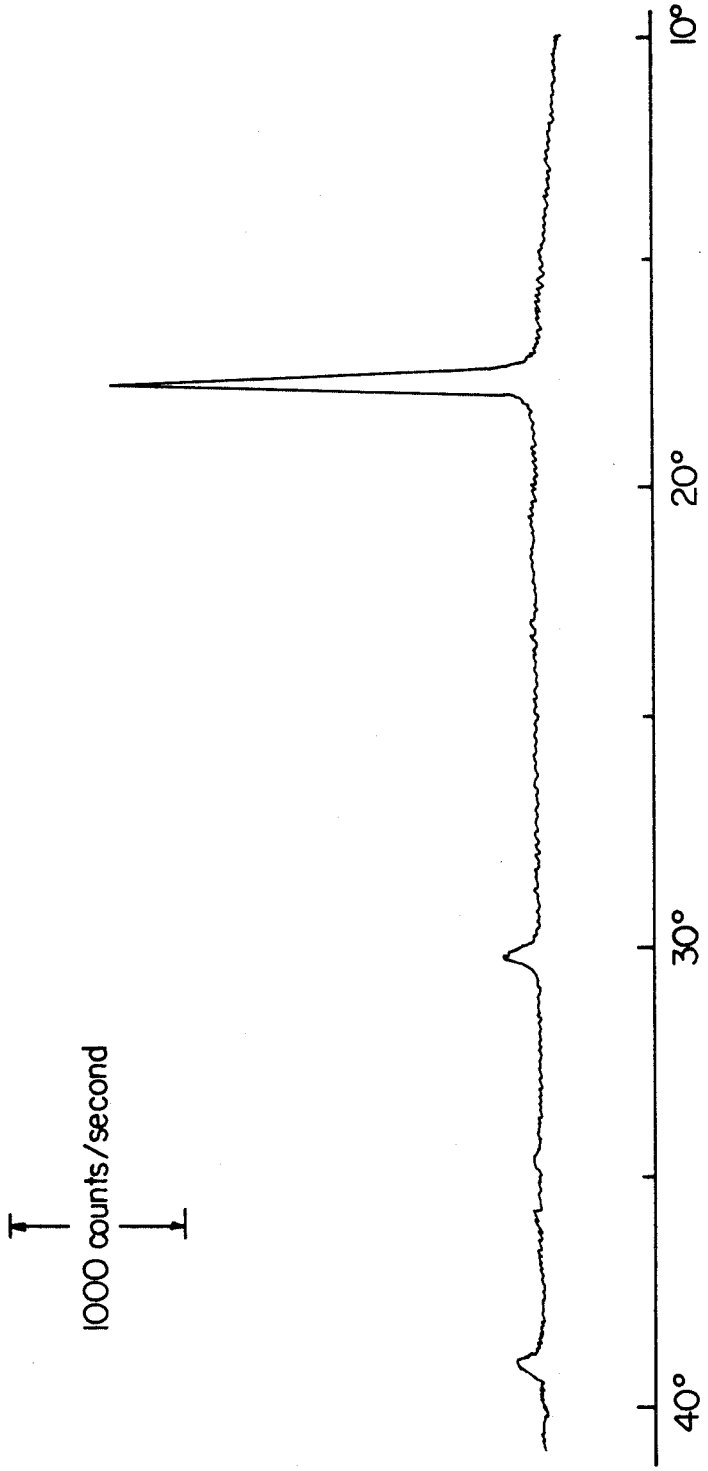

Figure 4.5. X-ray diffraction pattern of 40,000 psi-pressed FeS_{mack}.

and two S atoms per unit cell. The unit cell parameters are a = b = 3.68Å, c = 5.05 Å (Berner, 1962). These facts imply that the actual density of FeS_{mack} is 4.29 g/cc. The porosity of the FeS_{mack} pellets may therefore be calculated to be

$$(1.0 - \frac{2.9\ g/cc}{4.29\ g/cc}) \times 100\% = 32\%$$

Two of the SEM photographs which were taken of the surface of a freshly pressed pellet are presented in Figures 4.6 and 4.7. The individual crystals which comprise the pellet are clearly visible, and their particle size distribution seems indeed to be quite monodisperse; most crystals being on the order of 0.5 μ thick. The dimensions of the pores are approximately 0.1μ. Figure 4.8 is a photo of the edge of a pellet which has been broken open. The structure which appears at the surface in Figure 4.7 is present inside the pellet as well, as seen in Figure 4.8. The much greater surface roughness seen in Figure 4.8 as opposed to that in Figure 4.7 is due to the fact that when the pellet broke open, it did not break on a perfect plane. The freshly pressed surface, on the other hand, was very much flatter because it was formed against the surface of the mirror polished die.

In Figure 4.9 is found an SEM photograph of the surface of an FeS pellet from which a thin layer had been removed as described in Section 4.2.3. It is evident that this surface is rougher than that of a freshly pressed pellet. It was hoped that this would not be a problem, and that the stirring could be maintained at a level sufficiently

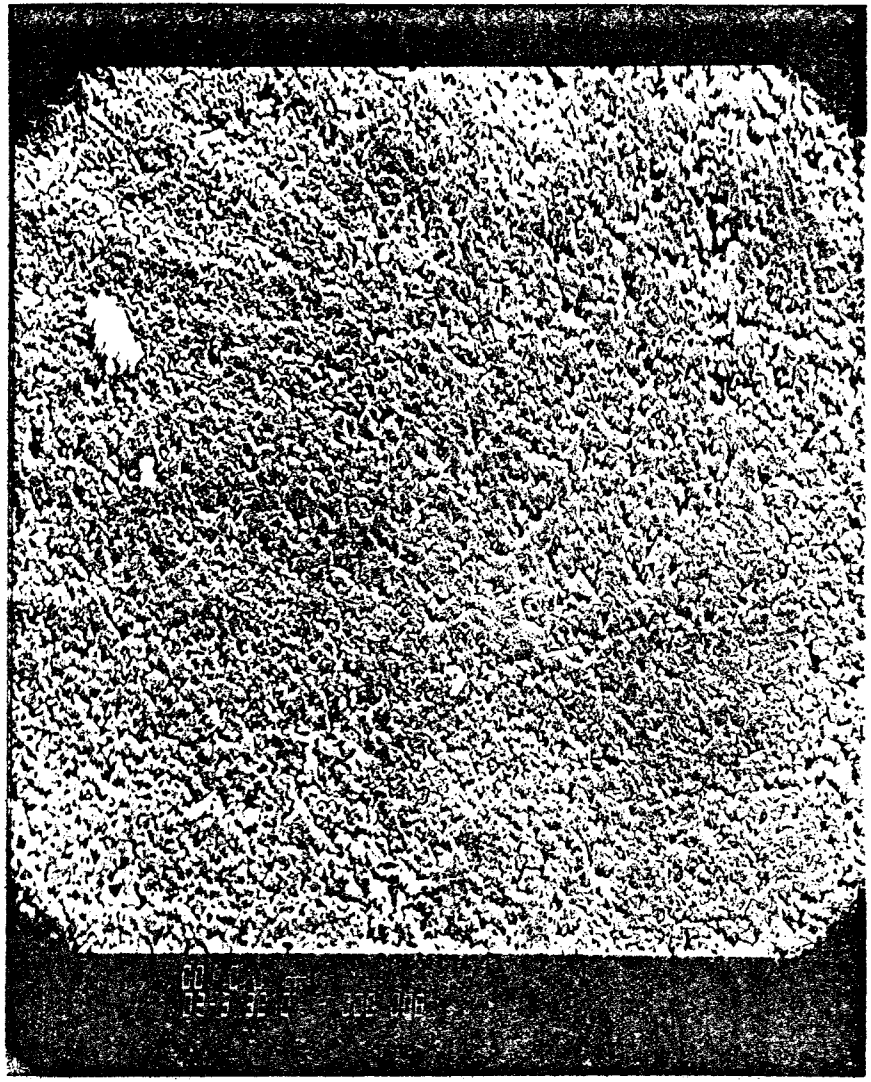

Figure 4.6. (Magnification - 2,000X)

Figure 4.7. (Magnification - 20,000X)

Figures 4.6 and 4.7. Scanning electron micrographs of freshly pressed FeS_{mack} pellet surface.

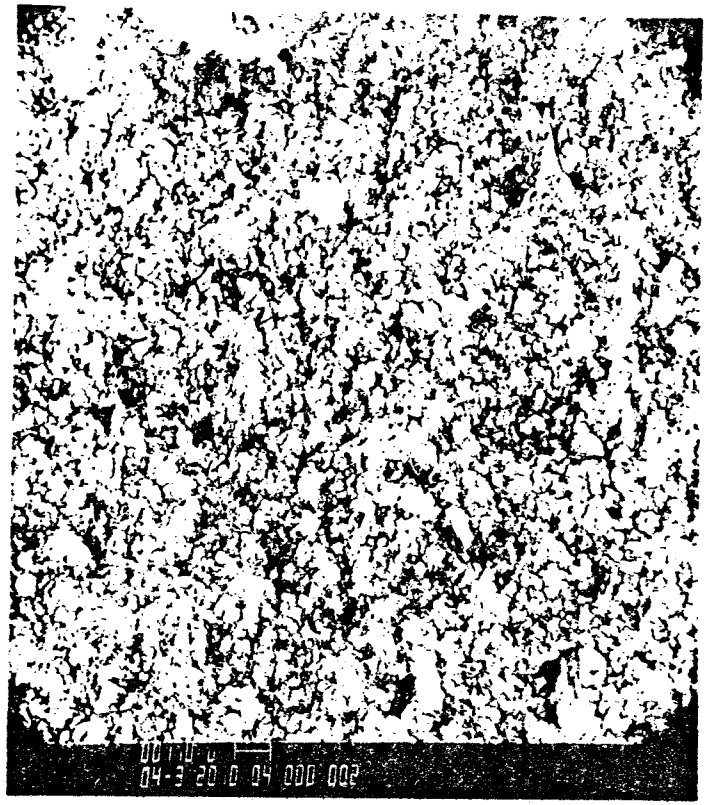

Figure 4.8 (Magnification 40,000 X)
Scanning electron micrograph of broken edge of pellet pressed from ∿1μ FeS_{mack} particles.

Figure 4.9 (Magnification 40,000 X)
Scanning electron micrograph of resurfaced FeS_{mack} pellet. Note scrape-marks left by cutting tool.

vigorous that diffusion into and out of these relatively large scale depressions would not limit the dissolution process in any way. This point will be discussed further in subsequent portions of this thesis.

4.4.2 Non-Porous FeS_{mack} Surface Characterization

The X-ray diffraction pattern obtained for the FeS-coated Fe disk is presented in Figure 4.10. The FeS_{mack} peaks are considerably less intense than those observed with pure mackinawite samples synthesized from elemental iron (Figure 3.4). The peak at 17.5° is clearly visible, but the one at 31° is barely discernible. The peak at 39° is not visible at all. The diffraction of X-rays from the underlying Fe (cubic) crystal lattice, evidenced by the strong peak at 45° 2θ (Fe-Fe d-spacing = 2.03 Å), indicates that this FeS coating is quite thin. This may be concluded because if it were not the case, the intensity of the incident and diffracted X-ray beams would be so attenuated (due to the absorption of the X-rays by Fe and S atoms) while passing through the FeS layer that the iron peak at 45° would not be observed. Based on the absorptivity coefficients of Fe and S for Cu K_α radiation, the FeS coating would have to be less than about 0.5 μ for the 45° Fe peak to appear at its observed intensity. The fluctuating background is probably due to the H_2S corrosion process not providing an adequately smooth and uniform surface for X-ray diffraction.

SEM photos of this surface are presented in Figure 4.11. It is not possible to see well-defined crystals in these photos. The 90 minutes of exposure to H_2S was apparently not long enough to allow the

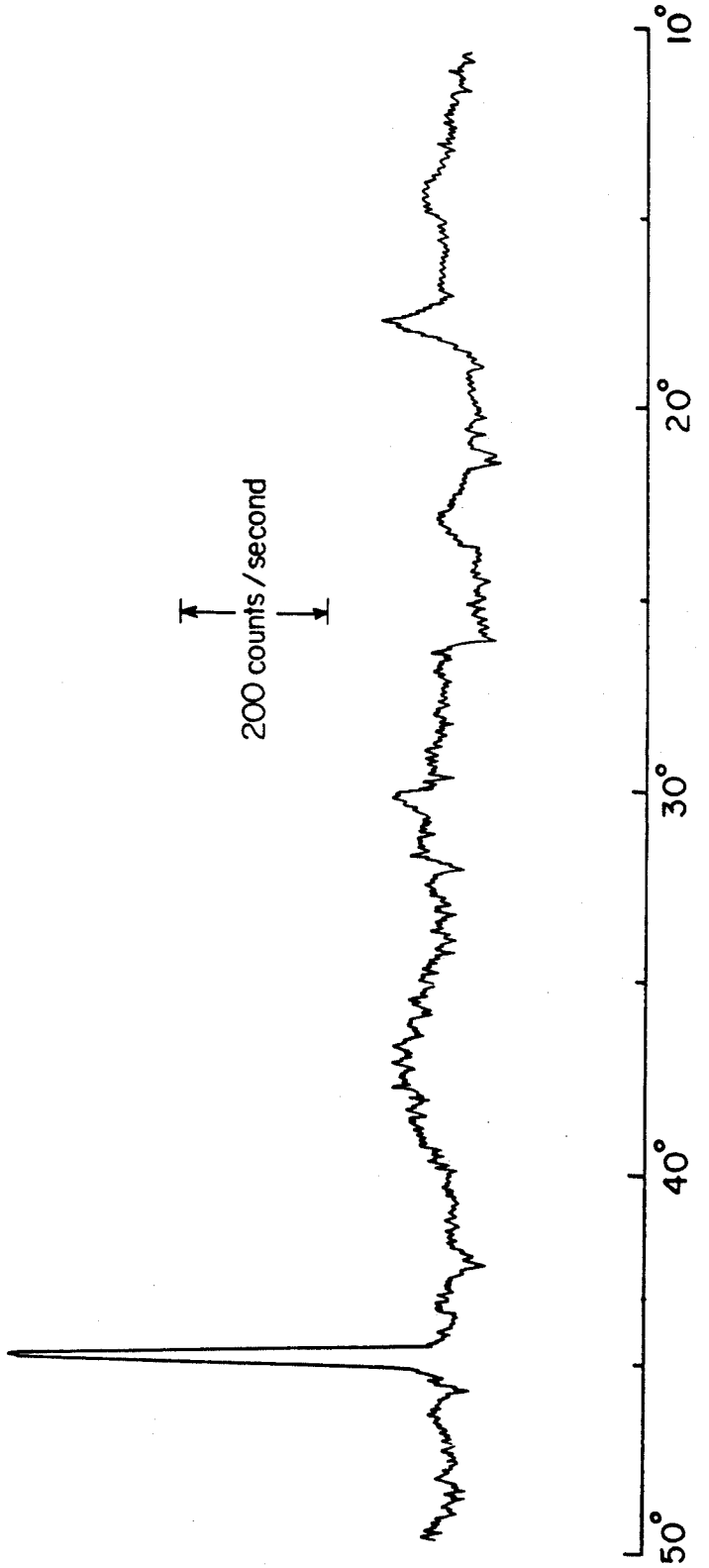

Figure 4.10. X-ray diffraction pattern obtained with FeS-coated Fe.
Note the strong iron peak (d = 2.03 Å) at 45° 2θ.

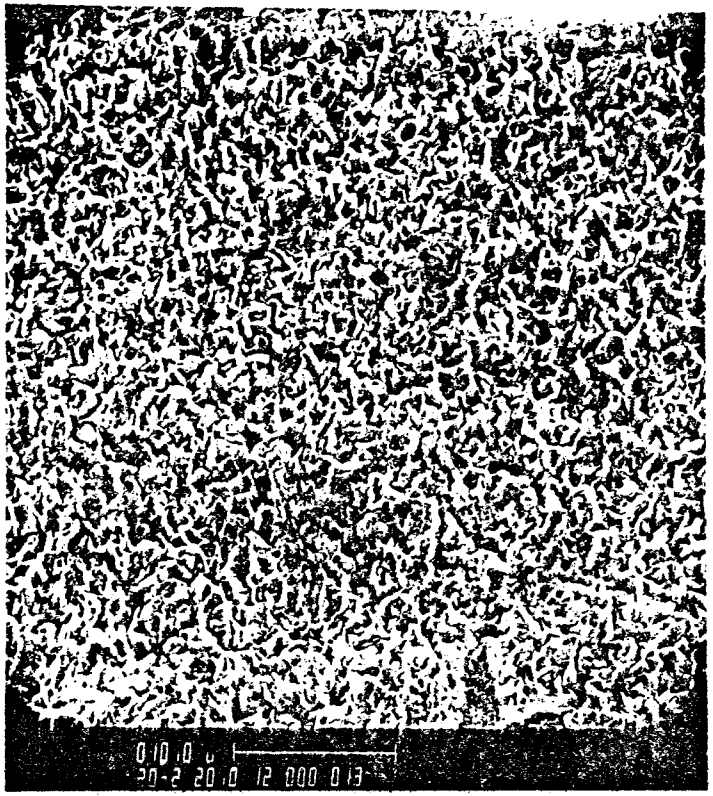

Figure 4.11a (Magnification - 2,000X)

Figure 4.11b (Magnification - 10,000X)

Figure 4.11. Scanning electron micrographs of surface of FeS-coated Fe disk.

formation of crystals on the Fe surface. Based on the Scherrer equation (see Section 3.1.1), the broadening of the peak at 17.5° implies a crystallite size of $\sim$ 200 Å. It is hoped that this small size will not affect the dissolution kinetics (see Section 3.3.1).

CHAPTER 5

MONITORING THE DISSOLUTION RATE

5.1 Extent of FeS Dissolution as a Function of pH

In experimental studies of chemical reaction rates, very often the rates per se are not directly measured. It is generally more convenient to follow the concentration of some reactant or product species (viz. extent of reaction) as a function of time. From these data one may then calculate the reaction rate. With a compound such as $BaSO_4$, one might follow its dissolution rate by intermittent aliquot removal/analysis. Since Fe^{2+}_{aq} and S(-II) species are very subject to oxidation by oxygen, such procedures are unattractive because of the considerable risk of admitting atmospheric O_2 to the reaction chamber. Fortunately, one can follow the dissolution of FeS in other ways.

The fact that S^{2-} and HS^- are basic species implies that during the non-oxidative dissolution of FeS the pH of the solubilizing aqueous medium will increase. We have:

$$FeS \rightarrow Fe^{2+} + S^{2-} \qquad (5.1)$$

$$S^{2-} + H^+ \rightleftarrows HS^- \qquad (5.2)$$

$$HS^- + H^+ \rightleftarrows H_2S \qquad (5.3)$$

A small amount of H^+ is produced as a result of the dissolution due to the production of hydrolyzable Fe^{2+} ions:

$$Fe^{2+} + H_2O \rightleftarrows FeOH^+ + H^+ \qquad (5.4)$$

When dissolving FeS into a dilute solution of a strong acid the proton balance equation (neglecting $[OH^-]$) for the reaction may therefore be written for any time

$$-\Delta[H^+] = -([H^+] - [H^+]_0) = [HS^-] + 2[H_2S] - [FeOH^+] \qquad (5.5)$$

where brackets denote concentration and $[H^+]_0$ represents the initial hydrogen ion concentration. The contribution of higher hydrolysis products of Fe^{2+} (such as $Fe(OH)_2$) have been neglected.

The equilibria which describe the pH-dependent speciation of sulfide and ferrous species may be written

$$\frac{\{H^+\}\ \{HS^-\}}{\{H_2S\}} = K_1 \qquad (5.6)$$

$$\frac{\{H^+\}\ \{S^{2-}\}}{\{HS^-\}} = K_2 \qquad (5.7)$$

$$\frac{\{FeOH^+\}\ \{H^+\}}{\{Fe^{2+}\}} = {}^*K_1 \qquad (5.8)$$

$$\frac{\{FeCl^+\}}{\{Fe^{2+}\}\ \{Cl^-\}} = K_{FeCl} \qquad (5.9)$$

where {} denotes activity.

The equation describing the complexation of ferrous ion by chloride has been included since the dissolution reactions will be carried out in chloride media.

If we define

$$S_{TOT} = [H_2S] + [HS^-] + [S^{2-}] \tag{5.10}$$

$$Fe_{TOT} = [Fe^{2+}] + [FeOH^+] + [FeCl^+] \tag{5.11}$$

we have

$$\begin{aligned} [H_2S] &= \alpha_0 S_{TOT} \\ [HS^-] &= \alpha_1 S_{TOT} \\ [S^{2-}] &= \alpha_2 S_{TOT} \\ [FeOH^+] &= \alpha_{FeOH} Fe_{TOT} \end{aligned} \tag{5.12}$$

where

$$\alpha_0 = \left(1 + \frac{K_1 \gamma_{H_2S}}{[H^+]\gamma_{H^+}\gamma_{HS^-}} + \frac{K_1 K_2 \gamma_{H_2S}}{[H^+]^2 \gamma_{H^+}^2 \gamma_{S^=}} \right)^{-1} \tag{5.13}$$

$$\alpha_1 = \left(\frac{[H^+]\gamma_{H^+}\gamma_{HS^-}}{K_1 \gamma_{H_2S}} + 1 + \frac{K_2 \gamma_{HS^-}}{[H^+]\gamma_{H^+}\gamma_{S^=}} \right)^{-1} \tag{5.14}$$

$$\alpha_2 = \left(\frac{[H^+]^2 \gamma_{H^+}^2 \gamma_{S^=}}{K_1 K_2 \gamma_{H_2S}} + \frac{[H^+]\gamma_{H^+}\gamma_{S^=}}{K_2 \gamma_{HS^-}} + 1 \right)^{-1} \tag{5.15}$$

$$\alpha_{FeOH} = \left(\frac{[H^+]\gamma_{H^+}\gamma_{FeOH}}{{}^*K \gamma_{Fe^{2+}}} + 1 + \frac{K_{FeCl}[Cl^-]\gamma_{Cl^-}[H^+]\gamma_{H^+}\ {}_{FeOH}}{\gamma_{FeCl}{}^*K} \right)^{-1} \tag{5.16}$$

and γ_A is the activity coefficient of species A.

Since $Fe_{TOT} = S_{TOT}$ at all times during the dissolution, by substituting (5.12) in (5.5) one obtains

$$S_{TOT} = -\Delta[H^+]/(2\alpha_0 + \alpha_1 - \alpha_{FeOH}) \qquad (5.17)$$

This equation describes the concentration of dissolved sulfide as a function of pH as well as such implicit variables as temperature T, pressure P, ionic strength I, etc. In the case of dissolution into a solution buffered by the acid/base pair HB/B^-, the proton balance equation (5.17) must be modified, and reads

$$S_{TOT} = ([B^-] - [B^-]_0 + [H^+]_0 - H^+])/(2\alpha_0 + \alpha_1 - \alpha_{FeOH}) \qquad (5.18)$$

A knowledge of the pK_A for the acid HB as well as the pH, T, etc. will allow the calculation of $[B^-]$. As in (5.17) the contribution of the OH^- ion is neglected. This approximation will introduce little error since the $([B^-] - [B^-]_0)/[OH^-]$ ratio will be greater than 500 in the buffered dissolution experiments discussed in this thesis.

It is apparent from equations (5.17) and (5.18) that in both buffered and unbuffered solutions one can monitor the rates of the non-oxidative dissolution of FeS simply by following pH. In this way, it is possible to completely isolate the dissolution process from the oxic atmospheric environment and still be able to follow the reaction very accurately and in as much detail as desired. The values for the equilibrium constants K_1, K_2, etc. and the method chosen for calculating

the activity coefficients are discussed in Appendix I. The pH electrodes which were selected for this research and how they were mounted in the dissolution reactor are described in the next section.

5.2 The Dissolution Reactor

5.2.1 Design Considerations

Mackinawite is a fairly insoluble compound. This implies that under most conditions, if some FeS is allowed to dissolve anoxically, only very small concentrations of O_2 would be required to completely oxidize the solubilized Fe(II) and S(-II), as well as, perhaps, the FeS/H_2O surface. For this reason, the solution which is to be used must be thoroughly de-oxygenated before being allowed to enter the reactor in which the dissolution is to be carried out. Oxygen must be kept from entering the system during all stages of a dissolution experiment. Special provisions must be made to seal the pH electrodes and solution delivery tubes into the reactor top as well as to seal the top to the reactor body. In addition, all reactor parts must be constructed of materials inert with respect to Fe(II) and S(-II). Finally, since pH will be used to follow the reaction, no H_2S may be allowed to enter a gas phase above the solution. Therefore, the reactor must be designed in such a way that all gas escapes upon filling the chamber.

5.2.2 Construction of Dissolution Reactor

A schematic of an apparatus which meets these requirements is found in Figure 5.1. The solution to be used in a given experiment is

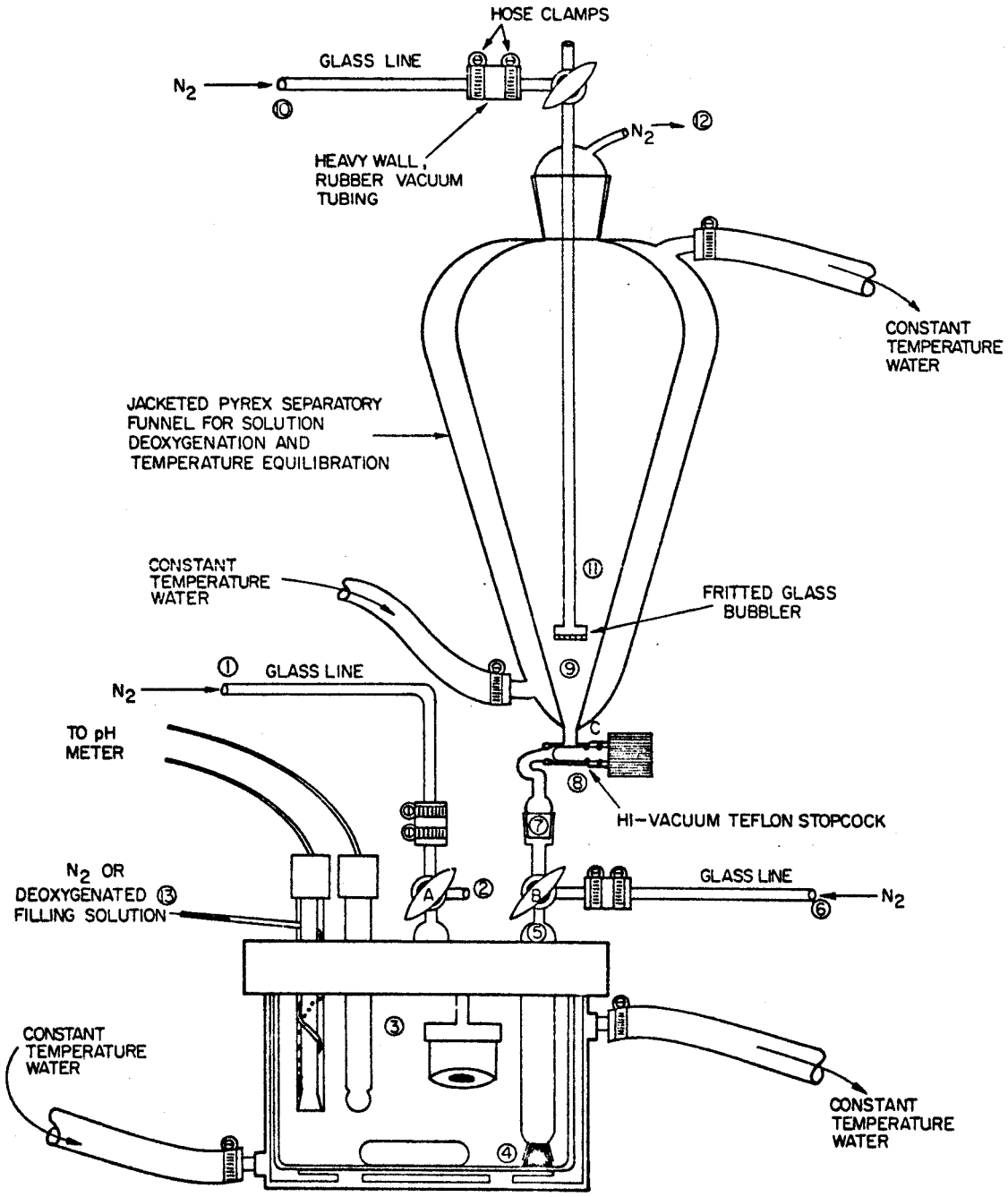

Figure 5.1. Dissolution apparatus

de-oxygenated in the jacketed, pyrex separatory funnel. The actual dissolution reaction is carried out in the reactor directly below it. A detailed diagram of this reactor is found in Figure 5.2. The reactor top was machined from TFE teflon. The "body" portion of the reactor, into which the top fits, was made by simply cutting off the bottom portion of a transparent Nalgene 32 oz. FEP teflon bottle. The sealing between the reactor top and cup pieces was accomplished by cutting grooves for and inserting two rubber O-rings into the reactor top. The reactor top was kept securely in place with an aluminum ring which screwed onto a plexiglas cup. The void volume of the reactor (with all electrodes, etc. in place) was usually very close to 310 ml.

The reaction temperature was controlled by pumping (Haake Corp. (Saddlebrook, NY) Model FS circulator) constant temperature water through the annular space between the inner (reactor) and outer (plexiglas) cups. When required, cooling was provided by a Haake model "Frigid Midget" refrigeration unit. To prevent the diffusion of oxygen into the reactor through the inner cup wall, the constant temperature water was bubbled with high purity grade N_2 during the entire course of an experiment series.

The addition of the de-oxygenated reaction solution was made through stopcock B, and the N_2 present in the reactor before any first experiment expelled through stopcock A. Three O-ring grooves and O-rings were placed in the reactor top around each of the stopcock arms entering the reactor, as well as around the pH and reference electrodes. The FeS powder pellets or Fe/FeS disks (with holders) were mounted in a

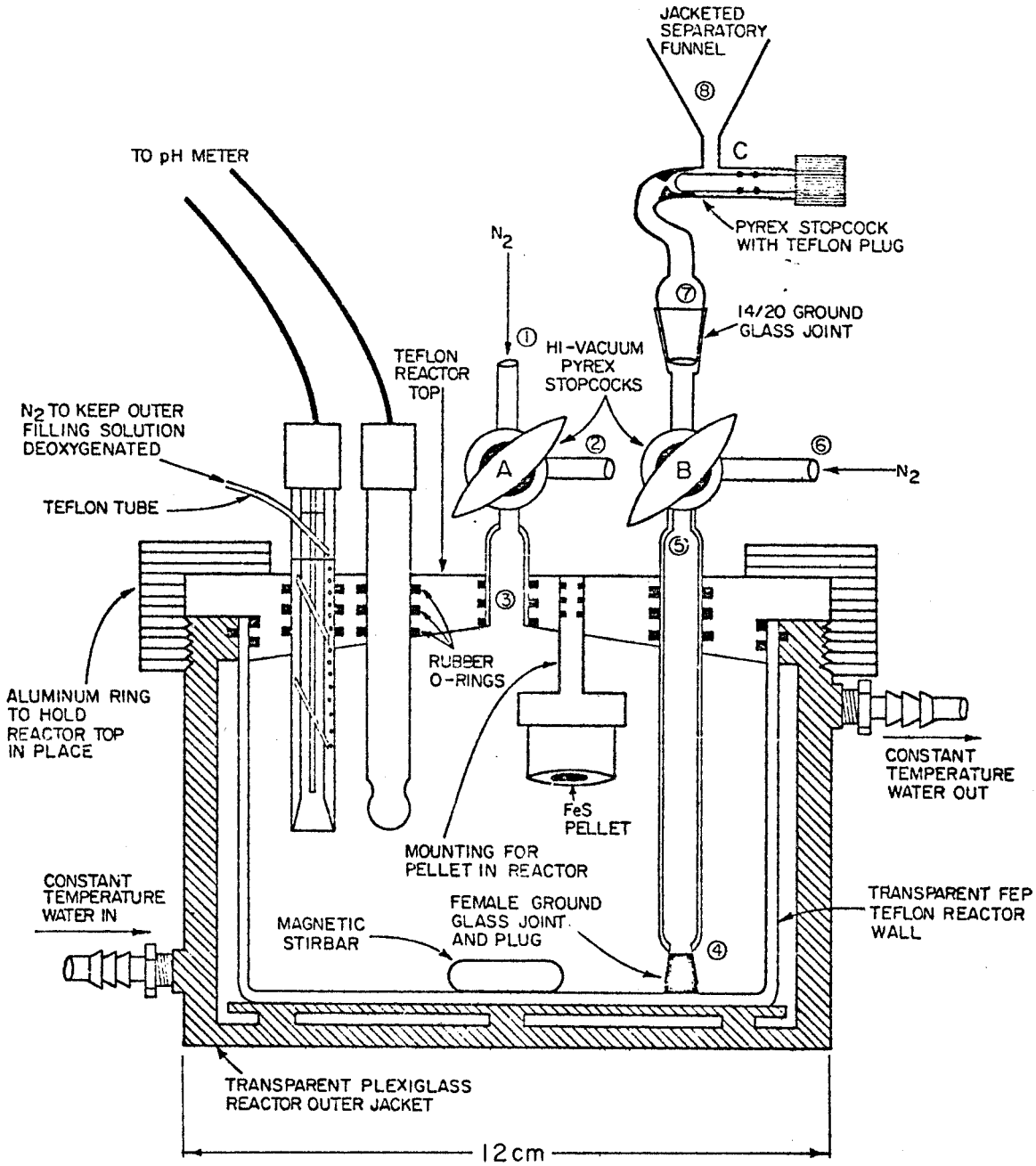

Figure 5.2. Schematic of dissolution reactor (Volume = 310 ml)

special cup machined from TFE teflon. The tube leading to the bottom of the reactor from the left stopcock was included to allow the removal of reactant solution at the conclusion of an experiment.

Stirring was accomplished by using a magnetic stirbar (10mm x 25mm). This stirbar was driven from outside the cell with a magnet mounted on the armature shaft of a motor (Bodine Electric Co. (Los Angeles, CA) Model W-14). It was felt that this method of stirring would be adequate, and that the diffusion boundary layer at the FeS surface could be kept thin enough that diffusion through it would not be a barrier to the dissolution process. This assumption was to be tested by stirring at different speeds.

5.2.3 Procedures for Use of Dissolution Reactor

The First Experiment of a Series.

The teflon reactor top and cup as well as the stopcocks and stirbar were cleaned in a hot solution of PEX[†] detergent (Peck's Products, St. Louis, MO), rinsed with deionized H_2O, soaked 24 hours in 85°C 4N HNO_3, soaked in distilled-deionized water (DDW) for 72 hours, thoroughly rinsed with DDW, and allowed to dry. All rubber O-rings were washed in hot PEX detergent, rinsed with distilled water, allowed to dry, and then lightly greased with Apiezon T stopcock grease (Apiezon Products, London) before they were fitted into their respective grooves in the reactor cap.

[†]Please see Section 3.2.1 for information about "PEX".

The reactor parts, along with the FeS pellet to be used (still stored under vacuum) were then assembled in an oxygen-free (less than 1 ppm O_2, balance He) dry-box. A minimum amount of Apiezon T grease was used to lubricate the stopcocks, which were then closed to prevent the entry of O_2 to the dissolution chamber. The ports for the electrodes were also sealed using special teflon plugs. The assembled reactor was then removed from the dry-box. Stopcocks A and B were connected with 5mm wall thickness rubber tubing and hose clamps to nitrogen lines 1 and 6, respectively, and the deoxygenation funnel was fitted to stopcock B (see Figure 5.1).

With stopcock C closed, the reactant solution for the first dissolution was added to the funnel. The solution was then deoxygenated by introducing N_2(O_2-free) to the funnel via 10 → 11 → 12 and 6 → 7 → 8 9 → 12.

This deoxygenation nitrogen was allowed to flow for at least 12 hours, and usually flowed for 24 hours or more. The flow rate was approximately 3-4 ml/sec. The entire system of reaction chamber plus deoxygenation funnel was then brought to the temperature selected.

The pre-conditioned glass pH electrode (Beckman Instruments, Inc. (Fullerton, CA), Model 39099) was rinsed with DDW, then allowed to dry five minutes. The teflon stopper sealing the port for this electrode was then opened, and simultaneously (to prevent the entrance of O_2 during insertion of the electrode) nitrogen at a flow rate of 20-30 ml/sec. was passed into the reactor from line 1, and allowed to escape

from the port into which the electrode was being inserted. Once the electrode was installed, the N_2 flow was stopped. A similar procedure was followed for the double junction reference electrode (Orion Research, Inc. (Cambridge, MA), Model 90-02-00). Prior to its insertion, however, the outer filling chamber was filled with deoxygenated solution of the same background electrolyte type and strength that was to be used in the dissolution reaction. It was introduced through tube 13, which later was used to pass N_2 into the reference electrode to keep the solution deoxygenated. With the reactor and funnel at the required temperature, and the electrodes in place, the solution was dropped into the reaction chamber at a flow rate not exceeding the deoxygenation flow rate from 10 (so that no O_2 would enter the funnel via 12). The appearance of solution at point 2 signaled the fact that the reactor had been filled completely, and that no N_2 remained in the cell. At this time, both stopcocks A and B were closed, and the stir motor and pH/mv meter (Orion Model 801) activated. Once the pH meter gave a stable reading, an automatic printer (Orion Model 751, interfaced with the pH meter) was activated so as to record the mv response from the electrodes every hour. A slow flow of N_2 from 1 to 2 was allowed to continue during the reaction (thereby keeping these lines O_2-free) so that O_2-free N_2 would be available on demand at the conclusion of the experiment.

Since this would be the first experiment of a series, it was assigned a code name of, for example, D1. Additional experiments

---

†Occasionally, some N_2 bubbles would cling to the cell walls, but the sum of their volumes never exceeded 1 ml.

performed immediately following D1 would be D2, D3, D4, etc. A series of experiments carried out with a different FeS pellet (whether freshly pressed or resurfaced) would be assigned a new letter, say E. The procedures which were used so that more than one dissolution experiment could be carried out per disk are now described.

Subsequent Experiments.

At the conclusion of a dissolution experiment, after making sure that N_2 was still flowing from 1 to 2, stopcock A was opened to the three-way position. Stopcock B was then carefully raised 0.5 cm. With 1-2 ml N_2/sec escaping at 2, stopcock A was turned so as to connect 1 and 3. Stopcock B was then opened to the three-way position, and a clean thin stainless steel rod was inserted at 7 and used to dislodge the stopper at 4. Stopcock B was then turned so that the reactant solution being displaced by the N_2 from 1 would be discharged through the horizontal arm of stopcock B. (N_2 line 6 had been removed prior to this operation, and a teflon tube connected in its place.) After the first 50 ml had been removed from the reactor, 100 ml was collected for Fe analysis in a 125-ml acid-washed, polyethylene bottle to which was added 2 ml of concentrated HCl (J. T. Baker (Phillipsburgh, NJ) Ultrex HCl). The Fe analyses were carried out with a Varian (Palo Alto, CA) Model AA-5 Atomic Absorption Spectrophotometer.

Once this sample had been removed, stopcock A was closed and the remaining Fe(II)/S(-II) solution was left in the reactor (to help maintain anoxic conditions). The separatory funnel was refitted at

point 7, and line 6 reconnected. If the next experiment was to be run at a different temperature, the thermostat of the water bath system was adjusted accordingly. Twenty-four hour deoxygenation of the next run's solution via 6 → 5 → 7 → 9 → 12 and 10 → 11 → 12 followed. Line 6 was then removed and the remaining old solution flushed out of the reactor (via stopcock B) with several large aliquots of deoxygenated water from the funnel. N_2 from line 1 was used to remove these washings. The final new solution was then dropped into the reactor. Stopcock B was relowered to close the stopper at 4, stopcocks A and B closed, and the printer activated: the new run had begun.

This procedure was used to introduce the new reaction medium for all runs after the first.

CHAPTER 6

RESULTS OF DISSOLUTION EXPERIMENTS

As was mentioned in Chapter 4, two different types of FeS_{mack} surfaces were prepared and used in anoxic dissolution experiments. They were: 1) pellets pressed from ~1 μ crystals of FeS synthesized from Fe and $H_2S(aq)$; and 2) non-porous coatings of FeS on elemental Fe. Extensive experimentation was carried out with the first type of surface and included experiments conducted in solutions of varying pH, T, and I (ionic strength) using pellets with a range of "surface areas" A.[†] The magnitude of pore-diffusion effects was investigated with FeS surfaces of the second type.

6.1 Results - Pellets of ~1 μ FeS_{mack}

In all cases, these pellets were prepared from Batch 6 FeS. The data presented in this section were always obtained using pellets which had been resurfaced as described in Section 4.2.3.

The dissolution behavior of these pellets was initially investigated using dilute, unbuffered HCl solutions of varying concentration

[†]The term "A" refers to the projected surface area of an FeS pellet, i.e., the area which it would have if it was completely flat. In reality, however, due to a certain degree of surface roughness, the real area of the exposed FeS was greater than A. It will be assumed in this thesis that the real surface area, A', was proportional to A, i.e., A' = fA, and that the "surface roughness factor" f ($\geq$ 1) was a constant from one disk to another. A discussion of what value would be a good estimate of f will appear in Chapter 7.

(10^{-5} - 10^{-3} M.)[†]. In these cases, the pH-time data were analyzed using Equation (5.18).

Preliminary experiments were conducted with 10^{-4} M HCl to determine the effects of stirring on dissolution rate. Stirring speed was varied between 50 - 900 rpm, the stirbar being located 2 cm directly below the disk. At speeds greater than 200 rpm, the dissolution rate became independent of stirring and therefore neither diffusion to the surface of reactant H^+ species nor diffusion away of product Fe^{2+}, HS^-, and H_2S species seemed to be limiting the dissolution rate of these FeS pellets. Unfortunately, one cannot now infer that diffusion is not playing any role in determining the dissolution rate of these FeS pellets. This is the case because the pores in the pellet are hydrodynamically isolated from the turbulent reaction mixture and consequently the transport of dissolved species into and out of these stagnant pores would be governed by the appropriate diffusion coefficients and concentration gradients. Estimates of the relative contributions of pore vs. surface dissolution will be discussed in Chapter 7.

Typical results of experiments carried out with 10^{-5} - 10^{-3} M HCl in 0.05 M NaCl (at a stirring rate of 600 rpm) are presented in Figure 6.1. The experimental data ($[H^+]$, M, vs. time, min.) are

---

[†]This pH regime (3-5) was selected for the first experiments because low pH solutions will tend to dissolve more FeS than solutions of higher pH. Consequently, the spectre of oxygen contamination would be less problematic since small amounts of O_2 will be less likely to oxidize large percentages of the dissolved FeS.

plotted for a number of different experiments. Corresponding to each experimental $[H^+]$ curve there is a calculated S_{TOT} curve which has been obtained using equation (5.17) and the $[H^+]$ data. The actual rates of any of these reactions evaluated at time t ($(dS_{TOT}/dt)_t$) may be similarly calculated.

For those experiments with an initial acidity of at least 5×10^{-5} M (pH = 4.3), the decay of $[H^+]$ is exponential (at least initially) inasmuch as a semilogarithmic plotting of $[H^+]$ vs. time is linear with a slope which is independent of the initial hydrogen ion concentration, $[H^+]_0$. In this pH regime then, this implies that the consumption of H^+ (viz. FeS pellet dissolution) follows an integrated rate law of the form

$$[H^+] = [H^+]_0 e^{-k_{obs} t} \tag{6.2}$$

Differentiating,

$$\frac{d[H^+]}{dt} = -k_{obs}[H^+]_0 e^{-k_{obs} t} = -k_{obs}[H^+] \tag{6.3}$$

where k_{obs} is the observed rate constant, dependent on many experimental parameters. We have for the unbuffered solutions:

$$-\Delta[H^+] = S_{TOT}(2\alpha_0 + \alpha_1 - \alpha_{FeOH}) \tag{5.17}$$

Since $\alpha_0 \simeq 1$ and α_1 and $\alpha_{FeOH} \simeq 0$ in this pH regime,

$$-([H^+] - [H^+]_0) \simeq 2\, S_{TOT} \tag{6.4}$$

Differentiating with respect to time

$$\frac{-d[H^+]}{dt} = k_{obs}\,[H^+] \simeq 2\,\frac{dS_{TOT}}{dt} \tag{6.5}$$

$$\frac{dS_{TOT}}{dt} \simeq \frac{1}{2}k_{obs}\,[H^+] \tag{6.6}$$

Equation (6.6) states that the rate of dissolution of the FeS pellets at pH $\leq$ 4.7 is proportional to the bulk solution $[H^+]$ value.

The results of experiments designed to determine whether this dissolution rate is first order in disk area A as well are presented in Figure 6.2. These data indicate that this is indeed the case. If it is assumed that the activity of the hydrogen ion, $a_{H^+} = \gamma_{H^+}\,[H^+]$, is the important variable here, and if account is also taken of the dependence on the reactor volume V, equation 6.6 may be rewritten:

$$\frac{dS_{TOT}}{dt} = \frac{1}{2}k_{obs}\,[H^+] = (k_1 A/V)\gamma_{H^+}[H^+] \tag{6.7}$$

$$k_{obs} = 2k_1 A\gamma_{H^+}/V \tag{6.8}$$

It is to be hoped that k_1 may be linked to some characteristic step in the overall process of FeS dissolution.

Table 6.1 contains data typical of those obtained with solutions of varying initial acidity (5×10^{-5} - 10^{-3} M). Experiments with $[H^+]_0$

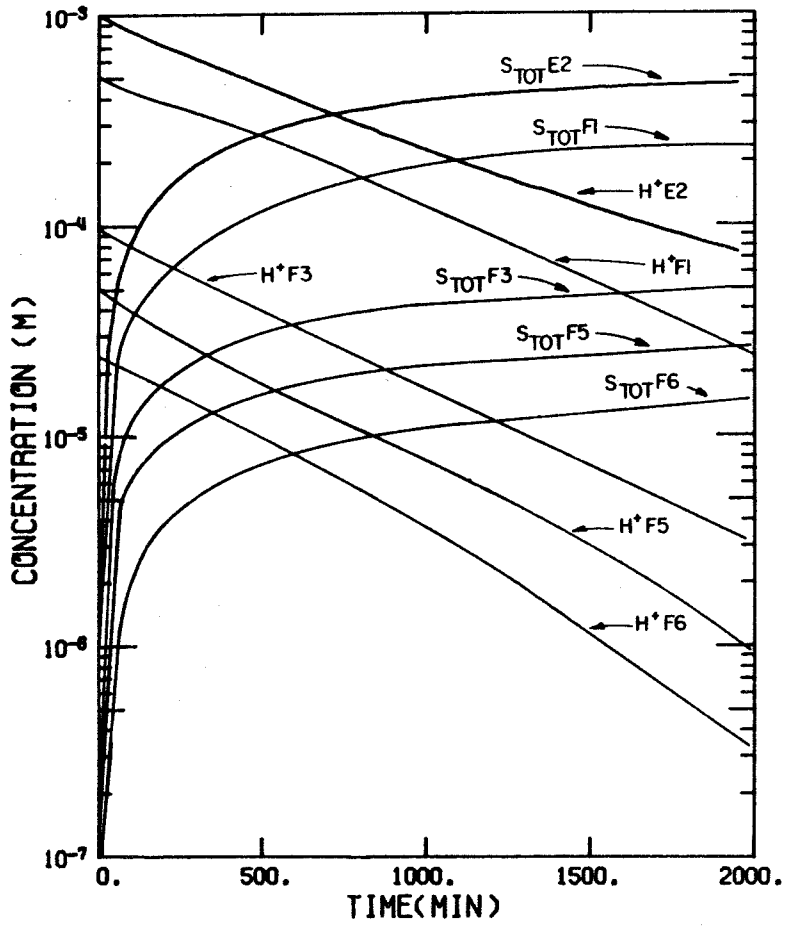

Figure 6.1a

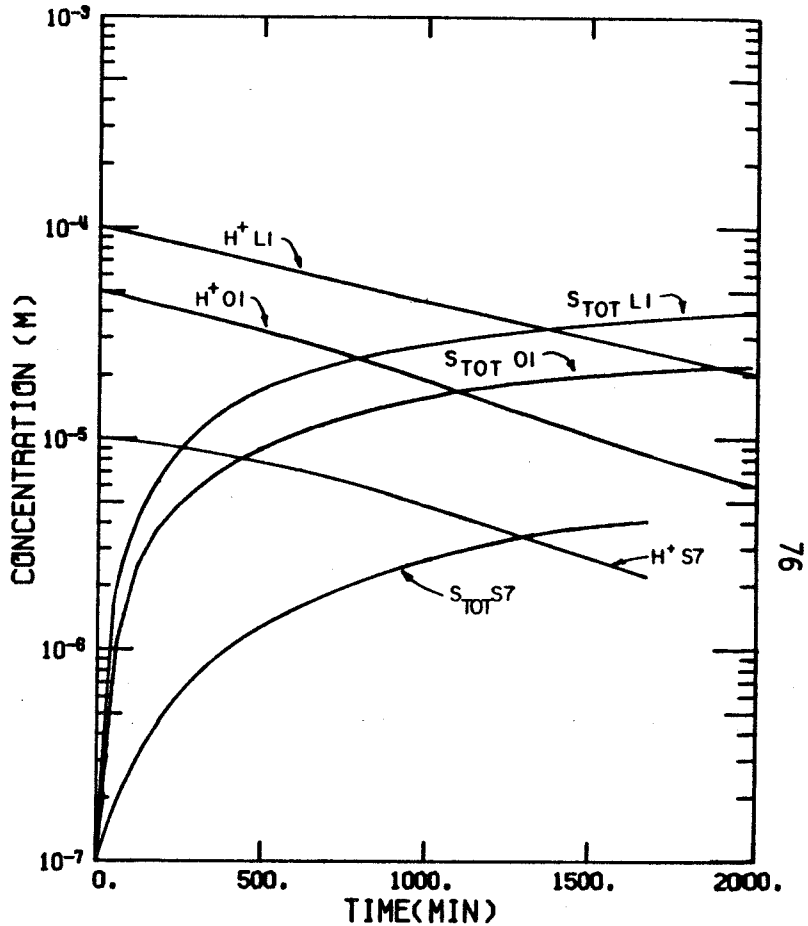

Figure 6.1b

Figures 6.1a,b Typical results of experiments carried out with 10^{-5}-10^{-3} M HCl solutions. Background electrolyte concentration is 0.05 M NaCl, T = 25°C, and reactor volume V = 0.31 ℓ. The H^+ curves were obtained experimentally, and the S_{TOT} curves were calculated using equation (5.18). In Figure 6.1a, the pellet surface area = 1.27 cm^2. In Figure 6.2b, A = 0.66 cm^2.

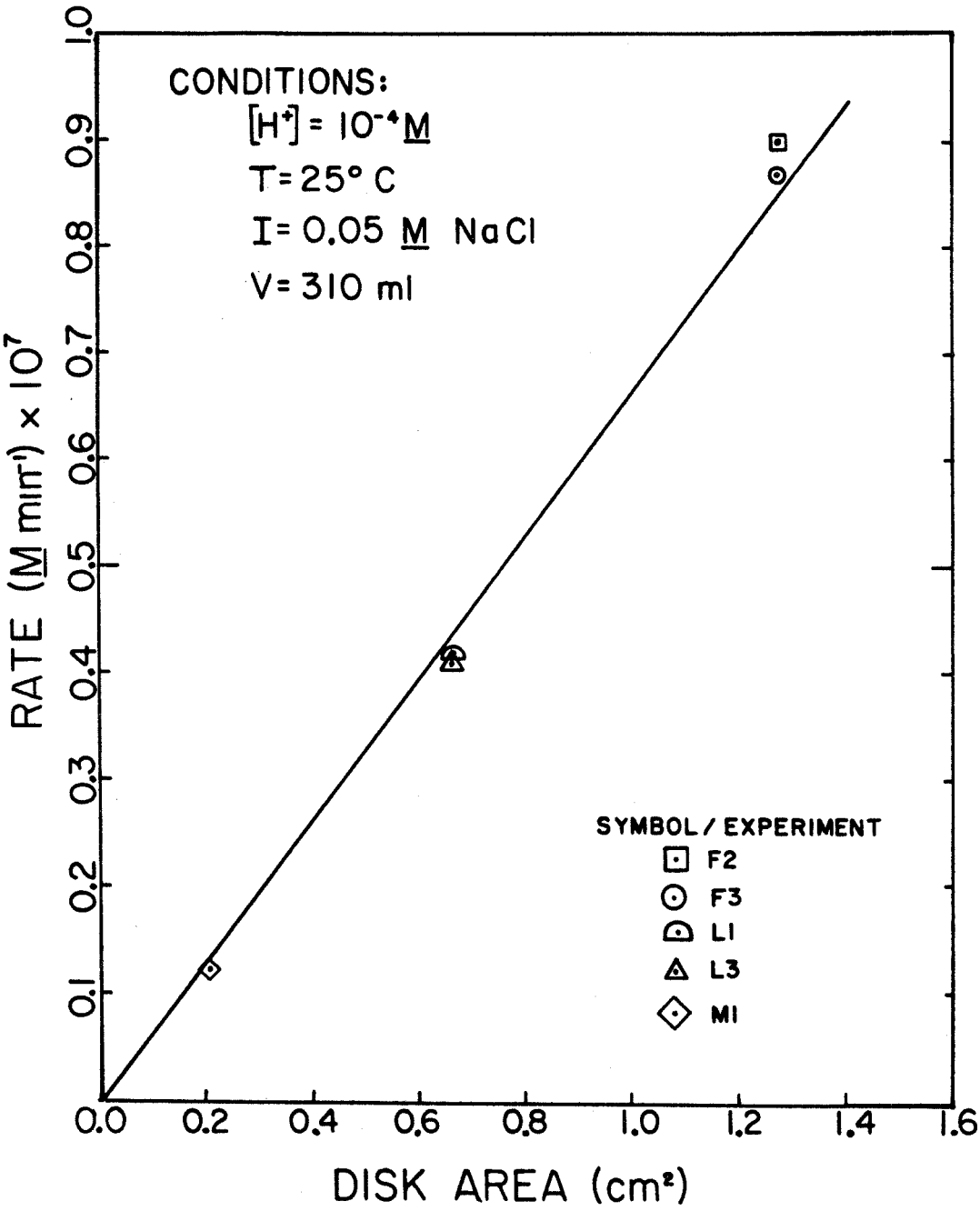

Figure 6.2. Rate of dissolution (ds_{TOT}/dt) vs. disk area A (cm^2) at 25°C and $[H^+] = 10^{-4}$ M.

Table 6.1 Results of experiments carried out with unbuffered solutions of varying initial acidity.

Experiment	$[H^+]$ initial, M	[Fe] x 10^4 M		Yield, %	k_1 (cm/min)
		Found	Predicted		
B1	10^{-3}	5.37	4.58	117	0.23
E1	10^{-3}	5.50	5.08	108	0.26
E2	10^{-3}	4.67	4.92	95	0.22
E3	10^{-3}	5.12	5.06	101	0.18
F1	$5x10^{-4}$	2.37	2.43	98	0.20
F2	10^{-4}	0.60	0.68	88	0.27
L1	10^{-4}	0.80	0.68	118	0.24
L3	10^{-4}	0.48	0.44	109	0.24
P6	$5x10^{-5}$	0.27	0.26	104	0.16
S1	10^{-4}	0.38	0.34	112	0.19
S13	$5x10^{-5}$	0.20	0.18	111	0.19
			Average:	105	0.22
			Std. Dev.:	9	0.04

Conditions:

H^+ added as HCl

[NaCl] = 0.05 M

T = 25°C

A = 0.66-1.27 cm

V = 0.310 ℓ

lower than 5×10^{-5} M are not included due to the deviation (see below) from the simple behavior characterized by equation (6.7). The column labeled "[Fe] predicted" is the [Fe] which was calculated (by Equation (5.17)) for the solution at the time at which that particular dissolution experiment was terminated and the sample for analysis was removed. The average yield of 105% is very good. The standard deviation on the yield was 9%. The values of k_1 were obtained from a least squares fit of the first 500 minutes of the data to the equation

$$\log_{10}[H^+] = \log_{10}[H^+]_0 - 2k_1 A \gamma_{H^+} t/(2.303V) \qquad (6.9)$$

The experimental agreement on k_1 is quite good, especially since the reaction being studied is heterogeneous in nature. The average value of k_1 for these experiments was 0.22 cm/min, and the standard deviation was 0.04 cm/min.

The effects of ionic strength (I) on k_1 are slight. Experiments conducted with 10^{-4} M HCl solutions indicated that k_1 may decrease by approximately 10% when I is increased from 0.05 M to 0.20 M, but as is evident from Table 6.1, a 10% change in observed k_1 values may not be meaningful.

An estimation of the dependence of k_1 on T was provided by experiments carried out over a range of temperatures (5°-25°C). In the analysis of these data, it was presumed that this dependence was of the so-called "Arrhenius" form, i.e., $k_1 = Ae^{-E_a/RT}$ (see, for example, Amdur and Hammes, 1966). A is termed the "pre-exponential" factor, E_a is the "activation energy", and R and T have their usual meanings.

A plot of $\log_{10}k$ vs. $\frac{1}{T}$ (°Kelvin^{-1}) will have a slope of $\frac{E_a}{2.303 \cdot R}$. Such a plot for k_1 is found in Figure 6.3. The line of best fit (calculated by least squares) has been drawn through the data and its slope implies an E_a of 6.8 kcal/mole.

Dissolution experiments which were initiated at pH values greater than 5 were carried out in solutions weakly buffered with a series of compounds with pK_a's in the 5-7 range: HOAc, $pK_a \simeq 4.7$; MES, $pK_a \simeq 6.2$; $pK_a \simeq 7.2$.[†] Since these solutions were buffered, Figure 6.4 presents the computed rate (dS_{TOT}/dt) vs. time data rather than the relatively uninteresting $[H^+]$ vs. time plots. In addition, for comparison, rate data obtained with unbuffered solutions with initial pH's of less than 5 were also plotted. The range of pH values cited in Figure 6.4 for each of the experiments represents the extent to which the pH varied over the time interval over which data has been plotted. For example, at the times 0 and 2100 min., the measured pH's for experiment E1 were 3.00 and 4.30, respectively.

The fact that when $[H^+]_0 > 10^{-5}\underline{M}$ the dissolution rate is proportional to $[H^+]$ is clearly evidenced by the logarithmic dependence of the initial rate (t = 0) on $[H^+]_0$ for experiments E1, F1, and L3. This observation is no longer valid, however, for experiments L2, L4, L6, and N7. Indeed, as the pH is increased above 5, it appears as though the dissolution rate becomes independent of pH.

[†]HOAc = acetic acid
MES = 2-(N-Morpholino)ethane sulfonic acid
MOPS = 3-(N-Morpholino)propane sulfonic acid

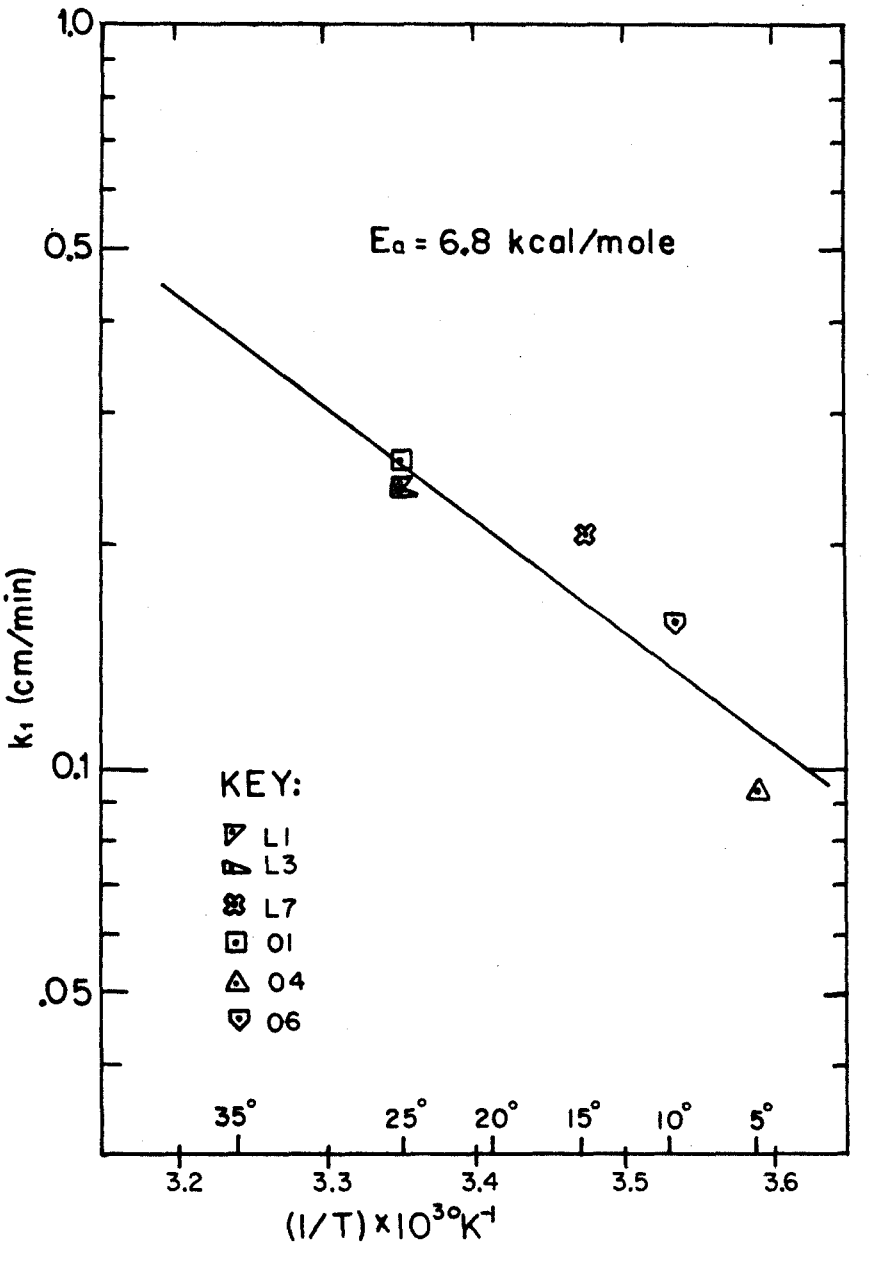

Figure 6.3. Estimation of Arrhenius activation energy E_a for k_1 based on slope of log k_1 vs. $\frac{1}{T}$, assuming $k_1 = Ae^{-E_a/RT}$. A = constant, R = gas constant, T = temperature, degrees Kelvin.

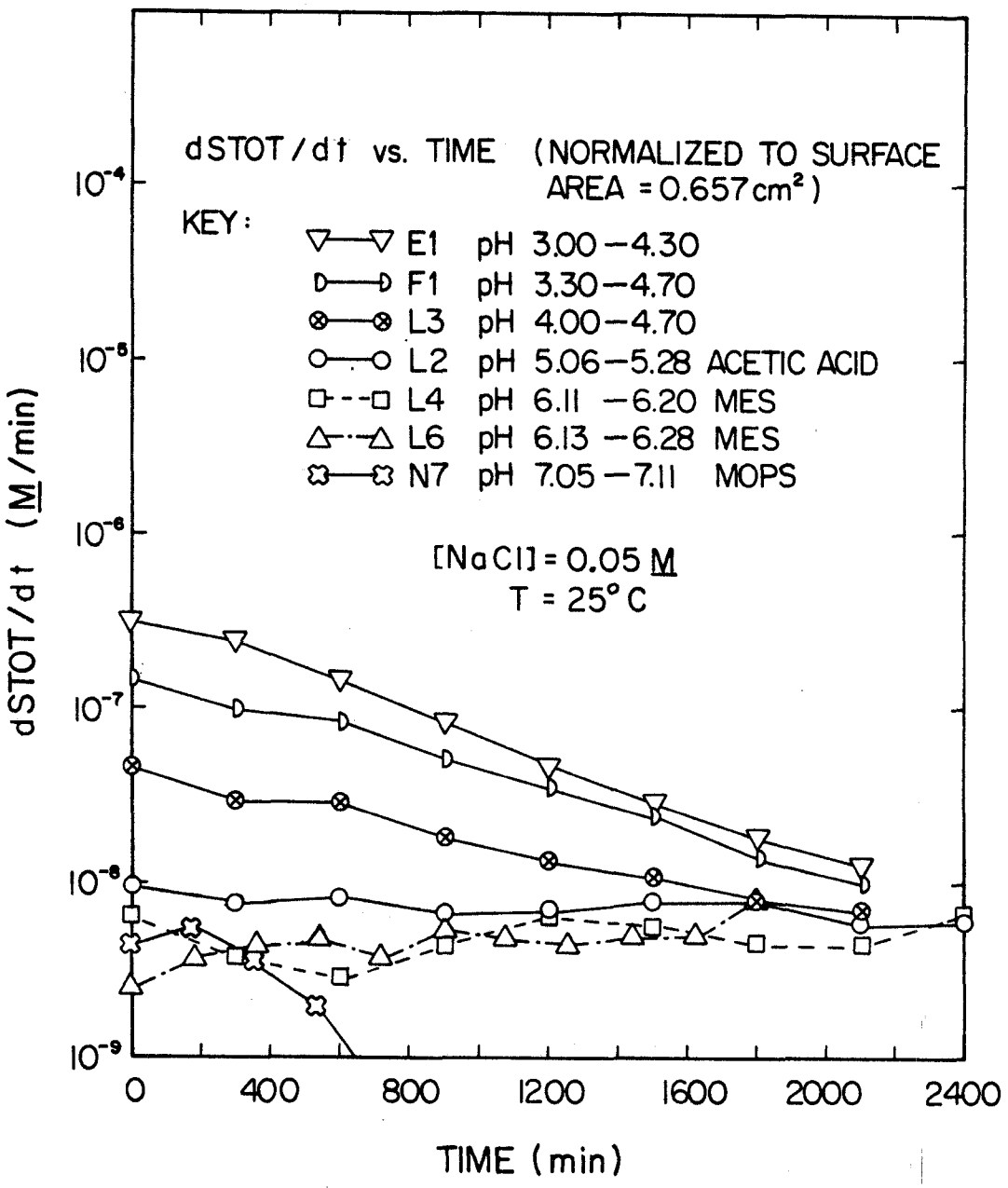

Figure 6.4. Dissolution rate (dSTOT/dt, M/min) vs. time (min) for experiments carried out over a range of pH values. A = .66 cm^2 for expts. L2,L3,L4,L6,N7. A = 1.27 cm^2 for expts. E1 and F1; the rate data for E1 and F1 has consequently been divided by 2 before being plotted so as to facilitate comparisons.

Thus, although Equation (6.7) represents very well the dissolution rate behavior when pH < 5, it seems to break down above this value. This observed deviation from Equation (6.7) suggests that there may be an additional term in the rate law which is independent of $[H^+]$. Assuming that the contribution of this term to the observed dissolution rate would be proportional to the exposed surface area of the pellet, these results imply that a more accurate formulation of the rate law may be

$$\frac{ds_{TOT}}{dt} = \frac{A}{V}\left(k_1 \gamma_{H^+}[H^+] + k_2\right) \tag{6.10}$$

If one divides Equation 6.10 by a_{H^+}, we obtain

$$\left(\frac{ds_{TOT}}{dt}\right)/a_{H^+} = \frac{A}{V}\left(k_1 + \frac{k_2}{a_{H^+}}\right) \tag{6.11}$$

When $k_1 >> \frac{k_2}{a_{H^+}}$ (i.e., low pH) the left hand side of (6.11) would be independent of a_{H^+}. Conversely, under high pH conditions, $\frac{ds_{TOT}}{dt}/a_{H^+}$ would be inversely proportional to a_{H^+}. The values of k_1, k_2, A, and V would determine the actual appearance of a plot of Equation 6.11. Experiments such as L2, L4, and N7 indicate that k_2 is close to 2×10^{-9} moles/cm^2minute. The solid line in Figure 6.5 has been drawn using this value of k_2, and with k_1 = 0.2 cm/min (see Table 6.1), A = 0.66 cm^2, and V = 0.31ℓ. In addition, experimental points from several experiments conducted over a range of pH have been plotted. The overall fit seems quite good. In several cases (E2, L1, and O1) the initial (higher a_{H^+}) points tend to agree better than later points (lower a_{H^+} values). A

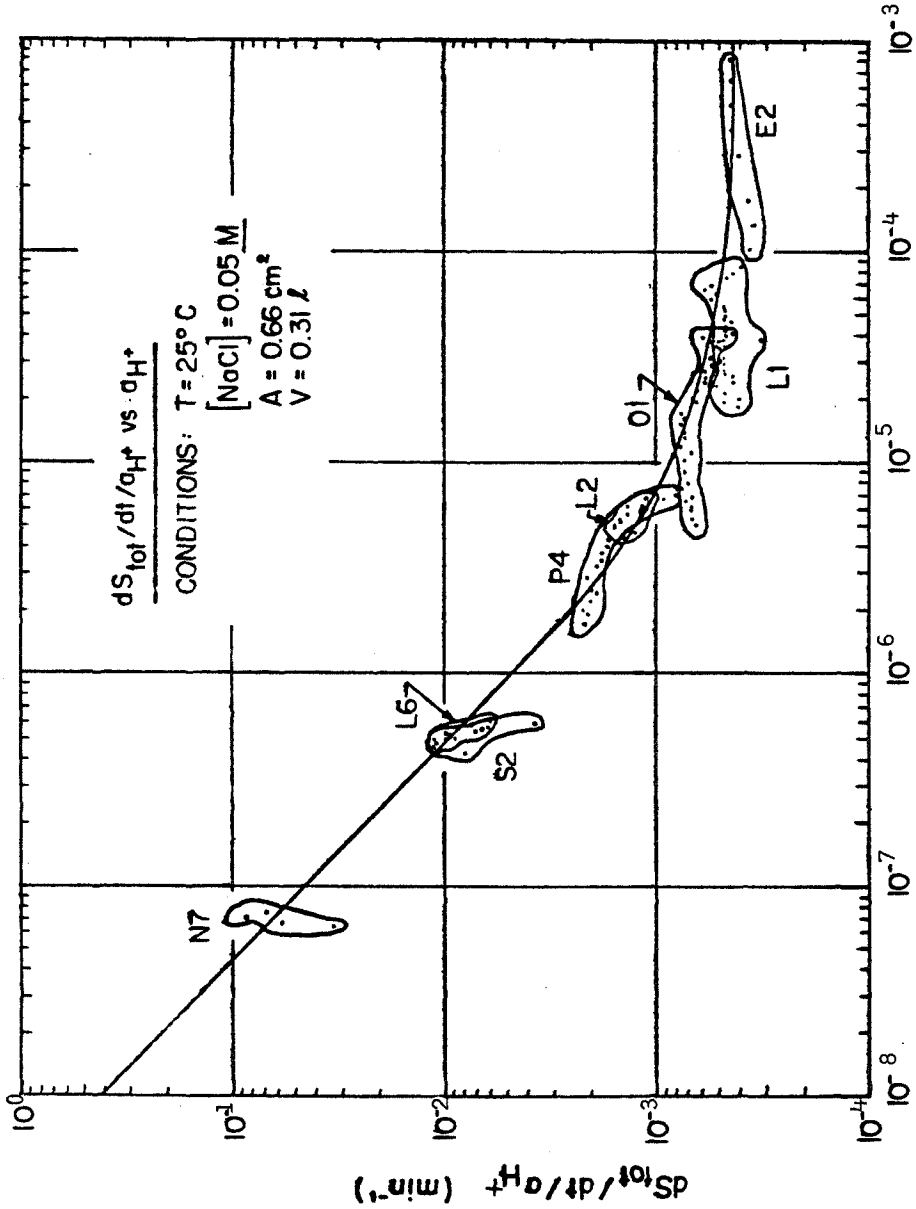

Figure 6.5 Plot of $dS_{TOT}/dt/a_{H^+}$ vs. a_{H^+} for several experiments. Solid line drawn for $k_1 = 0.2$ cm/min, $k_2 = 2 \times 10^{-9}$ moles/cm^{2}min. All experiments cited used pellets with A = 0.66 cm^2 except E2 in which A = 1.27 cm^2. Data from E2 consequently normalized to A = 0.66 cm^2 before plotting.

likely reason for this is that the concentration of dissolved ferrous sulfide is building up as the reaction proceeds and this undoubtedly slows down the observed dissolution rate due to the initiation of back reactions.

The data obtained from the higher-pH regime (4.7-7.5) experiments were therefore fit to Equation (6.10). For experiments carried out at pH $\geq$ 7, the dissolution medium contained up to 50% of the predicted saturation S_{TOT} after only 500 minutes of dissolution. In such cases, the observed rate did not hold constant and k_2 had to be estimated by extrapolating the rate back to time zero. Since the k_1 term makes a negligible contribution at pH $\geq$ 7, these reported values of k_2 were simply equated to $\frac{V}{A} \cdot (ds_{TOT}/dt)_{t=0}$. In the analysis of the pH $\leq$ 6 buffered runs the $k_1 \gamma_{H^+}[H^+]$ term is not negligible (at pH 5, $k_1[H^+] \simeq 2 \times 10^{-9}$ moles/cm^{2}min). In such cases, estimates of k_1 were obtained from the pH $\leq$ 4.7 runs of the same series (i.e., with the same letter prefix) and then used in the evaluation of k_2 through the arithmetic averaging of the quantity $\left[\frac{ds_{TOT}}{dt} \cdot \frac{V}{A} - k_1 \gamma_{H^+}[H^+]\right] \simeq k_2$ (measured every $\sim$ 200 minutes) over the first 2000 minutes of the dissolution reaction.

A summary of k_2 values obtained from experiments conducted at 25°C and at pH's where the k_2 term affects the rate law is contained in Table 6.2. When an arithmetic average was used to estimate k_2, the corresponding standard deviation is also listed. The average yield for the seven experiments was 90% and the standard deviation on the yield was 26%. The average of the measured k_2 values was 1.9 x 10^{-9} moles/cm^{2}minute. A priori, it seems possible that the k_2 term

Table 6.2 Results of experiments carried out with solutions buffered at varying pH's.

Experiment	Conditions*	[Fe] x 10^5M Found	[Fe] x 10^5M Predicted	Yield%	k_2 x 10^9 $\frac{moles}{cm^2 min}$	Standard deviation on k_2
L2	$4x10^{-4}$ M HOAc, $3x10^{-4}$ M NaOH; pH 5.06-5.28	1.80	2.00	90	2.1	0.29
L4	$4x10^{-4}$ M MES, $3x10^{-4}$ M NaOH; pH 6.11-6.20	1.00	1.37	73	2.2	0.64
L6	$2x10^{-4}$ M MES, $1x10^{-4}$ M NaOH; pH 6.13-6.28	1.09	2.14	51	1.9	0.44
N7	$1x10^{-4}$ M MOPS, $0.5x10^{-4}$ M NaOH; pH 7.05-7.12	0.38	0.34	112	1.9	-
P4	$2x10^{-4}$ M HOAc, $1.5x10^{-4}$ M NaOH; pH 5.06-5.71	1.66	2.21	75	2.4	0.36
P5	$1x10^{-4}$ M MES, $0.5x10^{-4}$ M, NaOH; pH 6.07-6.22	0.53	0.58	92	0.9	0.15
S2	$1x10^{-4}$ M MES, $0.5x10^{-4}$ M NaOH; pH 6.13-6.32	0.80	0.62	130	1.9	0.55
			Average:	90	1.9	0.41
			Standard deviation:	26	0.48	

*Batch 1, 0.05 M NaCl, T = 25°C

HOAc ≡ acetic acid, $pK_a \sim 4.7$

MES ≡ N-morpholino ethane sulfonic acid, $pK_a \sim 6.2$

MOPS ≡ 2-N-morpholino propane sulfonic acid, $pK_a \sim 7.3$.

simply reflects either an attack by, or diffusive step involving the conjugate acid HB. Therefore, while k_2 might be independent of pH, it might simply equal some k_2' times [HB]. That this is not the case is indicated by the fact that the experimental values of k_2 obtained seems independent of [HB] ($\simeq [HB]_{added} - [NaOH]_{added} = 10^{-4}$ M for Expt. L2).

Experiments were also conducted to investigate the effects of ionic strength and temperature on k_2. They were all carried out using solutions buffered with 10^{-4} M MES solutions which were equimolar (i.e., 5×10^{-5} M) in the conjugate acid and this conjugate base. Over the range 0.05 - 0.30 M NaCl, the effects of ionic strength on k_2 seem to be slight (Figure 6.6). The value of 4.4×10^{-9} moles/cm^{2}minute for k_2 observed at I = 0.06 M, however, was appreciably larger than the $\sim 2 \times 10^{-9}$ moles/cm^{2}minute typically observed in media of lower ionic strength.

An estimation of the Arrhenius activation energy E_a was obtained from experiments carried out over the temperature 5° - 25°C. The results have been plotted in the usual Arrhenius format (Figure 6.7). The line of best fit (calculated by least squares) has been drawn through the data and its slope implies an E_a of 7.3 kcal/mole.

After series M, an SEM photo of the surface of the pellet was taken (Figure 6.8). The type of scrape marks typical of resurfaced disks are no longer visible, and some of the details of the individual crystals are once again distinguishable. Apparently the scrape marks dissolve away.

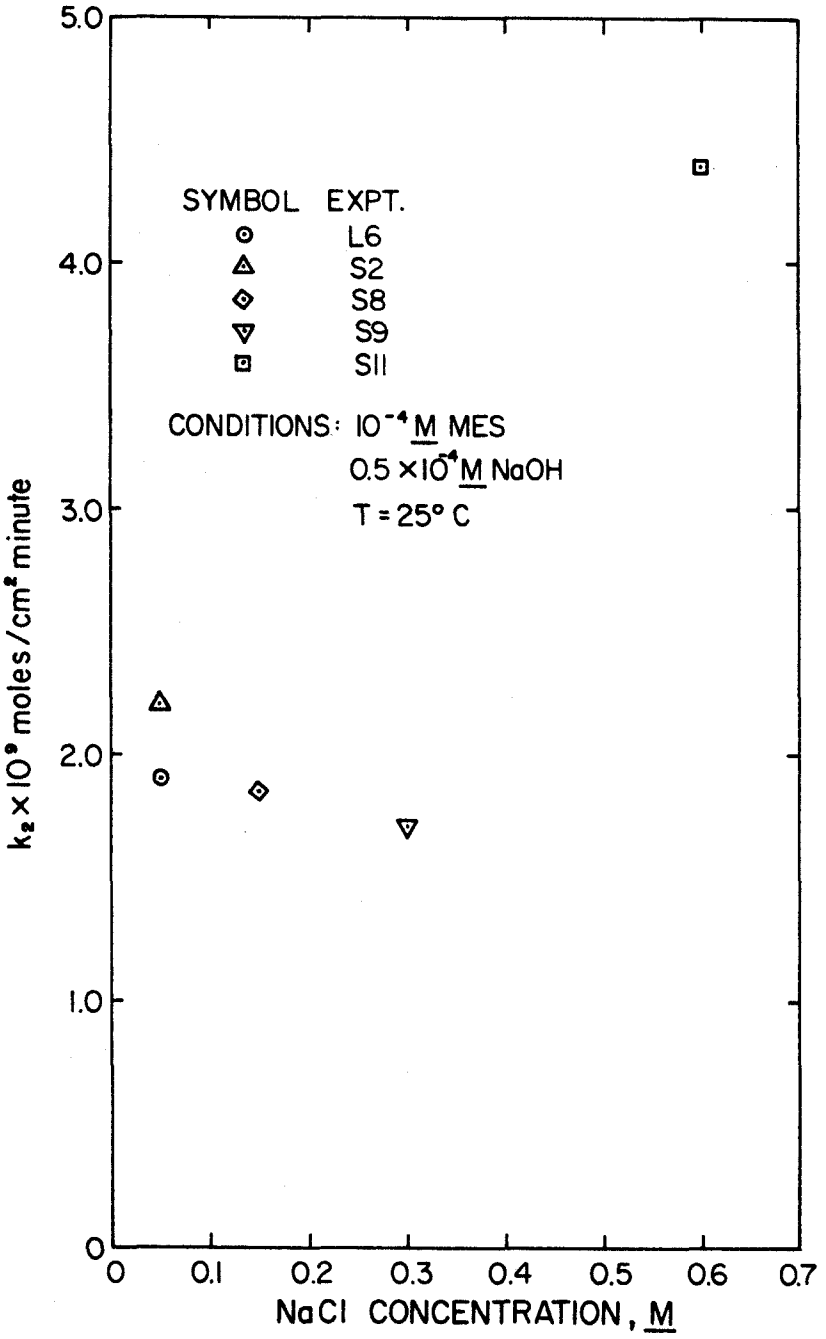

Figure 6.6 Effects of ionic strength on k_2. For I = 0.05 - 0.2 M, k_2 centers closely around 2×10^{-9} moles/cm^2 minute. The value of $\sim 4.5 \times 10^{-9}$ moles/cm^2 minute observed at I = 0.6 M seems anomalous.

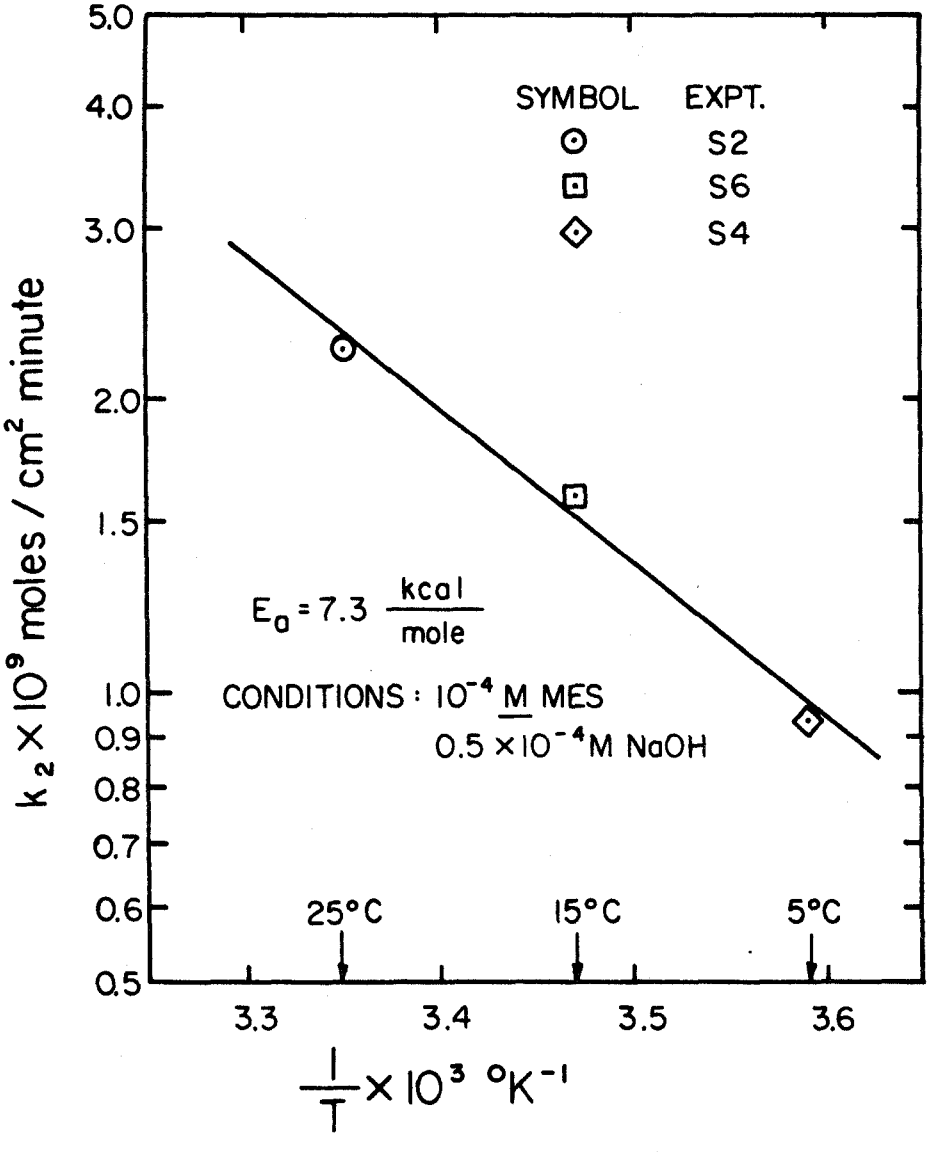

Figure 6.7 Estimation of Arrhenius activation energy E_a for k_2 based on slope of log k_2 vs. $\frac{1}{T}$.

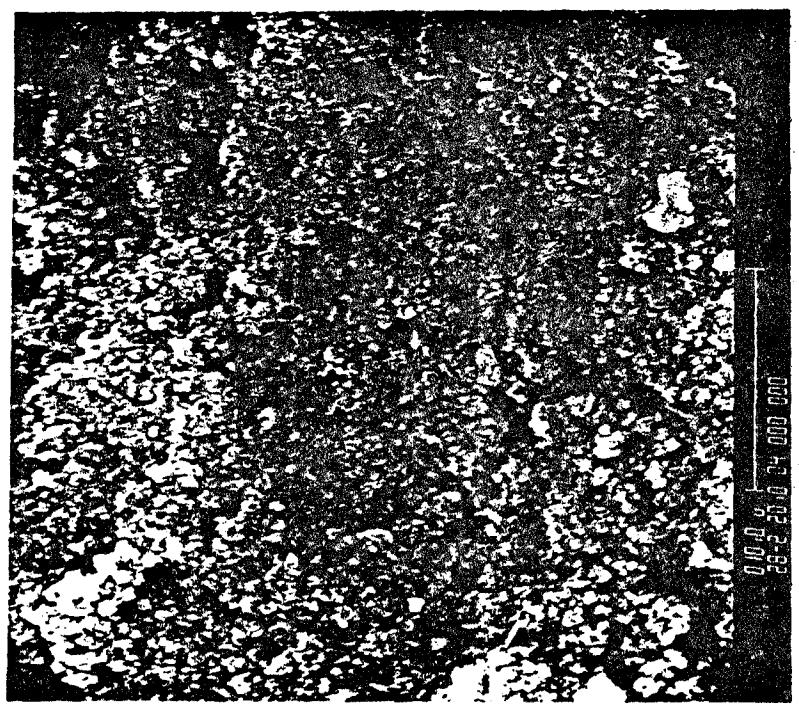

Figure 6.8 (Magnification 2,800 X)
Scanning electron micrograph of FeS_{mack}
pellet surface after series M.

The effects of trace levels of copper (added as $CuCl_2$) on the dissolution rates of the FeS pellets were also briefly investigated. Experiments were conducted in dilute HCl solutions of pH $\sim$5 (T = 25°C, I = .05 M NaCl) so that the effects on k_1 as well as k_2 might be simultaneously observed. For experiment S16, the $[H^+]_0$ and $[Cu]_0$ were 2×10^{-5} M and 0.052 ppm (= 8.20×10^{-7}M), respectively. The dissolution rates observed in this experiment were indistinguishable from those observed during S10 (same $[H^+]_0$, T, and I, but no copper). The [Fe] found at the conclusion of S16 was 1.03×10^{-5}M. Since the predicted [Fe] was 8.16×10^{-6}M, the yield was 120%. Interestingly, the [Cu] found at the end of S16 was only 4.10×10^{-7}, one half of the $[Cu]_0$. Experiment S18 was conducted with $[H^+]_0 = 10^{-5}$M and $[Cu]_0$ = 0.93 ppm (= 1.46×10^{-5}M). In Figure 6.9, the experimental $[H^+]$ curve and the computed S_{TOT} curve are compared to the corresponding curves of S7 which was conducted with [Cu] = 0. It is evident that ~ppm levels of Cu(II) can substantially retard the dissolution rates of these FeS pellets. It is, unfortunately, difficult to determine which of the two terms in the rate equation was more affected by the presence of the Cu(II) since the severity of this inhibition increases with time. This rate deceleration in S18 is evidenced by the concave-up nature of the $[H^+]$ curve.

The calculated terminal [Fe] for S18 is 1.43×10^{-6}M. In actuality, 9.90×10^{-6}M was found. This corresponds to a 692% yield! On the other hand, while the $[Cu]_0 = 1.46 \times 10^{-5}$M, the [Cu] found at the end of experiment S18 was only 8.78×10^{-6}M. It seems likely that

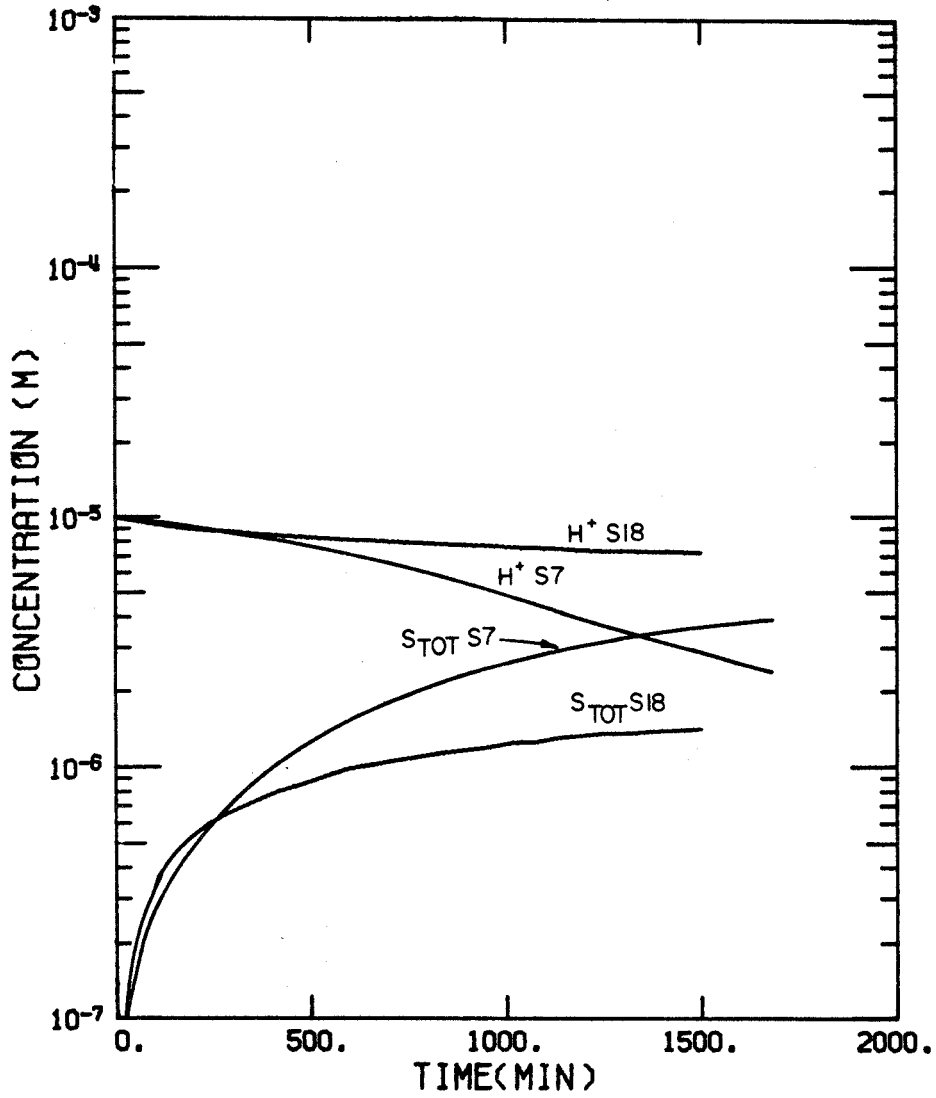

Figure 6.9 The results of dissolution experiments with FeS pellets. $[H^+]_0 = 10^{-5}$M HCl, background electrolyte is 0.05M NaCl, T = 25°, A = 0.66 cm^2, V = 0.31ℓ. The H^+ curves were obtained experimentally. The S_{TOT} curves were calculated using equation (2.18). $[Cu]_0$ for S7 = 0, $[Cu]_0$ for S18 = 0.93 ppm (= 1.5×10^{-5}M).

this depletion of Cu and the high Fe levels are linked. Since copper forms a very insoluble metal sulfide ($K_{so} \simeq 10^{-35}$), the depletion of the Cu and the excess Fe may be due to the reaction

$$Cu(II)_{aq} + FeS \rightarrow CuS + Fe(II)_{aq} \qquad (6.12)$$

Since the FeS dissolution reaction may still proceed, and since (6.12) neither consumes nor produces protons, the Fe found in the solution should equal the sum of the Fe predicted by equation (5.17) plus that solubilized by the ion exchange reaction (6.12). In other words, if (6.12) is the only reaction responsible for the loss of Cu from solution, the solution [Fe] should equal the quantity ($[Fe]_{predicted} - \Delta[Cu]$) where $\Delta[Cu]$ represents the change in the copper concentration. The equation for the theoretical % yield may therefore be modified to read

$$\% \text{ yield} = \frac{[Fe]_{found}}{[Fe]_{predicted} - \Delta[Cu]} \times 100 \qquad (6.13)$$

where $[Fe]_{predicted}$ is the value of [Fe] expected based on the pH change. Using equation 6.13, we calculate for experiment S18: % yield = $100 \times (9.9 \pm 0.5) \times 10^{-6} / [1.43 \times 10^{-6} - (8.8 \pm 0.4) \times 10^{-6} + (1.5 \pm .07) \times 10^{-5}] = 133\% \pm 25\%$. This calculation involved more than one analytical result, and an error ±5% was assumed for all analyses except that for pH. Thus, although a 133% yield is high, considering the ±25% error interval, it is not excessively large. The fact that (6.13) does give a value close to 100% is good evidence that the (6.12) is affecting the [Fe]. Although the [Cu] used in

experiment S16 (8.2×10^{-7} M = 0.052 ppm) was not high enough to affect the Fe yield, its reduction over the course of the experiment to 4.1×10^{-7} M provides further evidence for the importance of (6.12).

6.2 Results - Non-porous Fe/FeS_{mack} Surfaces

The dissolution behavior of these surfaces was investigated using dilute solutions of HCl (expts. T2, T3) as well as a solution buffered with MES (expt. T1). The results of T2 and T3 are plotted (along with S7 for comparison) in Figure 6.10. In general, it may be said that the dissolution rates of these surfaces are substantially greater than those observed for pressed pellets of FeS_{mack}. The agreement between T2 and T3 is good.

In order to determine if the rate data obtained exhibited the same type of functionality observed for the pellets, a plot of $dS_{TOT}/dt/a_{H+}$ vs. a_{H+} was prepared and is presented in Figure 6.11. The line which was fit to the pellet data, labeled "A" (calculated using (6.10) with k_1 = 0.2 cm/min and $k_2 = 2 \times 10^{-9}$ moles/cm^2min) is also included. Both line A and the data from Series T have the characteristics that:1) below a certain a_{H+} value, the slope is a constant, negative value; and 2) above this a_{H+} value, the slope approaches zero. In the case of line A, when $a_{H+} \lesssim 4 \times 10^{-6}$ M, the slope is -1 (because in this region $dS_{TOT}/dt/a_{H+} = \frac{A}{V} k_2 a_{H+}^{-1}$). The corresponding slope of the Series T data seems to be $\sim$-1.5. It is not immediately clear why these slopes should differ. Nevertheless, it will be assumed for the moment that the rate law describing the dissolution of these surfaces is

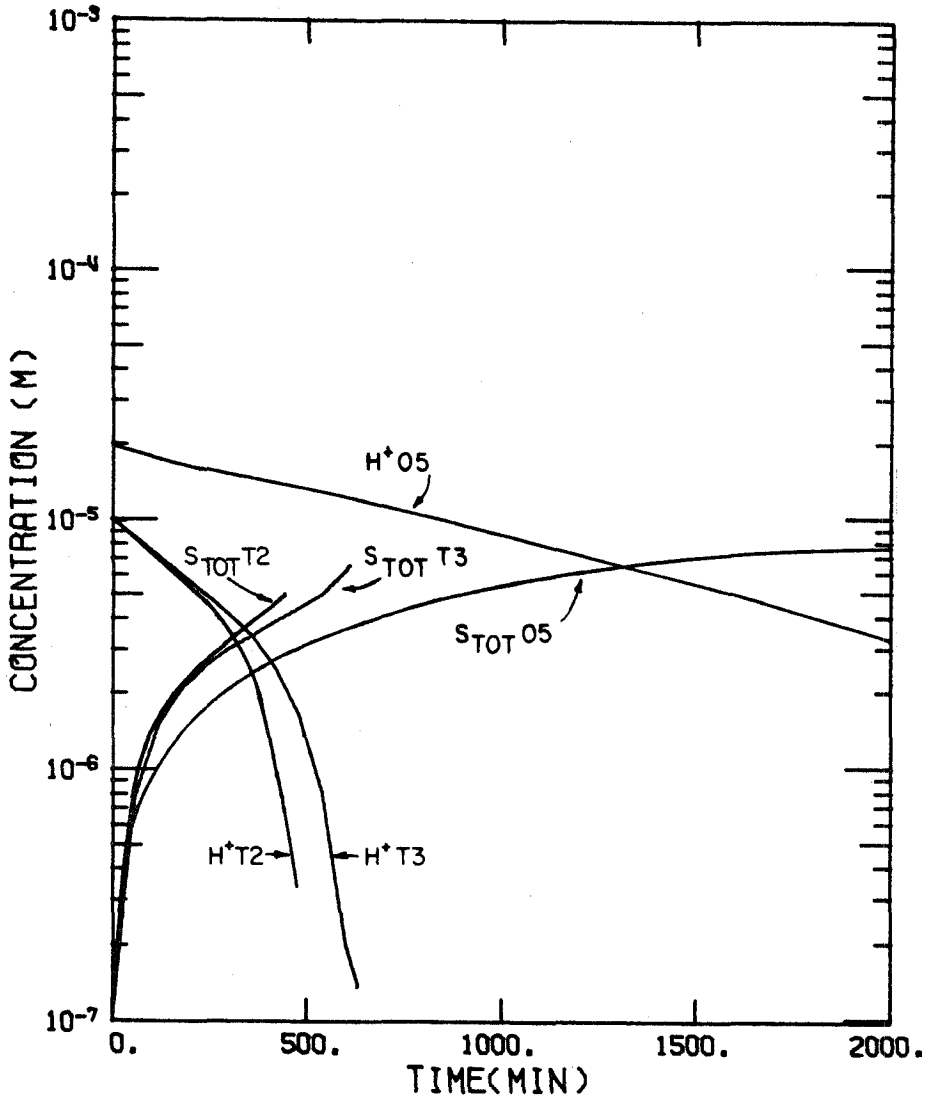

Figure 6.10 The curves labelled T2 and T3 are the results of dissolution experiments carried out with non-porous Fe/FeS surfaces. The 05 curves were obtained with FeS pellets. Background electrolyte is 0.05 M NaCl, T = 25°C, V = 0.3lℓ. A = 0.66 cm^2 for experiment 05 and 1.26 cm^2 for T experiments. The H^+ curves were obtained experimentally. The S_{TOT} curves were calculated using (5.17).

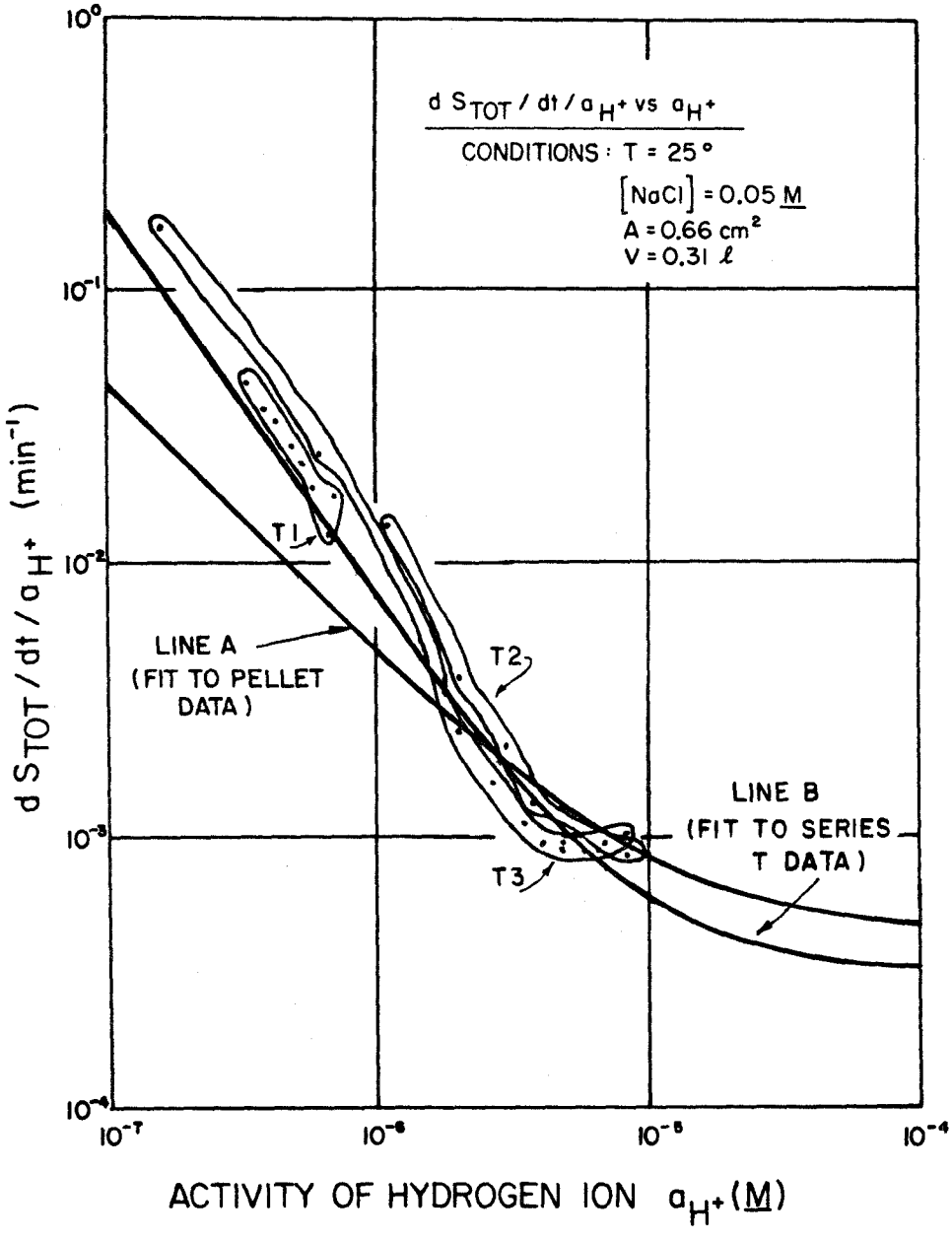

Figure 6.11 Plot of $d S_{TOT}/dt/a_{H^+}$ vs. a_{H^+} for several experiments carried out with non-porous FeS surfaces (Series T). The line fit to this data is Line B. Line A (area A = 0.66 cm^2), the fit to the pellet data is also shown. To facilitate comparisons between the pellet and non-porous data, the non-porous data (obtained using a surface area of 1.26 cm^2) was normalized to what would be expected for A = 0.66 cm^2.

$$\frac{dS_{TOT}}{dt} = \frac{A}{V} (k_1^* \gamma_{H^+} [H^+] + k_2^* [H^+]^{-0.5}) \qquad (6.14)$$

or, dividing by a_{H^+},

$$\frac{dS_{TOT}/dt}{a_{H^+}} = \frac{A}{V} (k_1^* + k_2^* \gamma_{H^+}^{0.5} a_{H^+}^{-1.5}) \qquad (6.15)$$

The k_1^* term would account for the leveling off of the $dS_{TOT}/dt/a_{H^+}$ vs. a_{H^+} curve, and the k_2^* term accounts for the slope of -1.5 in the low a_{H^+} region. Assuming this functionality for the rate law, a line has been fit by least squares to the Series T data and is labelled "B" in Figure 6.10. The values of k_1^* and k_2^* obtained from this fit are 0.15 cm/min and 1.2×10^{-13} moles$^{1.5}$/(cm$^{3.5}$min), respectively. It seems from the data of T2 and T3 that line B underestimates the rates at $a_{H^+} \geq 7 \times 10^{-6}$ M. There are too few data points above this value, however, to pull up the least squares fit. An attempt to obtain data at higher acidities so as to allow a more accurate determination of k_1^* was not successful: the thin FeS layer was quickly reduced to zero thickness at this high $[H^+]$, exposing the underlying Fe surface. If one assumes that the value of dS_{TOT}/dt is indeed being determined solely by a strong k_1^* term in this region ($a_{H^+} \sim 0.6 - 1.0 \times 10^{-5}$ M), the value of k_1^* would have to be close to ~ 0.5 cm/min.

CHAPTER 7

DISCUSSION OF RESULTS OF DISSOLUTION EXPERIMENTS

7.1 Introduction

As was mentioned in Chapter 2, the rate of a dissolution reaction may be controlled either by the rate of transport processes or by the velocity of the slowest step (also termed the "rate-determining step") in the chemical reaction sequence. Intermediate situations may also occur, with both transport and chemical processes active in determining the observed reaction rate. The available rate data must therefore first be examined for indications of either chemical or transport control. If it should be concluded that a given term in the rate equation is caused by some unknown chemical step in the dissolution process, conjectures may then be made as to its character. If transport effects seem important, it may still be possible to obtain a lower bound for the rate of the reaction sequence envisioned to be responsible for that term.

7.2 Discussion of Rate Constants

7.2.1 k_1

The rate law observed for the dissolution of pellets pressed from $\sim 1\mu$ crystals of FeS_{mack} was

$$\frac{dS_{TOT}}{dt} = \frac{A}{V}\left(k_1 \gamma [H^+] + k_2\right) \qquad (6.10)$$

where γ_{H^+} has been abbreviated to γ for convenience. We may rewrite

(6.10) in terms of the flux F_S (moles/cm^{2}min) of total sulfide (or iron, since $F_S = F_{Fe}$)

$$F_S = \frac{V}{A}\frac{dS_{TOT}}{dt} = k_1\gamma[H^+] + k_2 \qquad (7.1)$$

When the $[H^+]$ is greater than 5×10^{-5} (pH 4.3) the k_1 term dominates, and

$$F_S \simeq k_1\gamma[H^+] \qquad (7.2)$$

A rate-limiting step involving the attack of a proton at the FeS surface would lead to such first-order dependence on $[H^+]$. Alternatively, if the rate of dissolution of the basic FeS was limited by the diffusion of the solubilizing proton, F_S could again depend on the first power of $[H^+]$. The fact that k_1 was independent of stirring at speeds greater than 200 rpm seems to indicate that the dissolution rate was not being limited by diffusion between the bulk solution and the pellet surface.

The E_a measured for a rate constant ($k = Ae^{-E_a/RT}$) can often be used to distinguish between chemical and transport control of a reaction. In aqueous solutions at room temperature, diffusional activation energies are known to be small, in the neighborhood of 2-5 kcal/mole (Taylor, 1938). Thus, if a reaction is rate-limited by diffusion, the measured E_a must be small. (The converse, however, is not true.) For k_1, E_a was 6.8 kcal/mole with a standard deviation of 1.2 kcal/mole. This is smaller than the 8-20 kcal/mole which would clearly indicate

a chemical step and only somewhat larger than the 2-5 kcal/mole expected for diffusion-controlled reactions. Therefore, considering the magnitude of the standard deviation, 6.8 kcal/mole is not large enough to permit one to say with surety that, taken by itself, such a value indicates chemical control.

If the rate of dissolution were being controlled by the rate of "bulk solution ↔ pellet surface" diffusion, according to the Nernst model, we may write

$$F_{H^+} = D\frac{[H^+] - [H^+]_{x=0}}{\delta} \tag{7.3}$$

where $[H^+]$ is the bulk H^+ concentration, $[H^+]_{x=0}$ is the concentration of H^+ at the pellet surface, and D is the diffusion coefficient of H^+. From mass balance considerations, we have

$$F_S = 0.5\ F_{H^+} \tag{7.4}$$

If the dissolution rate is completely limited by the H^+ diffusion, then $[H^+]_{x=0}$ will be very low, i.e., $[H^+]_{x=0} << [H^+]$, and from (7.3) and (7.4) we obtain

$$F_S = \frac{D[H^+]}{2\delta} \tag{7.5}$$

which possesses the same dependence on $[H^+]$ as does (7.2). If such transport-controlled dissolution is indeed occurring, from (7.2) and (7.5) we would have

$$k_1\gamma = \frac{D}{2\delta} \tag{7.6}$$

From Table 6.1, at 25°C, $k_l \simeq 0.22$ cm/min. If $D \simeq 9.5 \times 10^{-5}$ cm^2/sec = 5.7×10^{-3} cm^2/min (Parsons, 1959) and $\gamma \simeq 0.8$ (I=0.05 M), then δ would be ~ 0.015 cm = 150μ. This is considerably thicker than the 10-30 μ reported to be typical for the diffusion-controlled dissolution of various materials under well-stirred conditions (see Chapter 2).

The independence of dissolution rate with respect to stirring rate would seem to indicate that a 150μ stagnant boundary layer is improbably thick. It might be argued, perhaps, the large, hydrodynamically-isolated depressions (of the order of $\sim$ 100μ) on the surface may be causing at least partial diffusion-control. This possibility may be ruled out on two accounts; 1) the SEM photos of the FeS pellets revealed these surfaces to be free of any such large depressions; and 2) the experiments T2 and T3 were carried out with a very flat non-porous surface and yet its dissolution behavior was very similar to that of the pellets (see Figure 6.11).

Taken together, the facts that: 1) the dissolution rate in this

regime was independent of stirring above 200 rpm; and 2) the behavior of both the pellets and the non-porous FeS surfaces was very similar at pH $\sim$ 5; indicate that "bulk solution $\leftrightarrow$ pellet surface" diffusion was probably not playing a role in determing k_1.

Two possibilities remain: either 1) the pores of the pellet are contiguous with one another and extend into the pellet for many microns, thereby contributing substantial reactive surface area for dissolution and allowing pore diffusion effects; or 2) the pores are not contiguous, there is thus no pore diffusion, and k_1 may be related directly to a chemical rate constant for a reaction step in the dissolution process. Both of these possibilities will now be considered.

Model 1. Pores are contiguous.

Some assumptions are required to make this problem more tractable. They are: 1) the pores may be considered to be straight cylinders; 2) there are no concentration gradients in directions perpendicular to a pore axis; and 3) that in the regime pH = 3.0-4.3 the rate of reaction of proton with FeS (in the pores as well as on the surface) is proportional to the H^+ concentration. It should be noted that the third assumption does not exclude diffusion control in the pores. It merely requires that the dissolution rate is proportional to the $[H^+]$. The supply of protons may be diffusion-controlled. The first two assumptions are reasonable, and simplify things considerably in that they one-dimensionalize the problem.

The third assumption is perhaps less easily justified. Locker and de Bruyn (1969) have shown that well stirred suspensions of cubic

ZnS (β-ZnS, sphalerite) and hexagonal CdS (CdS; greenockite) behave in this manner and dissolve in aqueous H_2SO_4 solutions (0.5-4.0 M) at a rate proportional to $[H^+]$: $F_S = k[H^+]$. A slow step involving first the desolvation of a proton and then its adsorption upon a lattice S(-II) species is proposed by these workers to be the rate determining step for the dissolution reaction. A faster desorption of both HS^- and metal ion is then envisioned to follow. Considering the basic nature of metal sulfides, it is not surprising that CdS and β-ZnS should dissolve at a rate proportional to $[H^+]$. In this analysis, it will be assumed that mackinawite behaves similarly in solutions of $pH \leq 4.3$. (for the sake of consistency with the earlier analysis of k_1, it will further be assumed that the important variable here is a_{H^+} rather than $[H^+]$. The rate constant will be denoted k_1' to distinguish it from k_1.

The overall porosity of the pellets was determined to be ∿30% (Chapter 4). For any cross-section through the pellet then, 30% of the area is accounted for by the pores, and 70% is taken up by the FeS. At the pellet surface, the FeS crystals do not lie flat. The random orientation of the crystals probably increases the exposed area by a factor of ∿2; the resultant exposed area is then about 2 x 70% = 140% of the projected surface area.

A schematic diagram of the rough surface including the hypothetical straight, cylindrical pores is presented in Figure 7.1. The distance x from the surface is measured positively into the pellet. The radius of the pore is r. The area and volume elements da and dv corresponding

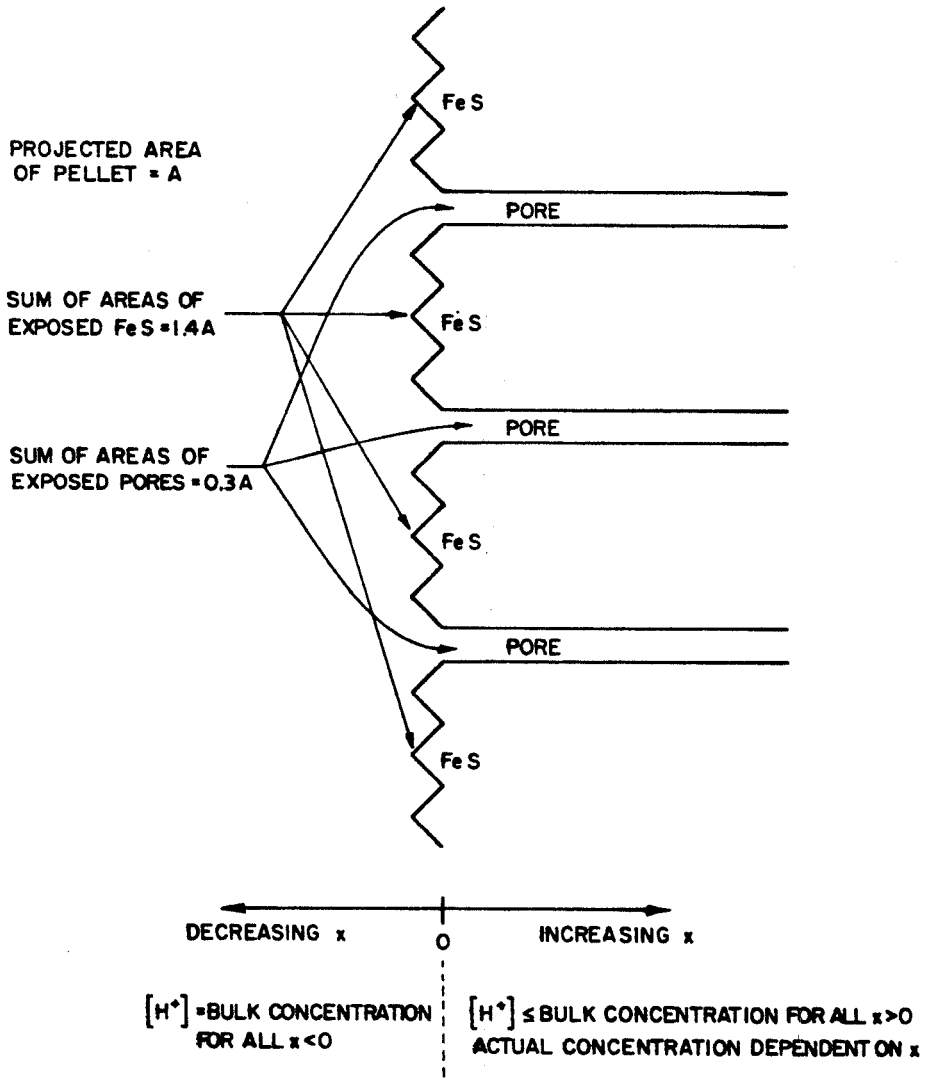

Figure 7.1 Schematic diagram of pellet surface for Model 1 of Section 7.2.1. The diameter of the hypothetical, straight pores is 2r. The variable x is zero at the pellet/solution interface, and increases positively into the pellet. The projected surface area of the pellet is A. The sum of the area of the pores is 0.3A. The non-pore projected area is 0.7A, but due to surface roughness it is estimated at 1.4A.

to the distance element dx are $2\pi r dx$ and $\pi r^2 dx$, respectively. From the assumption that the dissolution rate was proportional to $[H^+]$, the flux F_S from the pore walls would be

$$F_S = k_1' a_{H^+} \qquad (k_1' \neq k_1) \tag{7.7}$$

The rate of consumption R of H^+ per unit volume is therefore

$$R = \frac{2k_1' a_{H^+} da}{dv} = \frac{2k_1' a_{H^+} 2\pi r dx}{\pi r^2 dx} = \frac{4k_1' a_{H^+}}{r} \tag{7.8}$$

(The extra 2 results from the requirement of 2 moles of H^+ per mole of solubilized FeS.)

The basic differential equation which applies to this one-dimensional diffusion problem with a chemical reaction is

$$\frac{\partial c}{\partial t} = D\frac{\partial^2 c}{\partial x^2} - R \tag{7.9}$$

where c is the concentration of the material of interest. Accordingly, we have for $[H^+]$,

$$\frac{\partial [H^+]}{\partial t} = D\frac{\partial^2 [H^+]}{\partial x^2} - \frac{4k_1' a_{H^+}}{r} = 0 \tag{7.10}$$

where $\frac{\partial [H^+]}{\partial t}$ has been set equal to zero for steady state conditions. We can rewrite (7.10)

$$\frac{d^2 [H^+]}{dx^2} - \beta^2 [H^+] = 0 \tag{7.11}$$

where $\beta = \sqrt{\frac{4k_1'\gamma}{rD}}$. The boundary conditions are $[H^+]_{x=0} = [H^+]_{bulk}$ (no "bulk solution ↔ pellet surface" diffusion limitation); and $[H^+]_{x=\infty} = 0$ (the pore "mouth" is too far from $x = \infty$ to allow replenishment of H^+).

The solution is straightforward:

$$[H^+]_x = [H^+]e^{-\beta x} \tag{7.12}$$

The diffusive flux $F_{H^+,d}$ of H^+ into each pore mouth ($x=0$) would be

$$F_{H^+,d} = -D\left(\frac{d[H^+]}{dx}\right)_{x=0} = D[H^+]\beta \tag{7.13}$$

The flux $F_{H^+,s}$ due to the direct reaction of H^+ with the surface would be

$$F_{H^+,s} = 2k_1'a_{H^+} \tag{7.14}$$

This model predicts that the <u>total</u> flux of H^+ to the pellet surface would be given by

$$F_{H^+} = (0.3D\beta + 2.8k_1'\gamma)\ [H^+] \tag{7.15}$$

where the pores and exposed areas have been weighted according to their percentage area abundance.

When pH $\leq$ 4.3, the total flux F_{H^+} was observed to be given by

$$F_{H^+} = 2k_1a_{H^+} \tag{7.16}$$

If such pore diffusion is indeed having an effect, then by equating (7.15) and (7.16) we have

$$2k_1\gamma[H^+] = (0.3D\beta + 2.8k_1'\gamma)\ [H^+] \tag{7.17}$$

or

$$k_1\gamma = k_1'(0.30\sqrt{\frac{D\gamma}{rk_1'}} + 1.4\gamma) \tag{7.18}$$

When k_1' is large ($\sqrt{\frac{D\gamma}{rk_1'}} << 1.4\gamma/0.3$) the diffusion term may be neglected: although large concentration gradients develop near the pore mouths, the rate at the surface predominates. When k_1' is small, gradients still develop in the pores, but in this case, the reaction rate at the surface is not large and diffusion effects can influence the observed dissolution rate. If r is reduced while maintaining the same overall porosity, diffusional effects will be enhanced because the larger surface to volume ratio in the pores allows a more rapid depletion of the H^+. This results in higher concentration gradients (and therefore larger diffusion rates) at the pore mouths.

Equation (7.19) is a quadratic in $\sqrt{k_1'}$, and may be rewritten

$$k_1' + 0.2\sqrt{\frac{D\gamma}{r}}\sqrt{k_1'} - 0.7k_1\gamma = 0 \tag{7.19}$$

Using the same values of D, γ, and k_1 (T = 25°C, I = 0.05) utilized in equation (7.6), and taking $r \sim 0.2\,\mu = 2 \times 10^{-5}$ cm (see Figures 4.8 and 4.9), the solution to (7.20) yields a value of $\sim$ 0.005 cm/min for

k_1'. On the basis of this value, $\sim$ 3% of the dissolution is taking place on the surface, and $\sim$ 97% in the pores. If r is reduced to 0.05 μ, $k_1' = 0.001$, and the surface would be responsible for less than 1% of the observed reaction rate.

It is apparent that for these values of k_1', the observed reaction rate would be very much dependent on r. In this k_1' regime (where diffusion control into the pores would dominate), for the same overall porosity, the observed rate would go as $r^{-1/2}$ (see Equation (7.19)). Considering the somewhat crude method which was used to resurface the pellets, it would be very surprising if the same pore size distribution and overall surface porosity was present at the beginning of each series (compare Figures 4.8 and 4.9). The fact that k_1 did not seem to vary greatly from one series to the next (relative standard deviation = 15%) might therefore suggest that this model is incorrect.

Model 2. Pores are not contiguous.

This situation is relatively much easier to analyze. In this case, since "bulk solution $\leftrightarrow$ pellet surface" diffusion has already been ruled out, if the pores are not contiguous, then the measured k_1 would be directly relatable to the dissolution rate constant k_1'. The only factor to be accounted for is the surface roughness. In the analysis for Model 1, the actual exposed surface area of FeS was estimated to be $\sim$ 140% of the projected pellet area A. In Model 2, the bottoms of the pores must be included, and the resultant exposed area would be $\sim$ 170% of A. (It should be noted

that this estimation is of a very approximate nature.) The real value of the area will be denoted A' (equal to $\sim 1.7A$). Since we require that

$$k_1 \gamma A = k_1' \gamma A' \simeq 1.7 k_1' \gamma A \tag{7.20}$$

we have that $k_1' \simeq k_1/1.7 \simeq 0.13$ cm/min with a relative standard deviation of 15%.

The dissolution rate law which was observed for the non-porous FeS surfaces was

$$\frac{dS_{TOT}}{dt} = \frac{A}{V} (k_1^* \gamma [H^+] + k_2^* [H^+]^{-0.5}) \tag{6.15}$$

which reassuringly contains a term first order in $[H^+]$. If the general reactivities of the pellet and non-porous FeS were the same, and if the contiguous pore model was the correct one, then $k_1^* \gamma$ should have been of the order of 0.001 - 0.005 cm/min for $r = 0.05 - 0.20\ \mu$. In fact, experiments T2 and T3 indicated that $k_1^* \gamma$ was in the range 0.15- 0.50cm/min. At a minimum then, the ratio between k_1^* and k_1' would be of the order of 0.1/0.005 = 20. Alternatively, if the pores are not contiguous, the k_1^*/k_1' ratio would be of the order of 0.15/0.13 $\sim$1.2 A factor of $\sim$1.2 increase in reactivity due to poor crystallinity† seems much more reasonable than one which is of the order of $\sim$ 20.

†We know the non-porous FeS coating was less crystalline than the material used to prepare the pellets. This was apparent from their X-ray diffraction patterns, Figures 3.4 and 4.10.

Accordingly, the observations that:

1) the values of k_1 obtained for the somewhat crudely resurfaced pellets were much more reproducible than one would expect if Model 1 applied; and

2) the reactivity of the non-porous surface was very much closer to that predicted by Model 2 than that predicted by Model 1

both indicate that Model 2 (non-contiguous pores) provides a more accurate description of the pellet behavior, and that k_1 may be related to a chemical step in the dissolution reaction sequence.

However, the nature of mechanism responsible for the k_1 term remains unclear. Though we may probably presume that a proton is participating in the rate determining step (rds), it is unclear whether such protons are reacting with kink site and/or ledge site and/or surface site S(-II) lattice species.

In an experiment such as S16 where $[H^+]_0$ was 2×10^{-5} M, even after 10% of the H^+ was consumed, the ion activity product (IAP) for the dissolution reaction

$$FeS_{(s)} + H^+ \rightleftharpoons Fe^{2+} + HS^- \qquad (7.21)$$

($IAP = a_{Fe^{2+}}/a_{HS^-}a_{H^+}$) was still only 10^{-10} M. Based on the work of Berner (1967), a value of 2.5×10^{-4} M may be deduced for the equilibrium constant (i.e., the equilibrium IAP value) for reaction (7.21). Thus, $\Omega = \sim 2.5 \times 10^6$. With suitable estimates of σ and a, we may therefore use equation (2.4) to calculate the size of the critical radius r_c for this value of Ω.

In their study of the inhibiting effects of phosphate ion on calcite dissolution kinetics, Berner and Morse (1974) argue that the edge free energy σ (ergs/cm) may be approximated by $\sigma_s h$, where σ_s is the surface free energy (ergs/cm^2) and h (cm) is the height of the monomolecular wall which lines the hole. In other words, the energy required to lengthen the ledge of the hole by dl is assumed to equal the energy required to increase the area of the monomolecular wall by hdl, namely, $\sigma_s h dl$. If we take σ_s for FeS_{mack} to be $\sim$ 400 ergs/cm^2 (see discussion following equation (3.1)), and h $\sim$ 3Å = 3 x 10^{-8} cm, then $\sigma \simeq 1.2 \times 10^{-5}$ ergs/cm. A density of $\sim$ 4.3 g/cm^3 (see Chapter 4) implies a molecular volume of $\sim 3 \times 10^{-23}$ cm^3/molecule of FeS. Therefore, an estimate of the area density for any of the crystal faces would be $\sim$ 1 FeS molecule/9 Å^2 or a $\simeq 10^{15}$/cm^2.

Substituting these values into (2.4) we obtain that r_c, i.e., the radius of the smallest stable hole is only $\sim$ 2Å! Though such a value probably does not have much meaning, we may conclude that r_c is nevertheless very small under these conditions. This would perhaps explain why the dissolution rates observed during experiment S16 ($[H^+]_0 = 2 \times 10^{-5}$ M, $[Cu]_0 = 8.2 \times 10^{-7}$ M = 0.052 ppm) were indistinguishable from those observed during similar experiments where no Cu(II) was added. By the end of S16 (duration: 34 hrs), 50% of the initial Cu, i.e., 0.50 x 0.31ℓ x 8.2×10^{-7}M = 1.2×10^{-7} moles of Cu had been lost to the FeS surface. With a "true" FeS surface area of $\sim$1.7 x 0.66 cm^2 = 1.1 cm^2, and assuming a uniform distribution of Cu

on the surface, there would be ∿7 Cu(II) ions per $\mathring{A}^2$ (i.e., more than a monolayer of CuS) at the conclusion of S16, and fewer per $\mathring{A}^2$ during the early stages of the experiment. But despite the probable complete poisoning of S(-II) kinks during the very early stages of S16 the FeS dissolution rate was unaffected: the nucleation of new holes occurred with great facility and so dissolution continued. The extent of Cu coverage encountered in S18, however, (∿ 110 Cu(II) ions per $\mathring{A}^2$ at the conclusion of the experiment) was so great that even during the early stages, highly insoluble CuS probably coated the surface and so the consumption of protons was virtually halted.

It may therefore be concluded that under these conditions of extreme undersaturation, any surface S(-II) position is an active site for dissolution. In this case, the flux F_S of FeS dissolving from the surface is likely to be proportional to the area density n_s (moles/cm^2; $n_s = a/N_a$, N_A = Avogadro's number) of S(-II) sites as well as to a_{H^+}. The rate constant which applies to the reaction between H^+ and surface S(-II) species will be termed $\tilde{k}_1$:

$$F_S = k_1' a_{H^+} = \tilde{k}_1 n_s a_{H^+} \text{ (60 sec/min)} \qquad (7.22)$$

The units of $\tilde{k}_1$ are cm^3/(mole-sec). From before, $k_1' \sim 0.13$ cm/min with a standard deviation of 0.02 cm/min. Since $a \sim 10^{15}/cm^2$, $n_s \sim 1.6 \times 10^{-9}$ moles/cm^2, and therefore at 25°C, $\tilde{k}_1 \simeq 1.4 \times 10^6$ cm^3/mole-sec.

As discussed in Chapter 2, according to Eyring's (1935) "absolute reaction rate theory", the rate constant κ for any reaction is proportional to the quantity $\exp(-\Delta G^{\ddagger}/RT)$. The constant of proportionality is $\alpha\frac{kT}{h}$ (Glasstone, Eyring, and Laidler, 1941), where h is Planck's constant. The quantity $\frac{kT}{h}$ (sec^{-1}) represents the frequency at which the activated complexes decompose. α is termed the "transmission coefficient", and represents the fraction of activated complexes which decompose in favor of the products. For most reactions, α is between 0.5 and 1.0. Because there is no way of estimating α for this reaction from the data at hand, it will be assumed to be 1.

Since

$$\Delta G^{\ddagger} = \Delta H^{\ddagger} - T\Delta S^{\ddagger} \tag{7.23}$$

where $\Delta H^{\ddagger}$ and $\Delta S^{\ddagger}$ are the enthalpy and entropy of activation, respectively, we have

$$\kappa = \frac{kT}{h} e^{\Delta S^{\ddagger}/R} e^{-\Delta H^{\ddagger}/RT} \tag{7.24}$$

It can be shown (see, for example, Moore, 1972, p. 385) that for liquid systems, the so-called activation energy E_a may be related to $\Delta H^{\ddagger}$ by the equation

$$\Delta H^{\ddagger} = E_a - RT \tag{7.25}$$

and therefore

$$\kappa = e \frac{kT}{h} e^{\Delta S^{\ddagger}/R} e^{-E_a/RT} \tag{7.26}$$

With a measured E_a of $\sim$ 6.8 kcal/mole (standard deviation = 1.2 kcal/mole), at 25°C $\Delta H^{\ddagger}$ for the dissolution of FeS is $\sim$ 6.2 kcal/mole with a standard deviation of 1.2 kcal/mole. Locker and de Bruyn's (1969) data indicate $\Delta H^{\ddagger}$ values of 9.3 and 13.6 kcal/mole, respectively, for β-ZnS and CdS.

With standard states of 1 mole/cm^3 and 1 mole/cm^2 for a_{H^+} and n_s respectively (activation entropy values depend on the standard states selected), at 25°C we have for FeS

$$1.4 \times 10^6 = (2.7)(6.2 \times 10^{12})\, e^{\Delta S^{\ddagger}}(1.05 \times 10^{-5}) \tag{7.27}$$

$$\Delta S^{\ddagger} = -9.5 \text{ cal/mole-degree} = -9.5 \text{ eu/mole} \tag{7.28}$$

Similar calculations using the data of Locker and de Bruyn lead to values of -18 eu/mole and -7 eu/mole, respectively, for the $\Delta S^{\ddagger}$ of dissolution of β-ZnS and CdS.

7.2.2 k_2

At pH's higher than $\sim$ 5.7, the rate equation (6.10) is dominated by the k_2 term, and

$$F_s = k_2 \tag{7.29}$$

The value of E_a measured for k_2 was 7.3 kcal/mole with a standard deviation of 1.0 kcal/mole. Taken by itself, such a value is not large enough to be considered clearly indicative of chemical control (see discussion in Section 7.2.1). However, the facts that k_2 was observed to be independent of the concentration and nature of the

buffering agent (see Table 6.2) as well as of stirring are strong indications that k_2 is not reflective of some transport process involving the conjugate acid of the buffer. Since the saturation concentration for FeS will be a strong function of the pH, and because k_2 was also independent of the pH of the solutions, we may also rule out the possibility that the dissolution is rate-limited by the diffusion of the dissolved FeS. It appears, then, that diffusion is not influencing the magnitude of k_2. (This is an encouraging result as far as the analysis of k_1 is concerned because it makes pore diffusion effects even less likely.)

With the elimination of transport control, however, comes the problem of selecting a chemical reaction mechanism which is consistent with the data. Since the dissolution of the FeS must proceed via the formation and subsequent departure from the surface of "leaving groups" containing Fe and S, the rate-determining step (rds) must involve either the formation or the departure of such a leaving group. With k_1, the first order dependence on $[H^+]$ was used to argue for a protonated surface sulfide species as the important leaving group in the pH regime 3.0 - 4.3.

At a minimum, it is possible to say that in the case of k_2 the departure of $\equiv$S-H groups is not rate determining ("$\equiv$" denotes additional bonds to the lattice). Since H^+ is a potential determining ion for a metal sulfide surface, double layer theory predicts that the equilibrium surface concentration of these groups will be a strong function of pH (see for example Stumm and Morgan, 1970).

Therefore, the absolute number which leave the surface per unit time would also depend upon the pH. Because the k_2 term displayed no pH dependence, we may infer that under these pH conditions, a simple protonation is not enough to permit the departure of an HS^- group.†

A possible model for the rds would be one in which the thermal vibrations of the surficial lattice constituents (aided only by the solvating action of water molecules) wrest lattice sulfide species from their berths. The rate expected for one event of such a mechanism would show no dependence on pH or [HB], though we may be assured that any S(-II) making the transition from the solid to the aqueous phase would be doing so in a protonated form (as either HS^- or H_2S, depending on the pH). The thermal vibrations would alone control the actual rate of release, although the surface density of active sites (kinks?) for such a process might depend on the pH. For brevity, this model will be referred to as model A.

If this model does provide the correct description, however, it appears puzzling that the rate should be independent of pH and therefore also of Ω. The thermodynamic stability of embayments (each

---

†Under low pH conditions where k_1 dominates and where ledges, kinks and holes are likely to abound, however, many lattice S(-II) species are likely to be very exposed. Reaction with H^+ may be all that is needed to facilitate the solubilization of such S(-II) species, and F_S could well be proportional to $[H^+]$.

of which contains many kinks) increases with the degree of undersaturation Ω. Since the degree of attachment there is weakest, one might expect that kink positions would be favored sites for the mechanism of this model. Yet, the net rate is a constant at pH's greater than $\sim$ 5.6. This problem would be easily resolved if new kinks (and the ledges upon which they reside) are removed from the crystal surface before they can grow into embayments and thereby affect the area density of kink sites. That this may be occurring may be demonstrated as follows.

If we normalize k_2 by the "real" surface area A', then $k_2' \simeq 1.1 \times 10^{-9}$ moles/cm^2-min. With a molar volume of $\sim$19 cm^3/mole for FeS, this would imply that on the average, the faces of the exposed crystals are receding at a rate of $\sim 2 \times 10^{-8}$ cm/min = 2Å/min, or approximately one monolayer per minute. This is really quite fast, and it seems improbable that embayments large enough to affect the surface density of kink sites would have time to form.

An additional question requires consideration. That is, at pH > 6, why did the dissolution rate of the nonporous surfaces appear to be proportional to $[H^+]^{-0.5}$? Independence with respect to $[H^+]$ would have been the expected result. The reason for this difference in functionality is not clear. One conjecture would be that the iron ions in this poorly crystallized FeS may react with OH^- and are thereby released from the lattice, perhaps as $FeOH^+$ ions. This additional dissolution mechanism would account for the fact that the

rate was observed to accelerate as the pH, and therefore $[OH^-]$, was raised. Since only a limited amount of data were obtained with these non-porous surfaces, it does not seem possible to do anything more than speculate about the origin of this functionality difference. This question must consequently be left unresolved, and it will be assumed that model A provides the correct description of the mechanism.

Since this reaction is envisioned to be essentially unimolecular, the rate constant k_2' (moles/cm^2 min) may presumably be decomposed into a product of the area density (moles/cm^2) of active sites, n_{sa} (kink sites?), and a rate constant $\tilde{k}_2$(sec^{-1}) which describes the frequency at which the sites undergo solubilization:

$$k_2' = \tilde{k}_2 n_{sa}(60 \text{ sec/min}) \tag{7.30}$$

In order to facilitate the application of (7.26), the time scale chosen for $\tilde{k}_2$ is seconds.

The value of E_a measured for k_2' (and therefore also for k_2 and $\tilde{k}_2$) was 7.3 kcal/mole with a standard deviation of 1.1 kcal/mole. By (7.25) then, $\Delta H^{\ddagger}$ = (7.3 - 0.6) kcal/mole = 6.7 kcal/mole. To evaluate $\Delta S^{\ddagger}$, we require n_{sa} so that $\tilde{k}_2$ may be calculated and employed in (7.26). Unfortunately, with the data available, it would be virtually impossible to obtain a good estimate of n_{sa}, although an upper bound is provided by n_s. Thus, if $k_2' = 1.1 \times 10^{-9}$ moles/cm^2 min, and $n_{sa} = n_s \sim 1.6 \times 10^{-9}$ moles/cm^2, for this model, a lower bound on $\tilde{k}_2$ would be $\sim 10^{-2}$ sec^{-1}, and a lower bound on $\Delta S^{\ddagger}$ would be -45 eu/mole.

7.3 Summary and Conclusions

In this chapter, arguments have been advanced to the effect that neither k_1 nor k_2 are affected by the rates of transport processes such as diffusion. Rather, each has been attributed to a chemical reaction at the surface of the FeS crystal. Although the different FeS crystal faces may well exhibit different reactivities, no estimate of such differences were possible due to the fact that whole FeS crystals (and therefore several different faces) were subjected to dissolution during the experiments under discussion.

At pH's lower than $\sim$ 4.3, the k_1 term in (6.10) is dominant. A reaction between surficial S(-II) lattice species and protons with rate constant $\tilde{k}_1$ was proposed to be rate-determining. $\tilde{k}_1$ and k_1 are related as follows:

$$k_1 = (1.7)\tilde{k}_1 n_s (60 \text{ sec/min}) \qquad (7.31)$$

The factor of 1.7 was included to account for the difference between the "real" and projected surface areas. By assuming that $n_s \simeq 1.6 \times 10^{-9}$ moles/cm^2, an order of magnitude estimate for $\tilde{k}_1$ of $\sim$ 1.4 x 10^6 cm^3/mole-sec was obtained. For standard states of 1 mole/cm^2 and 1 mole/cm^3 for n_s and a_{H^+}, respectively, absolute reaction rate theory was used to estimate $\Delta S^{\ddagger}$ at -9.5 cm/mole. Considering the order of magnitude (factor of 10) nature of these estimates, the confidence interval on $\Delta S^{\ddagger}$ is probably no better than $\pm R\ell n10 = \pm$ 4.6 eu/mole. $\Delta H^{\ddagger}$ was estimated at 6.2 kcal/mole , with a standard deviation of 1.2 kcal/mole.

In the pH regime 4.3 - 5.6 there is a transition between dominance of the rate equation first by k_1 term and then by the k_2 term. Several possible rate-determining steps were discussed for the k_2 term. The one considered most reasonable relied primarily upon solvation by H_2O molecules and thermal vibrations of the lattice to liberate sulfide species. Consequently, it was proposed that

$$k_2 = (1.7)\tilde{k}_2 n_{sa}(60 \text{ sec/min})$$

where n_{sa} is the area density (moles/cm^2) of active sites for this dissolution process. $\Delta H^{\ddagger}$ was calculated to be $\sim$ 6.7 kcal/moles with a standard deviation of 1.0 kcal/mole. $\Delta S^{\ddagger}$ could not be estimated since n_{sa} was unknown.

However, as far as the application of the results of this thesis to natural systems is concerned, it is not necessary to know the $\Delta S^{\ddagger}$ values, or even the values of $\tilde{k}_1$ and $\tilde{k}_2$. For practical purposes, k_1' and k_2' are the important parameters. The fact that these latter rate constants are really averaged rate constants for the dissolution of FeS from the several different crystal faces does not diminish their applicability to problems involving natural systems. The FeS crystals or crystallites which might be present in such systems would, after all, have all of their several faces exposed and available for dissolution: averaged rate constants would be the ones needed for calculations anyway. If the laboratory and "real world" FeS had the same percentages of surface area distributed between the several

crystal faces, then the corresponding averaged rate constants would hopefully be the same.

Since we are not equipped to do otherwise, it will be assumed that this is the case, and the next chapter will present some analyses of how FeS might be expected to behave in natural systems.

CHAPTER 8

MACKINAWITE DISSOLUTION IN NATURAL WATER SYSTEMS: THE IMPLICATIONS OF THIS RESEARCH FOR THE CYCLING OF Fe, S, AND TRACE METALS IN THE ENVIRONMENT

8.1 Introduction

As has been discussed in Chapter 1, the kinetics of the non-oxidative dissolution of FeS_{mack} has a direct bearing on the rates of several environmentally important phenomena. They are:

1) the non-oxidative release of Fe, trace metals, and S from sulfide phases in anoxic sediments and sewage;
2) the oxidative release of these species from the same systems; and
3) the pyritization of recent sediments.

In order to be able to extrapolate the results of laboratory research to natural systems, it must be assumed that the experimental conditions and materials simulated those found in nature reasonably closely. This assumption will be made here, and the purpose of this final chapter will be to briefly discuss each of the above phenomena in the light of the results obtained from this research. Where possible, the errors which may accompany this assumption will also be considered. In addition, it will be assumed that the dissolution rate law for FeS_{mack} in natural systems is governed by k_2'. Since almost all natural water systems have a pH of at least 6, this is justified.

8.2 FeS_{mack} Dissolution in Natural Systems

8.2.1 Non-oxidative Dissolution

In order that the dissolution of sulfide phases should proceed non-oxidatively, oxygen must be absent. This condition is met in the same types of environments in which metal sulfides may originally form, i.e., anaerobic sewage sludge and anoxic sediments (as well as in the anoxic waters which often lie above these sediments). In this section we are interested in situations in which oxygen is still essentially absent, but the metal sulfide is now unstable with respect to non-oxidative dissolution.

8.2.1.1 Sediments

In the case of sediments which contain either naturally-formed or anthropogenic metal sulfides (as from sewage sludge), such an instability would require the lowering of the metal and/or sulfide concentration below the saturation concentration. Considering the extreme insolubility of most metal sulfides, barring oxidation reactions, such a lowering would be very difficult to accomplish by a chemical reaction (e.g., precipitation) in the pore waters surrounding the metal sulfide. The oxidation by O_2 of the dissolved sulfide and/or metal in neighboring sediments could, however, lead to the development of concentration gradients through the sediment medium and thereby the diffusive loss of sulfide and metal ions from pore waters which remain free of O_2. The types of processes which are responsible for such a juxtapositioning of oxic and anoxic sediments are: 1) the autumnal

return of oxygen to the anoxic bottom waters (and uppermost sediments) of certain lakes after the summer stagnation period; 2) the disruption of anoxic sediments by dredging operations; 3) the agitation of sediments by aquatic fauna (bioturbation); and 4) a reduction in the organic carbon loading to a sediment/water interface: oxic conditions could develop in sediments once protected by a blanket of materials high in organic carbon.

The undersaturation which would accompany the development of such concentration gradients would presumably then initiate the non-oxidative dissolution of residual solid metal sulfide. The flux F_S would depend on the fraction g(<1) of the area of the pore walls occupied by metal sulfide. Figure 8.1 presents a schematic diagram of this problem. The pores of the anoxic portion of the sediment are considered to be straight cylinders of radius r. The distance variable x is measured positively into the anoxic area, and is taken to be zero at the interface of the two regions. In sediments which contain substantial amounts (several percent) of organic carbon, the position of this interface may remain stationary or move only slowly into the anoxic region: while oxygen continues to diffuse down from the sediment/water interface, organics are also diffusing up towards the interface where they are oxidized.†

†For sediments of lower organic carbon content, the oxic front might advance through the anoxic sediment more quickly than the FeS may be able to dissolve non-oxidatively. In this case, any solubilization of Fe, S, and associated trace metals which may occur will take place according to oxidative reaction mechanisms. This type of situation will be discussed in a subsequent section.

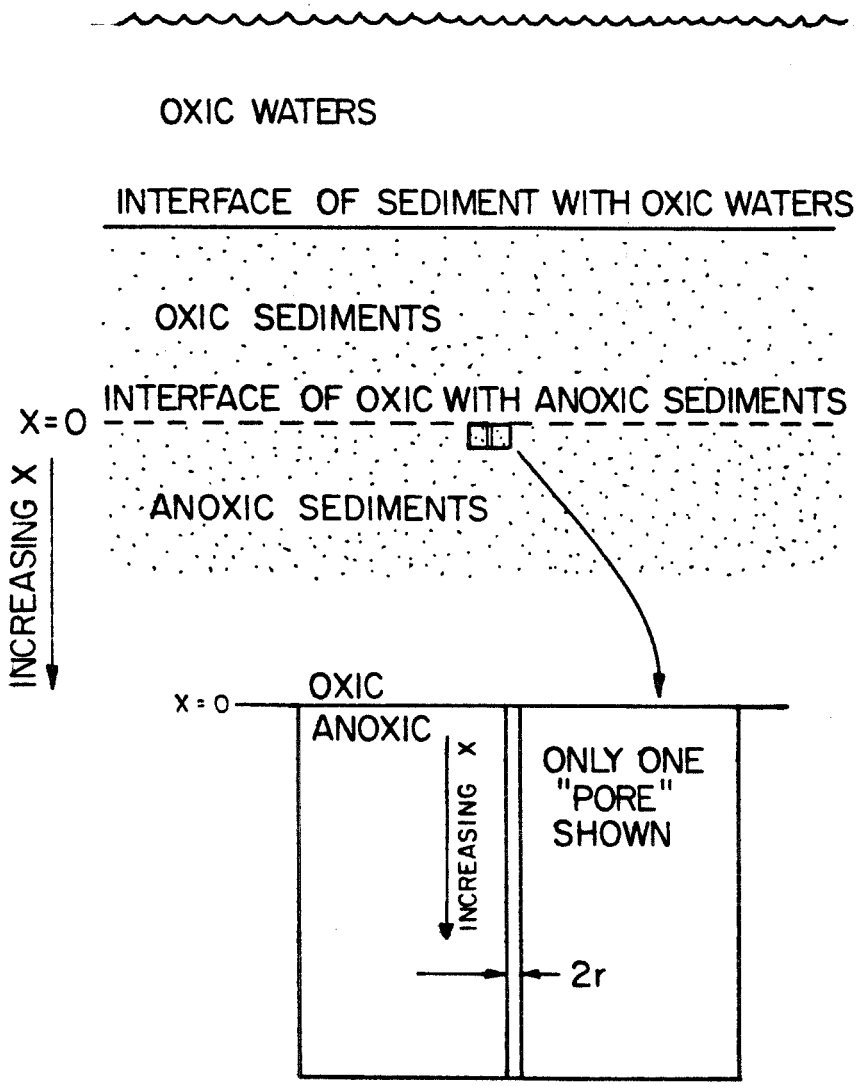

Figure 8.1 Schematic diagram of adjacent oxic and anoxic sediments. Diameter of hypothetical pores is 2r. The variable x is zero at the boundary of the two regions, and increases downward.

It would be very interesting to model this problem mathematically for FeS dissolution. To do so, however, it is necessary to know how the flux F_S from the sediment pore walls varies with c, the dissolved metal sulfide concentration. Although this was not studied in this thesis, for pure FeS (g = 1) it is known that $F_S = k_2'$ when c = 0 and also that $F_S = 0$ when $c = c_s$, the saturation concentration. For order of magnitude calculations then, it will be assumed that F_S from the sediment pore walls is given by

$$F_S = g(1 - \frac{c}{c_s})k_2' \tag{8.1}$$

This equation obeys these conditions, and also takes account of the factor g.

Proceeding as in the analysis of pore diffusion effects on k_1 (see Section 7.2), for the distance element dx, the area to volume ratio da/dv is equal to $\frac{2}{r}$. Thus, the rate of dissolution R' of FeS per unit volume of pore water is

$$R' = \frac{2g}{r}(1 - \frac{c}{c_s})k_2' \tag{8.2}$$

Being a "production" term, R' is a negative analogue of the consumption term R in (7.9). We have, therefore,

$$\frac{\partial c}{\partial t} = D\frac{\partial^2 c}{\partial x^2} + \frac{2g}{r}(1 - \frac{c}{c_s})k_2' = 0 \tag{8.3}$$

In this equation, D is the diffusion coefficient of the dissolved FeS in the sediment pores. $\frac{\partial c}{\partial t}$ has been set equal to zero for steady state conditions.

The logical choice for boundary conditions would be

$$\begin{aligned} c &= c_s, \; x = \infty \\ c &= 0 \; , \; x = 0 \end{aligned} \tag{8.4}$$

That is, at an infinite distance from the oxic sink, $c = c_s$, and at the boundary with the sink, c goes to zero. The solution is

$$\begin{aligned} c &= c_s(1-\exp[-(2gk_2'/Dc_s r)^{1/2}x]) \\ &= c_s(1-\exp(-\beta x)) \end{aligned} \tag{8.5}$$

where $\beta = (2gk_2'/Dc_s r)^{1/2}$.

Large values of g, k_2', and x tend to make c close to c_s. A large value of D, on the other hand, would tend to lower c below c_s because higher rates of diffusive loss from the pores would be favored. Increasing r would also lower c because large pores have small da/dv ratios: there is less reactive surface area per unit volume of pore. Finally, large values of c_s tend to favor greater undersaturation. The explanation here is that the absolute magnitude of the diffusive losses from the pores will be large when the concentrations in the pores are large. However, the rate at which the lost material can be replaced is limited by the magnitude of k_2', and so larger undersaturations tend to develop in the pores when c_s is large.

Even under those conditions which favor disequilibrium in the pores (e.g., large c_s and r), calculations based on (8.5) reveal that equilibrium (i.e., $c \simeq c_s$) is maintained at all but small distances from the oxic zone. For example, an upper bound on r for most sediments would be $\sim 10^{-2}$ cm, the particle size of fine sand. An upper bound on c_s in sediments would be $\sim 10^{-8}$ moles/cm^3, the saturation concentration for FeS at pH $\sim$ 7.0 in the absence of excess sulfide. A value of $\sim 5 \times 10^{-6}$ cm^2/sec may be taken for D. Berner (1964b) has found that anaerobic sediments often contain FeS at levels of $\sim$ 0.1%, and so an order of magnitude estimate of g might be $\sim 10^{-3}$. Using these values of c_s, r, D, and g, and the experimental value of 1.8×10^{-11} moles/cm^2-sec for k_2', a value of $\sim$ 9 cm^{-1} may be calculated for β. Thus, at a distance of only $\frac{1}{9}$ cm from the oxic zone, the $\frac{c}{c_s}$ ratio would have already climbed to $(1 - \frac{1}{e}) = 0.6$.

It appears from these calculations that the proximity of oxic sediments to anoxic sediments would affect the dissolved FeS concentration only near the interface itself. The bulk of the anoxic sediments would remain at equilibrium with respect to FeS dissolution. This is not to say that this model implies that the kinetics of FeS dissolution does not help determine the FeS release rate. That it could play an important role may be shown as follows:

The rate of diffusive release of FeS from the anoxic zone per cm^2 is

$$F_S = \phi D\left(\frac{dc}{dx}\right)_{x=0} \tag{8.6}$$

where Φ is the porosity of the sediment. It is included in (8.6) to account for the fact that only the sediment's pores are available for diffusion. From (8.5) then,

$$F_S = \Phi(2gk_2'Dc_s/r)^{\frac{1}{2}} \tag{8.7}$$

The flux F_S is proportional to $\sqrt{k_2'}$. Thus, if k_2' is lowered, perhaps by the action of large concentrations (∿ppm levels) of transition metals, under the conditions of this model, the dissolution rate would be reduced accordingly.

Another very interesting conclusion that may be drawn is that particular atoms of Fe, S and associated trace metals will remain essentially immobile until the oxic front has been able to advance to within short distances of them. This means that if these elements are going to participate in further diagenetic† reactions (e.g., adsorption, oxidation, etc.) once they are freed from the FeS, such reactions will have their first opportunity to occur near the oxic/anoxic interface. Consider, for example, the case of a transition metal ion which tends to associate with FeS, but which also has a marked affinity for metal oxides such as goethite (α-FeOOH). (Cu(II) would be a good example of such an ion.) As the FeS dissolves, then, such a species would probably become adsorbed on the goethite which is forming in the adjacent oxic sediments: it would not have time to migrate out of the area.

8.2.1.2 Particles in Suspension

Naturally-occurring FeS is likely to be limited to the sediment phase. When anaerobic sewage sludge is discharged to marine or lacustrine receiving waters, on the other hand, particulates containing metal sulfides would be suspended in the water column. If the water

†This term is used by sedimentologists to refer to changes which occur in sediments during and after burial.

is essentially free of oxygen (as would be the case for the discharge of anaerobic sewage sludge into the anoxic marine basins[†]), then such suspended FeS would be expected to dissolve in a nonoxidative manner. If there is some degree of continual mixing in the receiving water, then it might be sufficient to model such a dissolution as occurring with no transport control. Alternatively, after the initial dispersion of the sludge, the receiving waters might be relatively quiescent. The rate of diffusion of dissolved FeS away from the particle would then influence the lifetime of the particle. Both of these situations will be modeled.

Case 1. Particles dissolve with no transport control.

For a single particle of mass m (g), with no diffusion control,

$$\frac{dm}{dt} = -k_2' W s \tag{8.8}$$

where s is its surface area (cm^2) and W is the molecular weight (g) of FeS.

For an approximately cubic particle,

$$\begin{aligned} s &= 6\ell^2 \\ m &= \rho\ell^3 \end{aligned} \tag{8.9}$$

where ℓ is the approximate length (cm) of the crystal face, and ρ is the

[†]This is a proposed method of disposal for anaerobic sewage sludge from the Los Angeles area. An assessment of its feasibility, potential environmental impacts, etc. has been thoroughly studied by Jackson et al. (1978).

FeS density (g/cm^3). From (8.9),

$$s = 6m^{2/3}\rho^{-2/3} \tag{8.10}$$

Substituting (8.10) in (8.8),

$$\frac{dm}{dt} = -6k_2'Wm^{2/3}\rho^{-2/3} \tag{8.11}$$

This is easily integrated. The result is

$$1 - \left(\frac{m}{m_o}\right)^{1/3} = \frac{2k_2'W}{m_o^{1/3}\rho^{2/3}}\, t \tag{8.12}$$

where m_o is the mass of the particle at $t = 0$.

The dissolution of this particle will be essentially complete when $m << m_o$. The time for complete dissolution t_f will then be given by

$$t_f = \frac{m_o^{1/3}\rho^{2/3}}{2k_2'W} \tag{8.13}$$

Substituting for m_o in terms of the initial particle size ℓ_o, and using values of 4.3 g/cm^3 and 88 g/mole for ρ and W, respectively, equation (8.13) reduces to

$$t_f \simeq (0.02/k_2')\ell_o \tag{8.14}$$

If the experimentally obtained value of k_2' (1.1×10^{-9} moles/cm^2-min) is used, we have

$$t_f \simeq 2 \times 10^7 \ell_o \tag{8.15}$$

where t_f is in minutes and ℓ_o is expressed in cm.

According to (8.14), a plot of t_f vs ℓ_o would appear as a straight line in a log-log format. Line B in Figure 8.2 was drawn using (8.15). It indicates that a 0.25mm particle would require about one year to dissolve, while only one day would be required for a 0.7 μ size particle.

Considering the special conditions required for the synthesis of FeS crystals even as large as $\sim 1\mu$, if this model is correct and if k_2' is actually of the order of 10^{-9}moles/cm^2-min, it seems very unlikely that sewage sludge FeS particles would be large enough to last more than several hours. A lowering of k_2', perhaps through the action of poisoning metal ions, would increase the lifetimes of the particles proportionately.

Case 2. Particles dissolve with partial transport control

If there is partial transport control, then at the surface of the particle the dissolution flux F_S would be less than that given by k_2'. It will be assumed for the purposes of these order of magnitude calculations that it is given by

$$F_S = k_2(1 - \frac{c}{c_s}) \tag{8.16}$$

where c is the concentration at the surface of the particle. The factor $(1 - \frac{c}{c_s})$ is chosen for reasons discussed in Section 8.2.1.1.

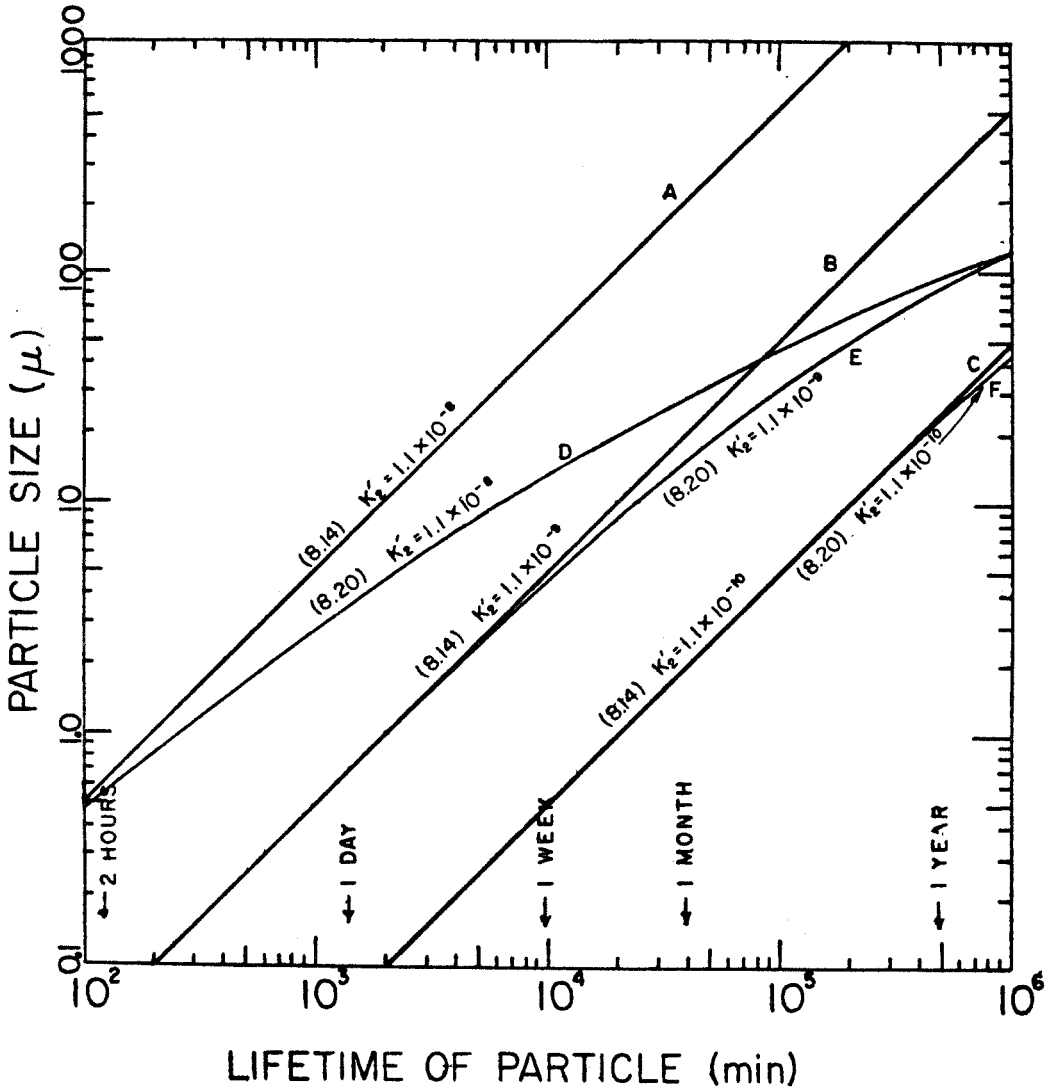

Figure 8.2 Particle size vs. particle lifetime for both non-diffusion- and partial-diffusion-controlled models. Lines A, B and C calculated using (8.14) with k_2' values of 1.1×10^{-8}, 1.1×10^{-9} and 1.1×10^{-10} moles/cm^2 - min, respectively. Lines D, E, F calculated using (8.20) with a c_s value of 2×10^{-9} moles/cm^3 and k_2' values of 1.1×10^{-8}, 1.1×10^{-9} and 1.1×10^{-10} moles/cm -min, respectively.

According to Berner (1971), when particles dissolve in a relatively quiescent medium, the diffusion boundary layer thickness is given approximately by the radius of the particle. The rate of diffusive flux away from the surface would therefore equal

$$F_S = \frac{D}{\ell/2}(c - c_{bulk}) \tag{8.17}$$

For simplicity, c_{bulk} will be assumed equal to zero. At steady state, we may equate (8.16) and (8.17). The result is

$$c = \frac{k_2'}{\frac{2D}{\ell} + \frac{k_2'}{c_s}} \tag{8.18}$$

Since $dm/dt = -WsF_S$, by (8.16) and (8.18),

$$\frac{dm}{dt} = -Wsk_2'\left(1 - \frac{k_2'}{c_s(\frac{2D}{\ell} + \frac{k_2'}{c_s})}\right) \tag{8.19}$$

After using (8.9) to make substitutions for s and ℓ in terms of m, (8.19) may be integrated. The result is

$$t_f = \frac{\rho\ell_o}{2k_2'W} + \frac{\rho\ell_o^2}{8DWc_s} \tag{8.20}$$

where t_f is again the time to complete dissolution and ℓ_o is the initial particle size. If k_2' is taken to be $\sim 1.1 \times 10^{-9}$ moles/cm^2-min, and $D \simeq 6 \times 10^{-4}$ cm^2/min,

$$t_f \simeq 2 \times 10^7 \ell_o + 10 \ell_o^2/c_s \qquad (8.21)$$

where c_s is expressed in moles/cm^3.

Equation (8.20) is similar to (8.14), but there is an additional term, $\rho\ell_o^2/8DWc_s$. The presence of this term reflects the fact that partial diffusion-limitation of the rate will increase the time required for complete dissolution. Depending upon the values of k_2', ℓ_o, and c_s, this effect may be either small or large.

Figure (8.2) contains plots of (8.20) for varying values of k_2', $D = 6 \times 10^{-4}$ cm^2/min, and for $c_s = 2 \times 10^{-9}$ moles/cm^3. This latter value would be the approximate saturation value in a medium at the typical natural water pH of $\sim$8 and initially containing no dissolved Fe(II) or S(-II).

The deviations from the corresponding lines calculated assuming no diffusion control (equation (8.14)) are large when k_2' and/or ℓ_o is large. The deviation between lines B and E (i.e., those calculated using the experimentally obtained k_2') becomes very small once the particle size is less than $\sim 2\mu$.

This analysis has implicitly assumed that the FeS in sewage sludge is present as a suspension of free particles, unassociated with the other particles and flocs. This may be somewhat unreasonable. There will no doubt be some aggregation of the FeS with other materials, and it might be that the dissolution would occur from within loose aggregates of sludge material. In this case, the ℓ in (8.19) would be replaced by d, the approximate dimension of the flocs. The integration

of the resultant equation would be similar to (8.14), but with the correction factor $[1-1/(\frac{2Dc_s}{k_2'd} + 1)]$. For the values of c_s, D, and k_2' used to obtain (8.21), and taking d to be 1, 10, 100, and 1000 , this correction factor would take on the values of 0.9, 0.7, 0.2, and 0.02, respectively. Faisst (1976) has estimated that the particle size distribution for anaerobic sewage sludge peaks at around 15μ, with a majority of the particles falling in the size range 2 - 30μ. For the conditions just discussed then, although this correction is not negligible, neither does it alter the general complexion of these results. For other values of k_2', c_s, and D, such corrections may or may not be needed.

These models are very informative. They clearly indicate the important roles which the variables k_2', D, c_s, and ℓ_o play in determining: 1) how long a given particle of FeS may be expected to last when subjected to anoxic dissolution; and 2) whether or not diffusion may be expected to play a role. A discussion of the implications of these models for trace metal release rates will be presented in Section 8.3.

8.2.2 Oxidative Dissolution

If oxygen is present, then the dissolution will proceed in an oxidative manner (equation (1.2)). This reaction has been studied in some detail by Nelson (1977). Oxidative dissolution experiments were carried out with suspensions of finely divided FeS (500-4,000Å particle size). Under the conditions of pH = 7, $[O_2]$ = 4 mg/ℓ ≃ 10^{-4} M, initial

FeS "concentration" of 800 mg/ℓ, and strong stirring, the observed FeS oxidative dissolution rate was $\sim 10^{-4}$ M min^{-1}.

This is a considerably greater rate of oxidation than would be predicted for the homogeneous oxidation of Fe(II) and S(-II) at their pH 7 saturation concentration. This may be shown as follows. At this pH, c_s for FeS would be $\sim 10^{-5}$ M. According to Stumm and Lee (1961), under these conditions, such a [Fe(II)] would be oxidized at a rate of only 5×10^{-6} M min^{-1}. Similarly, the data of Chen and Morris (1972) indicate that a [S(-II)] of 10^{-5}M would be oxidized to higher valence states at a rate of 10^{-10}M min^{-1}. Both of these rates are well below the observed 10^{-4}M min^{-1}. Consequently, it must be concluded that this oxidative dissolution involved the direct attack of oxygen at the FeS surface. Considering the extremely high FeS surface area available for reaction, however, (from $\sim 3 \times 10^3$ cm^2/ℓ for 4000 Å particles to $\sim 10^5$ cm^2/ℓ for 500 Å particles) the actual rate per cm^2 need not be large. (Depending upon the actual available surface area, this rate would be in the range 5×10^{-10} moles/cm^2-min to 4×10^{-9} moles/cm^2-min.)

For particles of FeS suspended in an oxic medium, the dissolution would undoubtedly take place oxidatively. Nelson (1977) discusses some possible mechanisms for this reaction. In sulfidic sediments which have become oxic, however, although the dissolution may be oxidative upon the introduction of O_2 to the system, this need not continue to be the case.

8.2.2.1 Sediments

Consider the case of a sulfidic sediment containing ~ 0.1% by dry weight of mackinawite. If the porosity of the sediment was ~ 0.3 and the density of the sediment particles ~ 3 g/cm^3, then there would be (.001) (700 cm^3 solids/ℓ)(3g/cm) = 2 g FeS/ℓ ≃ .02 moles FeS/ℓ (ℓ here refers to a liter of sediment). Similarly, if bioturbation or other mechanisms saturate the pore waters with O_2 at a level of ~10 mg/l = 3 x 10^{-4} M, there would be (0.3 l of pore water/ℓ)(3 x 10^{-4} M) ≃ 10^{-4} moles O_2/ℓ. If the FeS is to be oxidized to Fe(III) and S(0), three moles of electrons would be released per mole of FeS oxidized and therefore 0.02 moles FeS/ℓ would correspond to 0.06 equivalents of FeS/ℓ. Since one mole of O_2 can accept four moles of electrons, 10^{-4} moles O_2/ℓ would correspond to 4 x 10^{-4} equivalents O_2/ℓ.

If the reactivity of natural mackinawite towards oxidation by O_2 is similar to that of Nelson's synthetic mackinawite[†], this small amount of O_2 would be expected to last less than one minute! Thus, the oxygen would be removed quickly, and the sediment would be left pretty much anoxic.

The oxidation of the remaining FeS would require the diffusion of oxygen into the sediment. Providing that the short term presence of O_2 did not cover the surface of this FeS with a coating of FeOOH or

[†]There is reason to believe that this is the case. In addition to his work with laboratory synthesized FeS, Nelson also carried out oxidation experiments with natural FeS taken from anaerobic sediments. The results obtained with the two types of FeS were similar.

elemental sulfur[†], this FeS dissolution problem reduces to the same one discussed in Section 8.2.1.1. Thus, although the FeS dissolution initially takes place in an oxidative manner, the O_2 is soon consumed and the rates of non-oxidative dissolution may again become important.

8.2.3 Pyritization of Recent Sediments

The sulfur which forms as a result of FeS oxidation may go on to react with residual FeS to form pyrite (Berner, 1970):

$$FeS + S \longrightarrow FeS_{2\ pyrite} \qquad (1.6)$$

The amount of FeS which is ultimately converted to pyrite will depend upon the availability of elemental sulfur as well as upon the relative rates of: 1) the diffusion/oxidation process involving O_2; and 2) reaction (1.6). While approximate rates may be estimated for the first process, little is known about the rate of (1.6).

The pyrite formed by this reaction has been observed to crystallize on the surfaces of the elemental sulfur (Berner, 1970). It seems very likely, then, that the elemental sulfur reacts with solution phase Fe(II) and S(-II). This would be the final step in the mechanism of (1.6). The non-oxidative dissolution of the FeS as well as the transport of the resultant ions to the sulfur surface must precede it.

Since the non-oxidative dissolution may be envisioned to comprise the first step in (1.6), one wonders if it could be the rate-determining

[†]At neutral pH, the main sulfur oxidation product of FeS is elemental sulfur itself (Nelson, 1977).

step. The results of this research in conjunction with those of Berner (1970) indicate that this is probably not the case. During one investigation, Berner combined elemental sulfur with suspensions of finely divided FeS (particle size < 0.1μ). H_2S and HS^-, both at levels of 0.1 M, were also added. The pH of the resulting mixture was 6.9. Heating the solution at 65°C for two weeks was required to transform most of the FeS into FeS_2.

Since the E_a for k_2' was ∿ 7.3 kcal/mole, at 65°C k_2' should be of the order of 5×10^{-9} moles/cm^2-min. If the rate of (1.6) was limited by the dissolution rate, according to (8.14) the lifetimes of the particles (i.e., time to complete pyritization) should not have been greater than an hour or so. Although it no doubt had some effect on the dissolution rate, the presence of the H_2S could not have been responsible for retarding it enough so that the disappearance of these small FeS particles would require weeks. This is known because of earlier work by Berner (1967). He demonstrated here that only one hour of 60°C thermal aging was required to substantially increase the average size of very fine particles of FeS suspended in an H_2S-saturated solution. Because this increase could take place only if many of the smaller particles dissolved, and since this dissolution took place in the presence of the H_2S, the FeS dissolution rate may not be blamed for the slowness of (1.6). It seems that the final combination step between the aqueous Fe(II) and S(-II) with the elemental sulfur is responsible.

The above discussion should not be taken to imply that the rate of sediment pyritization is in general limited by the rate of (1.6). As Berner (1970) points out, other factors such as the availability of elemental sulfur might well determine the extent and rapidity of sediment pyritization.

8.3 Summary and Conclusions

The previous sections have discussed the various conditions under which both sedimentary and sewage sludge FeS may be expected to dissolve in natural water systems. Both oxidative and non-oxidative mechanisms have important roles to play in determining how this FeS and associated trace metals are solubilized in different situations.

Oxidative dissolution would be expected when: 1) anaerobic sewage sludge is discharged to oxic receiving waters; and 2) oxygen enters anoxic sediments containing FeS. In the first case, the FeS present would very likely be quickly oxidized. Also, since no transition metal ions are able to effectively retard the FeS oxidative dissolution rate (Nelson, 1977), any metal ions associated with this FeS would be released to the aqueous phase. In the second case, if a sediment of interest contains $\sim$ 0.1 percent-levels of FeS, then Section 8.2.2.1 indicates that the oxygen which enters the system is quickly spent oxidizing an equivalent portion of FeS to Fe(III) and S(0). This portion of the FeS "sacrifices" itself and helps to return the sediment to an anoxic state. Some of the sulfur formed during this partial oxidation no doubt combines with remaining FeS to form pyrite.

The boundary which this type of anoxic, FeS containing sediment may have with oxic sediments was termed the "oxic front". Its presence would lead to the diffusive loss from the anoxic area of various reduced compounds, including FeS. An expression was developed which may be used to calculate how the concentration of the metal sulfide in the pores varies with the distance from the oxic front. It was concluded that unless the distance to the oxic front is fairly small, under virtually all conditions, the pore waters remain saturated with FeS (i.e., substantial dissolution does not occur). This implies that any metal ions which are associated with the FeS will be released primarily at the oxic front.

The exact nature of these results depends strongly upon the dissolution rate of FeS at pH 7-8, and therefore on the magnitude of k_2'. If k_2' were substantially reduced by the action of poisoning metal ions, the dissolved FeS concentration would be lowered below the saturation concentration for greater distances from the oxic front than otherwise expected. If there is a source of oxygen for the sediment system (as in Figure 8.1), then the oxic front may be expected to slowly advance through the anoxic sediments. The relative proportions of FeS which dissolve oxidatively and non-oxidatively would depend on oxygen flux rates, reduced carbon content, porosity, as well as other variables. The proportion of FeS which becomes pyritized will depend on the amount of elemental sulfur available for reaction within the body of anoxic sediments, as well as on how well (1.6) can compete

with (1.2) at the oxic front. The discussion in Section 8.2.3 indicates that at least the non-oxidative dissolution rate does not limit the rate of (1.6).

If anaerobic sewage sludge is discharged to anoxic waters, however, the non-oxidative dissolution rate would be very important in determining the lifetime t_f of an FeS particle suspended in the water column. An expression was developed which relates t_f to k_2' and the initial particle size ℓ_o. In a second model, the relative importance of diffusion control was considered. For small k_2', ℓ_o, and c_s, the same t_f is predicted by both models.

If the value of k_2' obtained during this research (1.1×10^{-9} moles/cm^2-min) may be applied to sludge FeS, these analyses indicate that the lifetimes of the sludge FeS particles would be small. Since substantial amounts of various sulfide-forming transition metals are present in this sludge, k_2' (if it indeed is still an operative rate term) may be reduced and t_f correspondingly increased. The dissolution experiments carried out with copper certainly indicated that Cu^{2+} may act in this way: during experiment S18, both k_1' and k_2' were seemingly reduced by at least a factor of 10.

Considering the greater insolubility of metal sulfides such as CuS, if sludge FeS is contaminated with CuS and then dissolves, the inhibiting effects of the Cu^{2+} ions would very likely become more severe with time: the CuS would tend to be left behind on the surface where it could poison kink sites and even form a coating of CuS around the FeS particle.

These questions require more attention if we are to fully understand the role which iron sulfides play in determining the environmental cycling rates of Fe, S, and trace metals, It is hoped that this research has made a positive contribution toward that end.

APPENDIX I

The calculations of $S_{TOT}(t)$ depend upon a knowledge of how $[H^+]$ varies with time, and also upon the magnitudes of the equilibrium constants and activity coefficients involved (see Section 5.1). The values of K_1, $^*K_1$, and K_{FeCl} used in this thesis were taken from the critical compilation of Smith and Martell (1976). At 25°C, their values were 9.55×10^{-8} M, 3.16×10^{-10} M, and 1.00 M^{-1}. K_2 is known to be very small ($\sim 10^{-14}$ M). Consequently, the exact value of this constant is not needed since the species S^{2-} need not be considered when calculating α_0 and α_1 in the proton balance equations (5.17) and (5.18). K_w, the self ionization constant of water, was taken from tables in The Handbook of Chemistry and Physics.[†] At 25°C, $K_w = 1.01 \times 10^{-14}$ M^2. The values of the first acid dissociation constants for HOAc, MES, and MOPS were determined experimentally by measuring the pH imparted to a solution by known concentrations of B^- and HB, the conjugate base and conjugate acid, respectively.

The acitivity coefficients for the charged species were calculated using the Davies equation (Stumm and Morgan, 1970)

$$\log \gamma_i = - AZ_i^2 \left(\frac{\sqrt{I}}{1 + \sqrt{I}} \right) - 0.3\, I$$

where $A = 1.82 \times 10^6 (1/\varepsilon T)^{3/2}$, ε is the dielectric constant of water, and Z_i is the charge on the species i.

[†] The Handbook of Chemistry and Physics, 51st Edition, The Chemical Rubber Co., 1970, Cleveland, OH.

REFERENCES

Amdur, I., and G. Hammes, 1966, Chemical Kinetics: Principles and Selected Topics, McGraw-Hill, N.Y.

Barton, A., and N. Wilde, 1971, Trans. Farad. Soc., 67, 3590-3597.

Berner, R., 1964a, J. Geology, 72, 293-306.

Berner, R.,1964b, Marine Geology, 1, 117-140.

Berner, R., 1967, Am. J. Sci., 265, 773-785.

Berner, R., 1970, Am. J. Sci., 268, 1-23.

Berner, R., 1971, Principles of Chemical Sedimentology, McGraw-Hill, N.Y.

Berner, R., and J. W. Morse, 1974, Am. J. Sci., 274, 108-134.

Bovington, C. H., and A. L. Jones, 1970, Trans. Farad. Soc., 66, 2088-2091.

Bovington, C. H., and A. L. Jones, 1970, Trans. Farad. Soc., 66, 764-768

Burton, W. K., N. Cabrera, and F. Frank, 1951, Phil. Trans. Royal Soc., 243A, 299-358.

Cabrera, N., and D. Vermilyea, 1958, p. 393-410, Growth and Perfection of Crystals, R. Doremus, R. Roberts, and D. Turnbull, eds., Wiley, N.Y.

Campbell, J. and G. Nancollas, 1969, J. Phys. Chem., 73, 1735-1740.

Chen, K. and J. Morris, 1972, Envir. Sci. Technol., 6, 529.

Clark, A., 1966, Neues Jahrbuch Mineral Monatsheft, 6, 259-268.

Cullity, B., 1956, Elements of X-ray Diffraction, Wesley, N.Y.

Eyring, H., 1935, Chem. Rev., 17, 65.

Evans, H., C. Milton, E. Chao, I. Adler, C. Mead, B. Ingram, and R. Berner, 1964, U.S.G.S. Prof. Paper 475-D, p. D64-D69.

Faisst, W., 1976, Digested Sludge: Delineation and Modeling for Ocean Disposal, Ph.D. Thesis, Calif. Inst. Tech., Pasadena, CA.

REFERENCES (CONT.)

Flascka, H., 1955, Chemist Analyst, 44, 2.

Framson, P., and J. Leckie, 1978, Envr. Sci. Tech., 12, 465-468.

Frank, F., 1949, Farad. Soc. Disc., 5, 48-54.

Gallily, I., and S. Friedlander, 1965, J. Chem. Phys., 42, 1503-1511.

Glasstone, S., H. Eyring, and K. Laidler, 1941, The Theory of Rate Processes, McGraw-Hill, N.Y.

Goldhaber, M. B., and I. R. Kaplan, 1974, p. 569-655, in The Sea, vol. 5, ed. E. Goldberg, Wiley-Interscience, N.Y.

Haussühl, S. and W. Müller, 1972, Kristall und Technik, 7, 533-554.

Ives, M., 1963, J. Phys. Chem. Solids, 24, 275-281.

Ives, M., 1965, Ind. and Eng. Chem., 57, 34-40.

Ives, M., and J. P. Hirth, 1960, J. Chem. Phys., 33, 517-525.

Jackson, G., R. Koh, N. Brooks, and J. Morgan, 1978, Assessment of Alternative Ocean Sludge Disposal Practices, Report No. 14, Envr. Qual. Lab., Calif. Inst. Tech., Pasadena, CA.

Kossel, W., 1927, Nachr. Ges. Wiss. (Göttingen), 135.

Locker, L. D. and P. L. de Bruyn, 1969, J. Electrochem. Soc., 116, 1659-1665.

Morse, J., 1974, Am. J. Sci., 274, 638-647.

Morgan, J. and T. Sibley, 1975, Proc. Am. Soc. Civ. Engrs., Conference, Ocean Engineering, U. of Delaware.

Moore, W., 1972, Physical Chemistry, Prentice-Hall,Englewood Cliffs,NJ.

Nelson, M., 1977, The Oxidative Dissolution of Ferrous Monosulfides and the Behavior of Associated Trace Metals, Ph.D. Thesis,Stanford Univ., Palo Alto, CA.

Nernst, W., 1904, Z. Physik. Chem., 47, 52.

Nestaas, I., and S. Terjesen, 1968, Acta Chemica Scand., 22, 2111-2117.

REFERENCES (CONT.)

Nestaas, I., and S. Terjesen, 1969, Acta Chemica Scand., 23, 2519-2531.

Noyes, A., and W. Whitney, 1897, Z. Physik. Chem., 23, 689.

Parsons, R., 1959, Handbook of Electrochemical Data, Butterworths, London.

Rickard, D., 1969, Stockholm Contrib. Geology, 20, 67-95.

Rickard, D., 1975, Am. J. Sci., 275, 636-652.

Roberts, W., A. Walker, and A. Buchanan, 1969, Mineral Deposita, 4, 18-29.

Schindler, P., H. Althaus, F. Hofer, and W. Minder, 1965, Helv. Chim. Acta, 48, 1204.

Smith, R., and A. Martell, 1976, Critical Stability Constants, Vol. 4, Inorganic Complexes, Plenum Press, N.Y.

Stumm, W., and G. Lee, 1961, Ind. Eng. Chem., 53, 143.

Stumm, W., and J. Morgan, 1970, Aquatic Chemistry, Wiley-Interscience, N.Y.

Sweeney, R., and I.R. Kaplan, 1973, Econ. Geol., 68, 618-634.

Taylor, H.S., 1938, J. Chem. Phys., 6, 331-334.

Ward, J.C., 1970, Rev. Pure Applied Chem., 20, 175-206.